PEOPLE'S DEMOCRATIC REPUBLIC OF ALGERIA
MINISTRY OF HIGHER EDUCATION AND SCIENTIFIC RESEARCH

FRERES MENTOURI_CONSTANTINE 1 UNIVERSITY
FACULTY OF EXACT SCIENCES
DEPARTMENT OF PHYSICS

Phase transformations

Course intended for sudents of Master 1 (Applied physics, Nanophysics and physics of Materials)

Dr. BELAMRI Zehira

2023 / 2024

Contents

Chapter IV: Kinetics of Phase Transformations in Solid Materials and Alloys

Chapter V: Role of elastic strain energy and Interfacial energy

Chapter VI: Mechanisms of crystal growth during diffusionless transformations

Chapter VII: Types of diffusional transformations

Introduction

Materials science involves the development and study of materials' properties for specific purposes. Except in a few special cases, metals are rarely used industrially in their pure state. Generally, alloys consist of two elements (binary alloys), three elements (ternary alloys), and so on. Alloys can be composed of a single phase (single-phase alloys) or multiple phases (polyphase alloys). A phase (solid solution) is defined as a homogeneous part of the material with its own chemical composition and structure. These phases can undergo transformations during material use, driven by diffusion phenomena. Such phase changes are represented by equilibrium diagrams (or phase diagrams). Any phase transformation results in a reduction in the system's free enthalpy, which is the thermodynamic principle for reaching equilibrium, and can only begin from the nuclei of the new phase. These nuclei grow to eventually form an equilibrium phase. Thus, in all phase transformations, we observe both nucleation and growth phenomena.

The phase transformation mechanisms follow Avrami's law, which describes the variation in the nucleation rate as a function of time at a constant temperature. By analyzing different curves, we can construct the T.T.T. (transformation-temperature-time) diagram and describe phase transformations as a function of time.

In these chapters, students will learn the fundamental thermodynamic, crystallographic, and kinetic principles of phase changes in materials. Practical examples illustrate transformations considered essential from an engineering perspective. Each chapter should be thoroughly studied by students to:

- Distinguish between the fundamental types of changes in engineering materials based on thermodynamic, crystallographic, and kinetic features,
- Propose a realistic explanation for the phase changes that might occur under specific conditions during the technological processing of metallic materials,
- Identify the fundamental transformation products of engineering materials.

The books listed in the reference section at the end of this document can be consulted for additional information.

This document is intended for Master I students in the three specialties of Nanophysics, Applied Physics, and Physics of Materials at Frères Mentouri-Constantine 1 University. It is also suitable for students from other fields of study, provided they meet the essential prerequisites for enrolling in this course, which include completion of courses in Material Sciences, Structure and Properties of Solids, and Heat Treatment Essentials. The recommended approach for each chapter is to read the text section attentively and then complete the exercises provided.

At the end of this document, a trilingual glossary is provided as a fundamental tool for Master's students in physics, particularly in materials sciences. Its primary aim is educational; it is designed to alleviate the challenge of finding relevant bibliography in Arabic within the field. The glossary includes the majority of terms used in this manuscript.

Chapter

I

General thermodynamic aspects

I-1. Introduction

In a system at thermodynamic equilibrium, a phase is any part where the intensive quantities (such as temperature, pressure) are continuous functions of spatial coordinates. A phase change occurs when there is a discontinuity in at least one of these quantities. If all intensive parameters are homogeneous (independent of the specific point considered), the phase is considered homogeneous or uniform. In a solid or liquid substance, a phase can be defined as an arrangement of atoms, molecules, or particles, each arrangement corresponding to different properties of the solid or liquid material.

What is a phase transformation?

Phase transitions are physical phenomena that have been recognized for a long time. The experiment thus highlights phase transition phenomena (changes of state). For example, when a substance transitions from the liquid state to the solid state, it undergoes solidification. External manipulation of an intensive thermodynamic variable causes a phase transition.

At the microscopic scale, a phase transition begins to manifest itself through the phenomenon of nucleation. At the atomic or molecular level, the repulsive and attractive forces between atoms or molecules come into play in the processes of fusion and vaporization.

I-2. Kinetics of phase transformation

Phase equilibrium diagrams enable the determination, under equilibrium conditions, of the number, composition, and proportion of phases as a function of temperature and concentration. However, they do not provide information on the kinetics of phase transformations, the time required to form new phases when there is a change in temperature or pressure conditions.

Any phase transformation involves the reorganization of atoms or molecules. The mobility of atoms or molecules in both the liquid and solid states governs the formation of microstructures. Therefore, diffusion, which is the migration of atoms or molecules in solid or liquid materials, determines the kinetics of numerous phase transformations.

In thermodynamics, if a system is in equilibrium at a specific temperature and pressure, its free energy G is at its minimum. When the system is not in equilibrium under the given conditions, it naturally tends to return to an equilibrium state. During this transformation, its free energy decreases: $\Delta G<0$.

Figure I-1 shows the variation of the free energy as a function of temperature T. It illustrates the transformation of iron from the α phase to the γ phase. This figure demonstrates that the free energy of a phase decreases as the temperature increases.

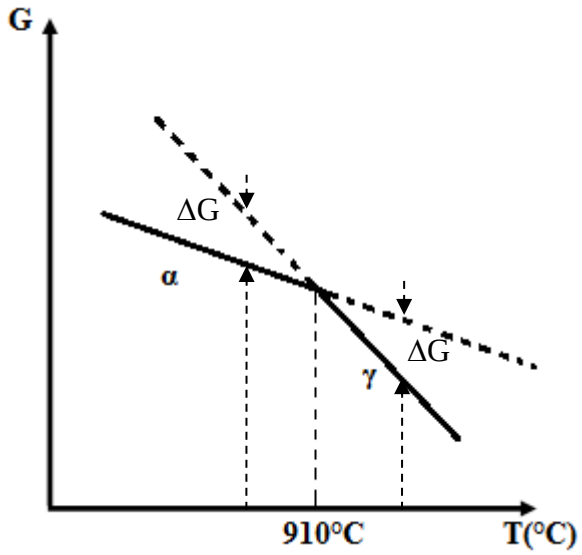

Fig. I-1- : Variation of the free energy as a function of the temperature T (example of the iron transformation from the α phase to the γ phase)

This is obvious because, by definition:

$$G = H - TS \qquad \text{(I-1)}$$

Where H is the enthalpy, T the absolute temperature, and S the entropy of the system.

However, when a system returns to the equilibrium state, not all particles undergo the transformation simultaneously. Otherwise, at every moment, all particles would be in an intermediate configuration, and neither the initial nor the final configurations could coexist during the transformation. The atoms that undergo transformation at any given time are those with higher kinetic energy.

The fact that the final states of a transformation are equilibrium states allows the use of thermodynamic approaches to describe these states configurations. As a system transitions from the initial state to the final state, it passes through a continuous sequence of intermediate configurations. Among these intermediates, one is assumed to be the transition state, which is close to equilibrium and corresponds to unique values of the thermodynamic functions.

A phase transition occurs when a phase becomes unstable under specific thermodynamic conditions, which are described using intensive variables. Therefore, it is essential to describe the thermodynamic conditions that govern a phase transition if we aim to predict it.

I-3. Activated state

As an atom evolves from an initial equilibrium state to a final one, it passes through a continuous sequence of intermediate states. Since the free energies of the two extreme configurations have, by definition, minimum values (and two minima must be separated by a maximum), the free energy of an atom or a group of atoms during the transformation first increases to a maximum and then decreases to its final value. This process is illustrated in Figure I.2.

This figure shows the variation of G according to the position x. G_I represents the average free energy of an atom in the initial configuration, and G_F corresponds to the end of the transformation. $\Delta G = (G_F - G_I)$ is negative and serves as the driving force of the transformation.

Any atom with a maximum free energy G^*_A is unstable because it can either return to its initial state or progress towards a final state by reducing its free energy. The configuration associated with this peak in the free energy curve is typically referred to as the transient state, transition state, or activated state.

It is evident that a necessary condition for an atom to participate in the reaction is that it possesses sufficient free energy to reach the transient state, i.e., its free energy is at least equal to:

$$G_A = (G^*_A - G_I) \qquad \text{(I-2)}$$

G_A is known as the activation free energy for the reaction.

The additional free energy required for an atom to overcome the thermodynamic barrier of transformation is provided by fluctuations. The distribution of energy among a set of particles is non-uniform. At any temperature above 0°K, particles are in motion, and collisions resulting from this random motion lead to wide variations in the energy of individual particles over time. Consequently, at any given moment, the system exhibits a broad energy spectrum, with some particles having energy equal to or greater than G_A^* undergoing the transformation. Particles lacking sufficient energy must wait until they receive the necessary activation energy from thermal fluctuations. This phenomenon is known as *thermal activation*.

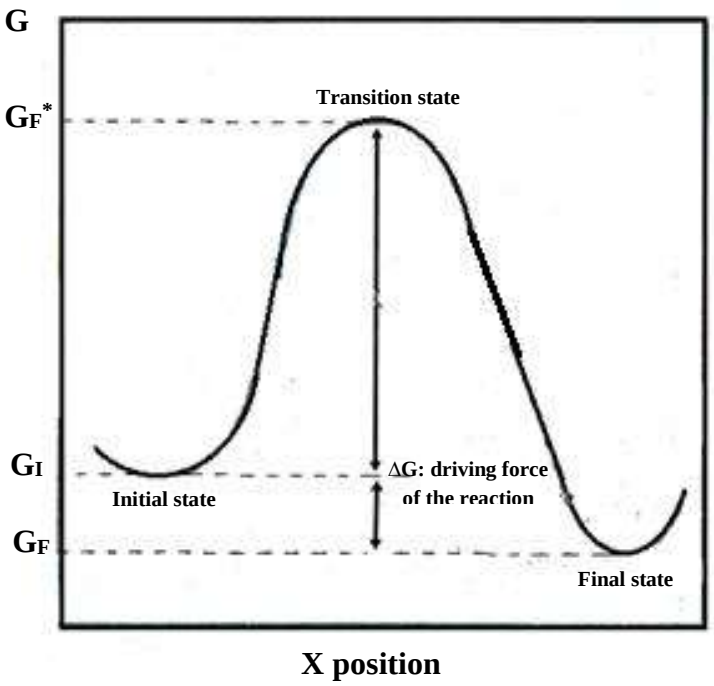

Fig. I-2- : Schematic variation of Gibbs free energy

I-4. Internal activation energy

Activation energy is the energy required by reactants to transition to another phase. On the other hand, the concept of an activated state naturally emerges from the equilibrium definition using G; it is often more convenient to study the thermodynamics of this state using an internal activation energy E_A and an activation entropy S_A. E_A and S_A are related by the following relationship:

$$G_A = E_A - TS_A \qquad \text{(I-3)}$$

The activation energy E_A is defined as the difference between the internal energy of an atom in the activated state and that of an atom in the initial state. The activation energy of a group of atoms can be subdivided into two parts:

a) The potential interaction energy of the atoms associated with the binding forces,

b) The kinetic energy due to the thermal vibrations of the particles.

Firstly, consider the interaction energy; equilibrium compels atoms to adopt positions of minimal potential energy in both the initial and final configurations. Thus, the potential energy of an atom during the transformation must evolve according to a curve akin to that shown in Figure I.2. However, a crucial distinction exists: E_F can be smaller or larger than E_I, while G_F is always less than G_I. If ΔE is positive, the reaction is endothermic; if ΔE is negative, it is exothermic. The potential energy of the transition state relative to that of the initial state is E_A[1].

As temperature increases, thermal energy causes all particles, including atoms, to exist at higher energy levels. At any given temperature, each atom within the system does not occupy the same energy level. Thermal fluctuations result in atoms distributing themselves among the available energy levels.

The activation energy value can assist us in estimating the relative rate of a reaction. A high activation energy value suggests a slow reaction because few reactants possess sufficient kinetic energy to surmount the barrier and produce new products. In contrast, a low activation energy value indicates a fast reaction.

I-5. Distribution of kinetic energy

Statistics help to determining the most probable distribution of energy among the particles of a system. This distribution corresponds to the greatest number of possible arrangements because it can be achieved through the most numerous pathways. According to this hypothesis, calculations show that the fraction of atoms with thermal energy equal to or greater than a given value E_A at temperature T is:

$$\frac{n}{N} = \exp\left(-\frac{E_A}{K_B T}\right) \qquad \text{(I-4)}$$

Where K_B is the Boltzmann constant.

For an atom to transition from one phase to another, it must possess thermal or kinetic energy at least equal to the activation energy E_A.

We can then seek the expression for the rate of the single process, which constitutes the transition of an atom from the α structure to the γ structure (as in the case of iron), that is, the fraction of the total number of atoms reaching the final configuration per unit time dy/dt. Indeed, it is proportional to:

- The vibration frequency ν, which is assumed to be the same for all atoms, signifies that each atom encounters conditions conducive to undergoing the transition ν times per second.
- The probability that an atom has thermal energy at least equal to E_A during each vibration, that is:

$$P = \exp\left(-\frac{E_A}{K_B T}\right) \quad \text{(I-5)}$$

- The probability p that, when an atom has sufficient energy, it meets the geometric conditions required for the transformation. For example, in the case of iron, p will vary from 1/8 to 1/12 (because in the BCC and FCC systems, the number of neighboring sites of a given atom is 8 and 12, respectively). So:

$$\frac{dy}{dt} = pv\ exp\left(-\frac{E_A}{K_B T}\right) \quad \text{(I-6)}$$

I-6. Study of the reaction kinetics

Isoconversional analysis methods rely on accurately calculating the evolution of the activation energy E_A from kinetic data. Various linear integral methods proposed in the literature include:

❖ KISSINGER-AKAHIRA-SUNOSE (KSA) method

This method allows the estimation of E_A for a system from the following relation:

$$ln\frac{\beta}{T_p^2} = -\frac{E_A}{RT_p} + C \quad \text{(I-7)}$$

❖ BOSWELL method

It is based on the following linear expression, which enables the calculation of E_A across a series of temperature-scanning experiments:

$$ln\frac{\beta}{T_p} = -\frac{E_A}{RT} + C \quad \text{(I-8)}$$

❖ **STARINK method**

The method provides the following equation (I-9). According to Starink, the latter is significantly more efficient and yields better results compared to other linear integral methods.

$$ln\frac{\beta}{T_p^{1.92}} = -1.0008\frac{E_A}{RT} + C \qquad \text{(I-9)}$$

In the three methods:

C : constant which depends on the step of the reaction according to the kinetic model,

β: is the rate of heating,

Tp : the temperature of the maximum of the peaks

R = 8.314 J.mole^{-1} is the constant ideal gases.

Practice exercise

We consider an iron-based alloy with the addition of 9% at. Cr. The alloy is homogenized at 1000°C for 1 hour then water quenched. We want to determine the activation energy of the ordering process of the ordered phase Fe_3Al of $D0_3$ structure during heating of this alloy (the formation of Fe_3Al).

Figure 1 shows the differential scanning calorimetric analysis (DSC) test curves obtained with different heating rates. These curves show an exothermic peak around 300° C. which is linked to the formation of the ordered phase of $D0_3$ structure.

1. Based on the Starink method, give the variation curve of the straight line Y as a function of (1000 / Tm) for this alloy.
2. Deduce the activation energy value of of the ordered phase of $D0_3$ structure formed in this alloy.

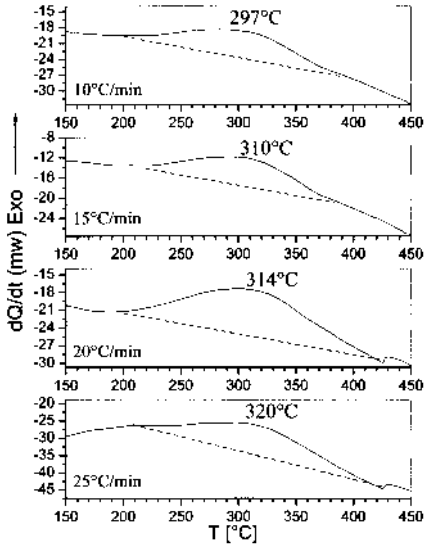

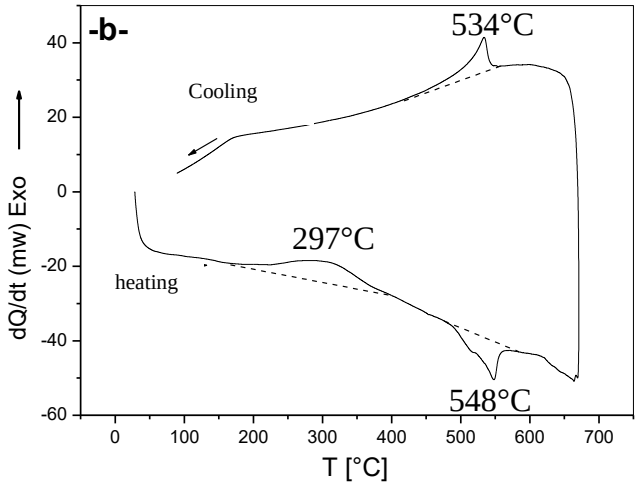

DSC curve of Fe- 25% at. Al- 9% at. Cr studied alloy obtained with a heating rate of 10°C/min

Figure 1

Answers

1- According to Starink equation (see course)

$$ln\frac{\beta}{T_p^{1.92}} = -1.0008\frac{E_A}{RT} + C$$

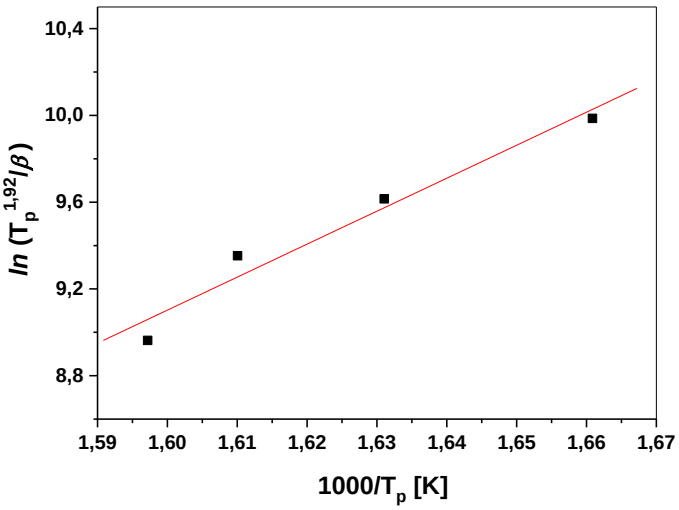

The slope of the line = 9.188

$E_{act} = \frac{9.188*1000R}{1.0008}$ = 18.22 Kcal/mol = 0.79 eV

Chapter

II

Crystal growth and solidification

II-1. Introduction

The properties of metallic materials, whether in a pure state or as a mixture of two or more elements, depend on the phase transformations they undergo. The majority of phase transformations that occur in materials are accompanied by a change in the number of phases present.

Depending on the types of phases present in the system under consideration, we distinguish between two main categories: transformation from the liquid phase to the solid phase, and transformation from one solid phase to another. In this chapter, we will study the first category of these transformations (liquid ↔ solid), specifically focusing on the phenomenon of solidification.

Solidification is defined as the transition of material from the liquid phase to the solid phase. In metallic alloys, this phase change leads to significant alterations in mechanical, physical, and chemical properties. The study of this phase transformation in metals has continued for several decades to enhance understanding of solidification principles.

The structures formed after solidification influence the mechanical properties of castings and partially determine the type of treatment required to achieve desired properties. Specifically, the size and shape of grains depend on solidification conditions.

II-2. Liquid state and solid state

In the crystalline solid state, at the atomic scale, atoms are considered to have well-defined average positions held together by cohesive forces, arranged in a motif (unit cell). Moreover, the structure of solids typically includes a significant number of defects such as vacancies, dislocations, and stacking faults, etc...

Crystalline materials exist in either monocrystalline or polycrystalline forms. Commonly used metallic materials typically have a polycrystalline structure composed of numerous microcrystals (grains) interconnected by less ordered regions known as grain boundaries. Each grain in a metallic material is a single crystal. Decreasing the grain size leads to an increase in material strength at room temperature.

In the liquid state, atoms no longer have well-defined positions. The first neighboring atoms of a given atom occupy positions close to those they occupy in a crystal, while the positions of second and third neighbors are less well-defined, and beyond that, order does not

exist. This partially disordered arrangement results from the existence of empty spaces between groups of atoms or molecules. It is the mobility of these empty spaces that gives liquids their fluidity.

The key fact is the sudden change in certain physical characteristics when transitioning between different physical states.

- Liquids are generally less dense (except for certain elements: Bi, Ge, Ga, Si, water, and cast iron). This results in a volume loss or shrinkage during solidification (e.g., copper experiences a 4.8% shrinkage).
- Atom mobility (diffusivity) is greater in liquids (self-diffusion and chemical diffusion of alloying elements and impurities are slower in solids compared to liquids).

II-3. Solid/liquid interface

The solid-liquid interface is the intermediate zone between the last atoms constituting the solid and the atoms of the liquid phase, with a thickness typically only a few atoms of the material. Once the solid phase nucleus forms, its growth continues and is limited by:

- The kinetics of atom attachment at the solid-liquid interface,
- Heat diffusion from atoms in both the solid and liquid phases. The significance of each of these factors depends on the substance under study and the conditions of solidification.

In general, creating an interface is a process that requires energy and is thermodynamically unfavorable. The presence of interfaces increases the free energy of a material. Similar to phase boundaries, grain boundaries represent a specific type of interface as they delineate the boundary between two crystalline grains of the same composition and structure but different orientations. Fine-grain systems, characterized by numerous interfaces, possess higher free energy compared to coarse-grained systems.

From a thermodynamic standpoint, an interface is characterized by its specific interfacial energy, denoted as γ. This energy is independent of the interface area and can be determined by measuring the work required to create a unit area of the interface.

❖ Interfacial structures

The solid-liquid interface can assume various growth forms (flat, cellular, or dendritic) depending on the cooling conditions (solidification). Among the parameters controlling the morphology of the solid-liquid interface are the temperature gradient in the liquid and the growth rate of the nuclei.

At low solidification rates, with a fixed temperature gradient in the liquid, the solid-liquid interface remains flat. Achieving this ideal growth state is practically challenging because heat exchange between the molten material and the sample creates a temperature gradient in the liquid region. The planar interface becomes unstable beyond a critical value of the growth rate or temperature gradient.

However, if the growth rate is increased beyond a critical value Vc, and the temperature gradient is reduced, the solid-liquid interface becomes unstable. This instability leads to the formation of a cellular morphology, where the spacing λ typically ranges from tens to hundreds of micrometers. At even higher growth rates, this cellular structure can transform into a dendritic form. These different cases are illustrated in Figure II-1.

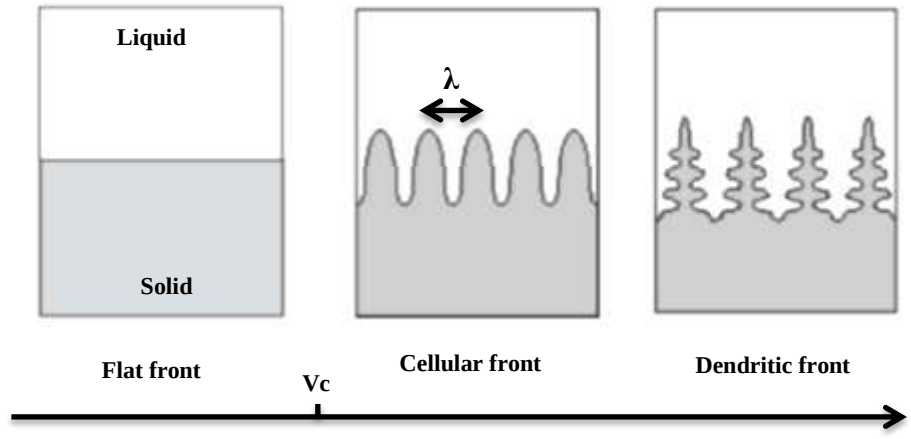

Fig. II-1- : Schematic representation of the different morphologies of the solid-liquid interface.

Solidification occurs in two stages: nucleation and growth. Nucleation is the stage where many small solid particles (nuclei) form from the liquid. Each of these solid nuclei must reach a certain critical size to remain stable. Growth then occurs as the solid nuclei increase in size at the expense of the surrounding liquid until the liquid phase is completely consumed.

II-3-1. Nucleation

There are two types of nucleation: homogeneous nucleation, where solid nuclei form within the liquid without contact with walls or impurities, and heterogeneous nucleation, where nuclei form on foreign particles submerged in the liquid or on the cold walls of the mold.

II-3-1-1. Homogeneous nucleation

Some nuclei can form within the liquid without any solid support (such as mold walls or inclusions). These nuclei are called homogeneous nuclei, and their formation requires very high supercooling, typically around 20% of the melting temperature (T_f).

a. Latent heat and volume free energy

The change in free energy per unit volume (ΔG) that accompanies solidification of a pure substance A can be expressed as:

$$\Delta G_v = G_v^s - G_v^l = \Delta H - T\Delta S \qquad \text{(II-1)}$$

where:

- G_v^l is the free energy per unit volume in the liquid state,
- G_v^s is the free energy per unit volume in the solid state.
- H and S are respectively the enthalpy and the entropy per unit volume of A at the considered temperature.

This expression represents the difference in free energy per unit volume between the liquid state G_v^l and the solid state G_v^s of substance A during solidification.

For a pure metal, the transformation from liquid to solid occurs at a specific temperature characteristic of the metal. This temperature is where the free energies of the solid (G_v^s) and liquid (G_v^l) phases are equal: $G_v^s = G_v^l$. The latent heat (L) is defined as the amount of heat released during solidification or absorbed during fusion, where $L = \Delta H$.

Now studying the variations of free energy per unit volume as a function of temperature for this material:

- At $T=T_F$, the two phases, liquid and solid, coexist in equilibrium, with their free energies being equal: $G_v^s = G_v^l$.
- For $T>T_F$, the liquid phase is stable, so $G_v^l < G_v^s$.
- For $T<T_F$, the solid phase is stable, so $G_v^s < G_v^l$.

In summary, T_F represents the temperature at which the solid and liquid phases of the material are in equilibrium, and the stability of each phase relative to the other depends on whether the temperature is above or below T_F.

Figure II-2 schematically represents the evolution of the free energy per unit volume (G_v) of the metal as a function of temperature. This observation can be generalized to any phase transformation: the phase with the lowest free energy is the most stable, or equivalently, the phase whose formation reduces the free energy of the system.

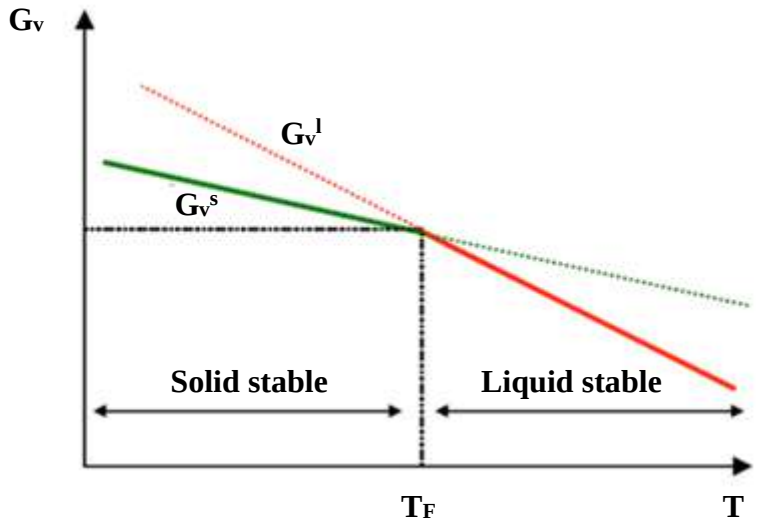

Fig. II-2- : Variations of free energy per unit volume as a function of temperature.

Consider the solidification of a pure metal initially maintained at a temperature above its melting point to keep it in the liquid state. The metal is then cooled to a temperature T well below its melting point. For solidification to occur, ΔG_v must be less than zero ($\Delta G_v<0$).

This clarifies that solidification will only occur when the Gibbs free energy change per unit volume (ΔG_v) is negative, indicating that the solid phase is more stable than the liquid phase under the given conditions.

At a temperature T different from T_F (where $T \leq T_F$), $\Delta G_v = 0$ and $\Delta H = -L$ (the minus sign indicates the release of latent heat of solidification):

$$\Delta G_v = 0 \quad \text{(II-2)}$$

$$G_v^s - G_v^l = 0 \quad \text{(II-3)}$$

$$H_v^s - T_F S_v^s = H_v^l - T_F S_v^l \quad \text{(II-4)}$$

$$H_v^s - H_v^l = T_F S_v^s - T_F S_v^l \quad \text{(II-5)}$$

$-L = T_F \Delta S$ which give: $\Delta S = \frac{\Delta H}{T_F} = -\frac{L}{T_F}$

If the temperature T differs from T_F, the change in free energy ΔG_v is not zero, and it can be evaluated assuming that ΔH and ΔS are not significantly affected by temperature.

$$\Delta G_v = \Delta H - T\Delta S \quad \text{(II-6)}$$

Where:

$$\Delta G_v = (-L) - T\left(\frac{-L}{T_F}\right) = -L\frac{T_F - T}{T_F} \quad \text{(II-7)}$$

For solidification to occur ($\Delta G_v < 0$), the term ($T_F - T$) must be positive, indicating $T_F > T$. The difference ($T_F - T$) is referred to as *supercooling*.

The minus sign in the ΔG_v relation indicates that the liquid → solid transformation occurs with a decrease in the free energy of the system, because at $T < T_F$, $G_v^s < G_v^l$. This decrease in free energy is proportional to the volume of the nucleus (germ):

$$\Delta G_1 = \Delta G_v * V \quad \text{(II-8)}$$

b. Supercooling and surface energy

During cooling under equilibrium conditions (i.e., at very low rates), the thermal analysis curve T=f(t) typically resembles that shown in Figure II-3-(a): the isothermal plateau indicates solidification occurring at a constant temperature for the pure metal. However, under usual cooling conditions in industrial settings, it is observed that the liquid phase does not immediately solidify just below the equilibrium temperature T_F.

In practice, the thermal analysis curve obtained resembles that shown in Figure II-3-(b). Solidification initiates at a temperature T_B significantly lower than T_F, requiring an 'undercooling' ΔT, also known as supercooling (portion AB of the curve). Once the first nuclei (germs) form, the release of latent heat causes a temperature increase (portion BC of the curve).

In the case of an alloy (solid solution), the thermal analysis curve corresponds to that shown in Figure II-3-(c), where one can determine the starting temperature of solidification, T_s , by extrapolation. Supercooling reflects a delay in solidification. This delay is explained by the formation of an interface between the solid nuclei and the liquid. This interface consumes an amount of energy ΔG_s per unit area of interface created ($\Delta G_s>0$, indicating that interface formation is an endothermic process). The presence of nuclei increases the free energy of the system by an amount ΔG_2 proportional to the surface area of the nuclei, where:

$$\Delta G_2 = \Delta G_s * S \qquad \text{(II-9)}$$

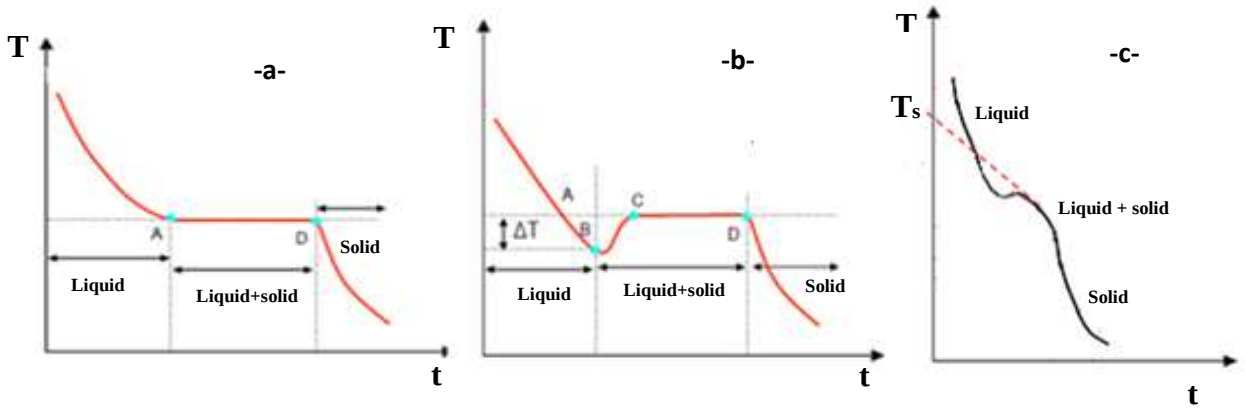

Fig. II-3- : Cooling curves for:
(a) a pure metal without supercooling,
(b) a pure metal with supercooling,
(c) a supercooled binary alloy.

c. Free energy of nucleus formation

Consider an initial volume of liquid undergoing solidification. When a solid nucleus forms with volume V and surface area S, the total change in free energy of nucleus formation (ΔG_g^f) is the sum of two components: the free energy related to volume and the free energy related to surface area:

$$\Delta G_g^f = \Delta G_1 + \Delta G_2 \qquad \text{(II-10)}$$

The formation of this nucleus will only be possible if $\Delta G_g^f < 0$. The first term, being negative, drives the solidification process, while the second term, being positive, opposes it. The most probable shape of the nucleus will therefore correspond to minimizing surface energy consumption (minimum surface area) and maximizing volume energy release (maximum volume). The spherical shape satisfies this condition (see Figure II-4).

Suppose, therefore, that the nucleus is spherical in shape with radius r. We then have:

$$\Delta G_g^f = \Delta G_1 + \Delta G_2 \quad \text{(II-111)}$$

$$\Delta G_g^f = \Delta G_v * V + \Delta G_s * S \quad \text{(II-12)}$$

$$\Delta G_g^f = \Delta G_v * (4/3\ \pi\ r^3) + \gamma_{s\text{-}l} * (4\pi r^2) \quad \text{(II-13)}$$

So, the total change in free energy of nucleus formation (ΔG_g^f) is:

$$\Delta G_g^f = -\frac{4}{3}\frac{\pi L \Delta T}{T_F} r^3 + 4\pi\gamma r^2 \quad \text{(II-14)}$$

Where: L, T_F, γ (the specific interface energy) are constants which depend only on the nature of the metal.

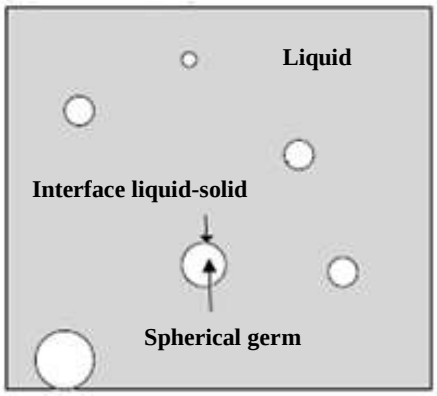

Fig. II-4- : Formation of the spherical solid nucleus

The free energy of nucleus formation then depends on two parameters: one is experimental, the temperature T or the supercooling ΔT, and the other is the size of the nucleus. Let us fix the temperature, hence the supercooling $\Delta T = T_F - T$, and examine the evolution of the free energy of formation as a function of the nucleus size (see Figure II-5).

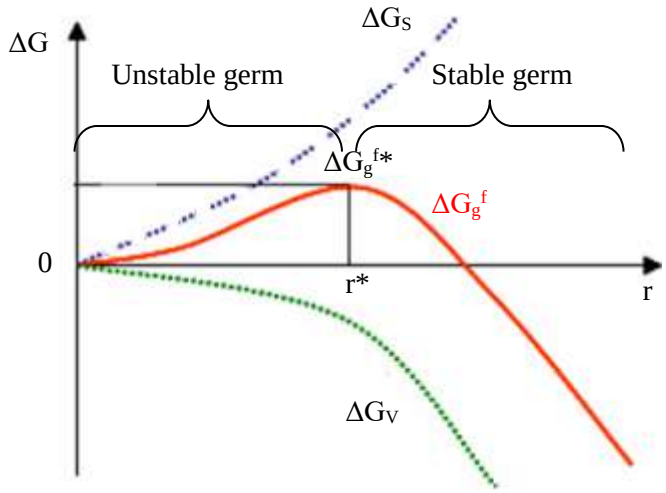

Fig. II-5- : Free energy variation curves as a function of nucleus size.

❖ **Influence of germ size**

As the size of the nuclei increases, the free energy first increases before reaching a maximum ΔG_g^{f*} at a critical size r = r*, then decreases for larger values of r. The critical size r* can be determined by setting the derivative of ΔG_g^f equal to zero at r*:

$$\frac{d\Delta G_g^f}{dr} = 0 \qquad \text{(II-15)}$$

$$-\Delta G_v\, 4\pi\, r^2 + \gamma_{s\text{-}l}\, 8\pi r = 0 \qquad \text{(II-16)}$$

$$r^* = \frac{2\gamma T_F}{L\Delta T} \qquad \text{(II-17)}$$

The critical value of the free energy is:

$$\Delta G_g^{f*} = \frac{16\pi\gamma^3 T_F^2}{3L^2\Delta T^2} \qquad \text{(II-18)}$$

ΔG_g^{f*} is the potential barrier that a nucleus must overcome to reach the critical size r*.

Figure II-6 shows that only nuclei that have reached a critical size can be stable. Indeed, the growth of a nucleus larger than r* (for example, a nucleus with radius $r=r_3$ becoming a nucleus with radius $r=r_4$) leads to a decrease in free energy:

$$\Delta G_g^{f}{}_{3\to4} = \Delta G_g^{f}{}_4 - \Delta G_g^{f}{}_3 \qquad \text{(II-19)}$$

As $\Delta G_g^{f}{}_4 < \Delta G_g^{f}{}_3$, we will therefore have $\Delta G_g^{f}{}_3 \rightarrow 4 < 0$.

On the other hand, the growth of a nucleus smaller than the critical size (for example, a nucleus with radius $r=r_1$ becoming a nucleus with radius $r=r_2$) implies an increase in free energy:

$$\Delta G_g^{f}{}_{1\rightarrow 2} = \Delta G_g^{f}{}_2 - \Delta G_g^{f}{}_1 > 0 \qquad \text{(II-20)}$$

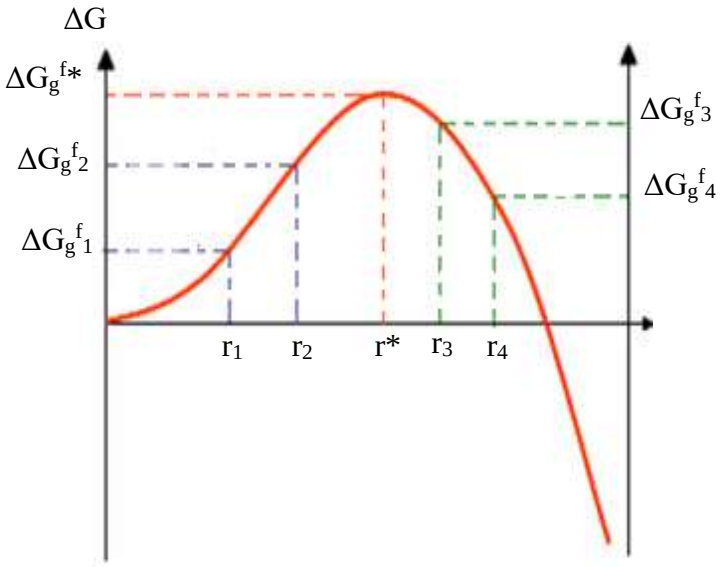

Fig. II-6- : The variation of the free energy of nucleus formation according to its radius r shows the stability domain of the nucleus.

❖ **Influence of temperature**

The influence of temperature can be deduced from the previous relations; that is, the potential barrier decreases when the supercooling ΔT increases (up to moderate values), and the same applies for r^* (the critical size and the energy barrier are lower as the supercooling increases). This means that increasing supercooling allows smaller nuclei to stabilize. In other words, the number of stable nuclei increases, and solidification is favored when supercooling is high.

II-3-1-2. Heterogeneous nucleation

In practice, there are supports that provide a surface on which the metal can solidify. These supports consist of either insoluble impurities (see Fig. II-7) or the walls of the mold or crucible. Under these conditions, a nucleus with a radius of curvature greater than the critical

radius forms with a minimal liquid-solid surface area. Moreover, the number of atoms required to form a nucleus of critical size is much smaller compared to that of a homogeneous nucleus.

The nucleus assumes the shape of *a spherical cap* with radius r. Various contact surfaces contribute with their interface energies: γ_{gl} (the interface energy between the liquid and the nucleus), γ_{gs} (the interface energy between the nucleus and the support), γ_{sl} (the interface energy between the support and the liquid).

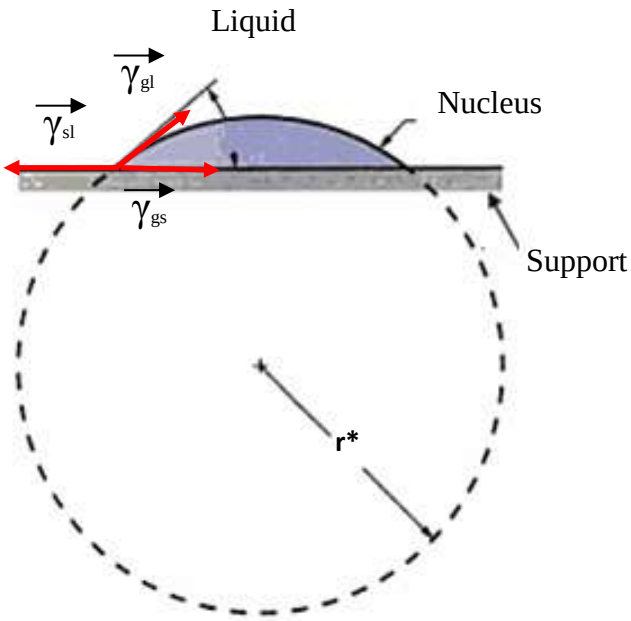

Fig. II-7- : Heterogeneous nucleation on a solid support.

Let θ be the contact angle between the support and the nucleus: this angle measures the tendency of the solid nucleus to spread more or less on the support. The stability of the nucleus-support-liquid system requires a relationship between the surface energies, namely:

$$\vec{\gamma}_{sl} + \vec{\gamma}_{gl} + \vec{\gamma}_{gs} = 0 \qquad \text{(II-21)}$$

By projection on the axis of the support:

$$\gamma_{sl} = \gamma_{gl} \cos\theta + \gamma_{gs} \qquad \text{(II-22)}$$

In this case, the total change in free energy of nucleus formation (ΔG_g^f) is:

$$\Delta G_{het} = \Delta G_{hom}\, f(\theta) \qquad \text{(II-23)}$$

Where:

$$f(\theta) = \frac{(2+\cos\theta)(1-\cos\theta)^2}{4} \quad \text{(II-24)}$$

II-3-1-3. Nucleation rate

In the liquid, there are nuclei of all sizes. Each nucleus size corresponds to a critical formation energy ΔG_g^{f*}. We can then evaluate the number of nuclei (n*) of critical size (r*) by the following relationship:

$$n^* = N.exp\left(-\frac{\Delta G_g^{f*}}{KT}\right) \quad \text{(II-25)}$$

Where N is the total number of atoms in the system.

It is observed that the number of nuclei reaching the critical size increases with the degree of supercooling. However, nuclei of critical size become stable only if they capture additional atoms. This condition depends on the ability of these atoms to diffuse toward the nucleus. This phenomenon involves an activation energy for diffusion in the liquid, ΔG_d (the potential barrier that must be overcome for an atom to attach itself to the growing nucleus). We can introduce the concept of nucleation rate, which can be expressed by the following relationship:

$$V_G = C.exp\left[-\frac{\left(\Delta G_g^{f*}+\Delta G_d\right)}{KT}\right] germ.m^{-3}.s^{-1} \quad \text{(II-26)}$$

In the case of homogeneous nucleation, a simplified calculation allows us to establish that the nucleation rate strongly depends on supercooling (ΔG_g^{f*} depends on ΔT). Figure II-8 shows the evolution of the nucleation rate as a function of temperature. We observe that:

- The nucleation rate is zero when:
- $T=T_F$: Few nuclei reach the critical size at this temperature.
- The supercooling is very high: The temperature is then too low, which greatly slows down the diffusion of the species and makes it difficult for the atoms of the liquid to reach the nucleus to enhance its stability.

- The nucleation rate is higher for moderate supercoolings, which allows for the presence of a large number of critical nuclei and facilitates their subsequent growth due to reasonable diffusion.

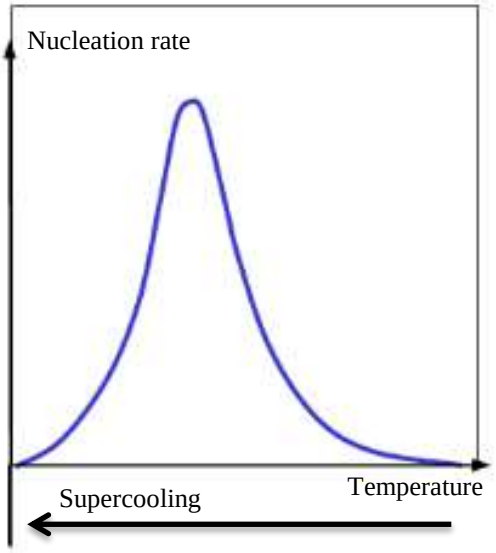

Fig. II-8- : Influence of supercooling on the nucleation rate.

The heterogeneous nucleation rate can be expressed similarly, but in this case:

$$\Delta G_g^{f*}{}_{het} = \Delta G_g^{f*}{}_{hom}\, f(\theta) \qquad \text{(II-27)}$$

II-3-2. Growth

As soon as a stable nucleus is formed, its growth begins with the addition of atoms to its surface. This growth is determined by the rate at which atoms arrive at the interface and by their ability to adhere to it. In other words, the growth rate of the solid depends on the diffusion coefficient of the atoms and the structure of the interface.

At the atomic scale, the growth of the nucleus is controlled by the ability of its surface to capture new atoms. Growth is therefore favored by an irregular surface containing sites on which atoms can easily attach themselves (vacancies...).

III-3-2-1. Growth of the solid in the case of pure metal

For a pure metal, once the initial nuclei are formed, growth continues through their development. These nuclei assume a regular geometric form during their growth. However, when they come into contact with other nuclei during growth, their regular form is disrupted, and the initial crystals become irregular, forming what are known as grains.

If the cooling of the pure metal is very slow (under equilibrium conditions), as a layer of solid forms, the thickness of the solidified layer increases as heat diffuses outward. It is at the

interface where the release of latent heat occurs and where a discontinuity in thermal gradients is established between the liquid and the solid. At this stage, growth occurs with a flat front.

The heat balance is based on the continuity of the heat fluxes at the solid/liquid interface; we can write:

$$Q_S = Q_L + Q^* \quad \text{(II-28)}$$

Where Q_S: is the quantity of heat that the solid can extract,

Q_L: heat evacuated by the liquid,

Q^*: latent heat of solidification

We define:

$$Q_S = J_S.A.dt \quad \text{(II-29)}$$

$$Q_L = J_L.A.dt \quad \text{(II-30)}$$

$$Q^* = -L.A\ .dx \quad \text{(II-31)}$$

L is the latent heat of solidification per unit volume, released (hence the sign -). J_S and J_L are the heat fluxes in the solid and the liquid, respectively. A is the interface area which advances with a speed dx/dt.

The thickness of the solid increases by an infinitesimal quantity dx during dt, and according to Fourier's law which expresses the heat fluxes as a function of the thermal conductivities (K_S and K_L) and the temperature gradients (T'_S and T'_L):

$$J = -KG \quad \text{(II-32)}$$

$$J_S.A.dt = J_L.A.dt - L.A\ .dx \quad \text{(II-33)}$$

$$-K_S T'_S\, dt = -K_L T'_L dt - L\, dx \quad \text{(II-34)}$$

Which gives the solidification rate as follows:

$$V_s = \frac{(K_s T'_S - k_L T'_L)}{L} \quad \text{(II-35)}$$

In reality, this front is subject to disturbances that result in the presence of a protuberance (an advanced part of the solid) ahead of the interface (see Figure II-9).

The solid/liquid interface is at the melting temperature T_F, while the liquid has a higher temperature as one moves away from this interface.

Heat tends to concentrate on the protuberance that develops at the interface. This results in a local increase in the temperature gradient, T'_L, which slows down the solidification rate. The protrusion's growth is then halted until the remainder of the interface has advanced to catch up. This mechanism is known as *planar growth*, which happens as a smooth interface progressively advances through the liquid.

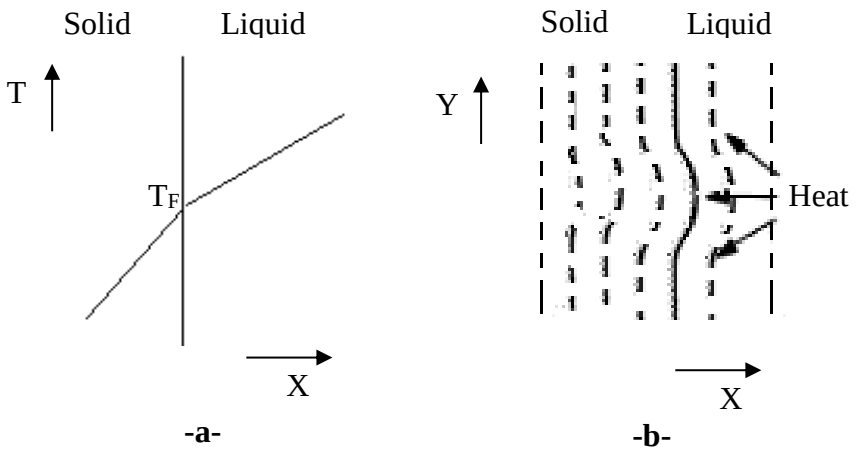

Fig. II-9- : Mechanism of protrusion development at the solid/liquid interface, with the liquid at a higher temperature than the solid:
(a) Temperature distribution curve
(b) Formation of a protrusion.

- If a pure metal cools rapidly, the liquid near the interface can reach a temperature lower than T_F before many nuclei form. In these circumstances, a solid protrusion that forms ahead of the interface will immediately find itself in a region of supercooling. This leads to an exaggerated growth of the protrusion ahead of the interface.

The latent heat of solidification L initially flows towards the supercooled liquid, causing its temperature to increase. Secondary and tertiary branches then form on the primary trunk (this assembly of trunk + branches is called a dendrite) to accelerate the removal of the latent heat of solidification (Fig. II-10). In the solidification of pure metals, these dendrites are referred to as thermal dendrites to distinguish them from dendrites formed in alloys.

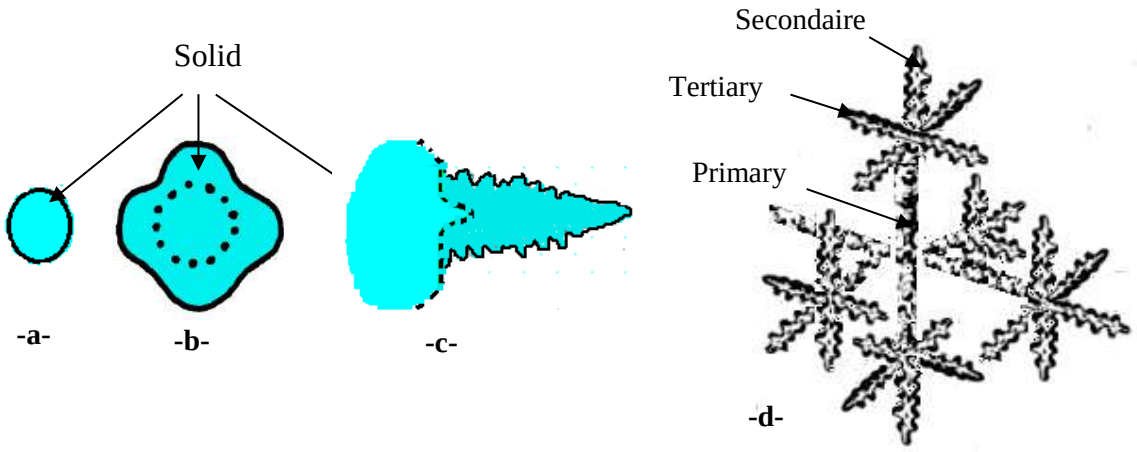

Fig. II-10- : Mechanisms of dendrite development: (a) spherical germ crystal, (b) development of protuberance on the crystal surface, (c) first stage of dendrite formation; (d) developing dendrite.

Fig. II-11 shows a dendrite during growth more clearly. The size of dendrites is typically characterized by the distance between the axes of the secondary branches, denoted as λ. This distance is smaller when the liquid solidifies more rapidly.

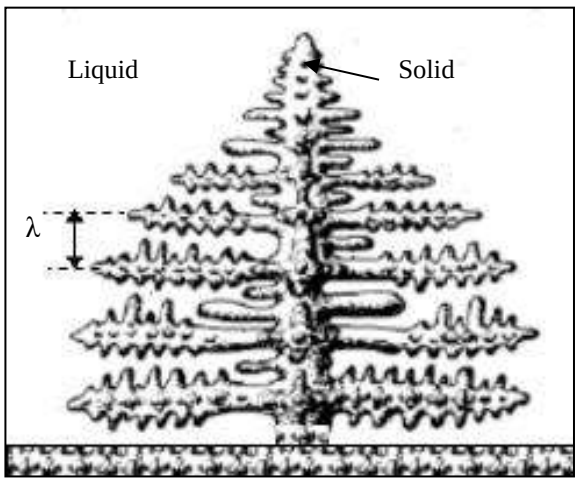

Fig. II-11-: Dendrite during growth.

III-3-2-2. Solidification Process in Alloys

In practice, the solidification of pure solids is rare because pure metals typically contain impurities that alter their solidification characteristics, effectively transforming them into alloys. Therefore, solidification of alloys is more commonly encountered in industry.

What we have just described for a pure metal also applies to alloys: before solidification begins, there must be nucleation. Solidification must also involve simultaneous redistribution of solute between the solid and the liquid.

A- Case of a single-phase alloy

❖ Solidification of a single-phase alloy under equilibrium conditions

Consider an alloy A-B with a nominal composition C_0 of element B (Fig. II-12-a). Under equilibrium conditions, cooling a liquid alloy of composition C_0 from temperature T′ results in progressive solidification within the temperature interval between T_0 and T_f . At a specific temperature T, the solid phase formed has composition C_s, while the remaining liquid phase has composition C_L. Once solidification is complete, the cooled alloy is homogeneous, and its composition throughout is C_0.

At a given temperature within the solidification interval, there is coexistence of both liquid and solid phases, with their masses following the law of conservation. This occurs under the assumption that the solid phase forming has sufficient time to continuously homogenize through the diffusion of alloying elements in the solid state.

❖ Solidification of a single-phase alloy under non-equilibrium conditions

In practice, the cooling rates used (such as cooling in air outside the furnace) are high, and diffusion in the solid state remains extremely limited. However, diffusion is always possible in the residual liquid that has not yet solidified. These factors mean that the composition of the solid and the liquid does not evolve as described in the equilibrium diagram.

We consider the binary alloy A-B with composition C_0 (Fig. II-12-a). If this alloy is cooled under equilibrium conditions (i.e., with a very slow cooling rate) as described in the previous paragraph, the point representing the overall composition of the solid follows the solidus curve from S_0 to S_f. In this scenario, the time required for the solid composition to become uniformly continuous through solute diffusion would be extensive.

Due to the slow diffusion in the solid state (when the alloy is cooled at a rate such that diffusion is negligible in the solid phase but still possible in the remaining liquid), the actual situation often resembles the following:

- The initial nuclei deposited at T_0 have a composition close to their equilibrium composition C_{S0}.
- During cooling, these nuclei maintain a composition closer to their initial values rather than reaching equilibrium values, i.e., richer in A (point B in Fig. II-12-a).

As a result, the overall composition of the solid is positioned in Fig. II-12-a- to the left of the ideal solidus line. Solute B is rejected from the centers of the solid grains towards their boundaries (grain boundaries). This heterogeneity in composition is known as *minor segregation*: the clustering of solute atoms along the grain boundaries of a material.

Solidification therefore ends at a temperature $T_{f'}$, which is below the steady-state solidification temperature T_f.

From a microstructural perspective, the initial nuclei formed at temperature T_0 with concentration C_{S0} exhibit a dendritic morphology (Fig. II-12-b). As temperature decreases, solidification progresses along the dendrite branches, forming lines that represent surfaces of equal concentration, with each line corresponding to a different concentration (Fig. II-12-b). The solidification interval expands from T_0 to T_f , rather than from T_0 to $T_{f'}$.

This phenomenon can be observed in alloys with a eutectic point. The shift in the solidus can cause the eutectic phase to appear at the grain boundaries (Fig. II-13) for compositions that theoretically lie outside the eutectic range. This results in the unexpected appearance of a phase with a lower melting point, posing a risk of local melting under conditions of use that were initially considered safe (melting at the grain boundary leading to material failure).

We also distinguish segregation on the scale of the piece, known as major segregation: during the solidification of a metal part, the center solidifies last and is therefore richer in solute compared to zones that solidified first.

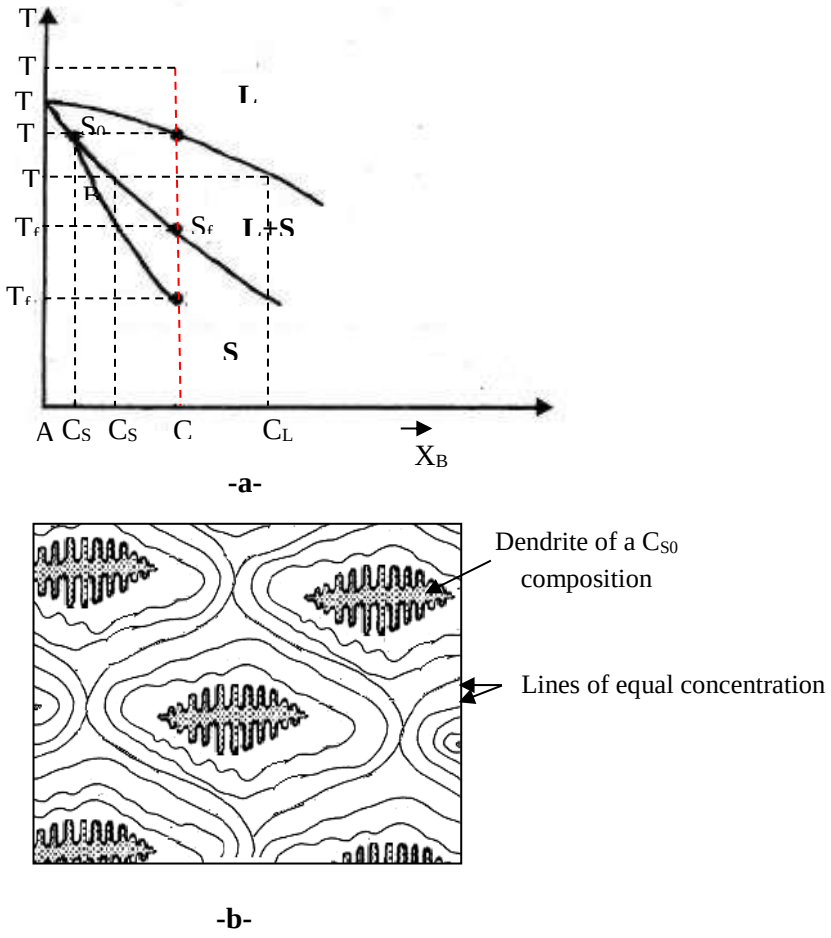

Fig. II-12-: Illustration of minor segregation:

(a) Portion of the phase diagram illustrating deviations from equilibrium during the solidification of a single-phase binary alloy.

(b) Lines of equal concentration in a single-phase alloy exhibiting minor segregation.

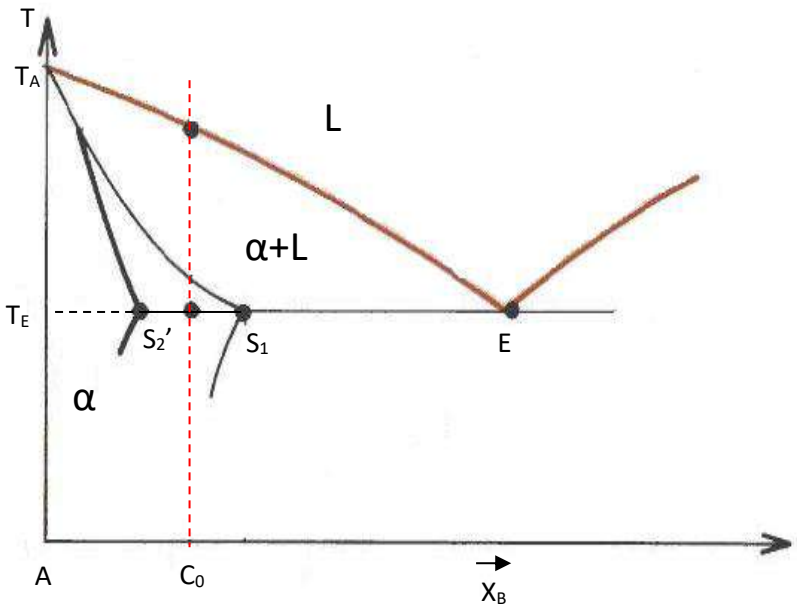

Fig. II-13- : Part of the Phase Diagram with Eutectic Point: Illustration of Deviations from Equilibrium during Solidification of a Binary Alloy.

B- Case of a two-phase alloy:

❖ **Eutectic growth:**

Eutectic growth involves the cooperative growth of two solid phases of different compositions from a single homogeneous liquid phase. During eutectic growth, there is an accumulation of species B in the liquid in front of one phase and species A in front of the other phase (Fig. II-14).

The redistribution of solute in the liquid destabilizes the planar interface during the growth of a single-phase solid and promotes the proximity of solid phases during eutectic growth. Various eutectic microstructures have been observed and are classified as regular (in lamellar or rod forms) and irregular (Fig. II-15).

If, during coupled growth, the two solid phases are characterized by isotropic interfacial energy, the eutectic lamellae grow parallel to the heat flow. This results in a regular structure of the eutectic after solidification. The lamellar structure of eutectics can be described as the periodic and alternating stacking of parallel ribbons of the two phases.

In some alloys, irregular structures are observed where the lamellae or fibers are not evenly spaced. In these eutectics, the interlamellar spacings are disorderly and vary significantly throughout.

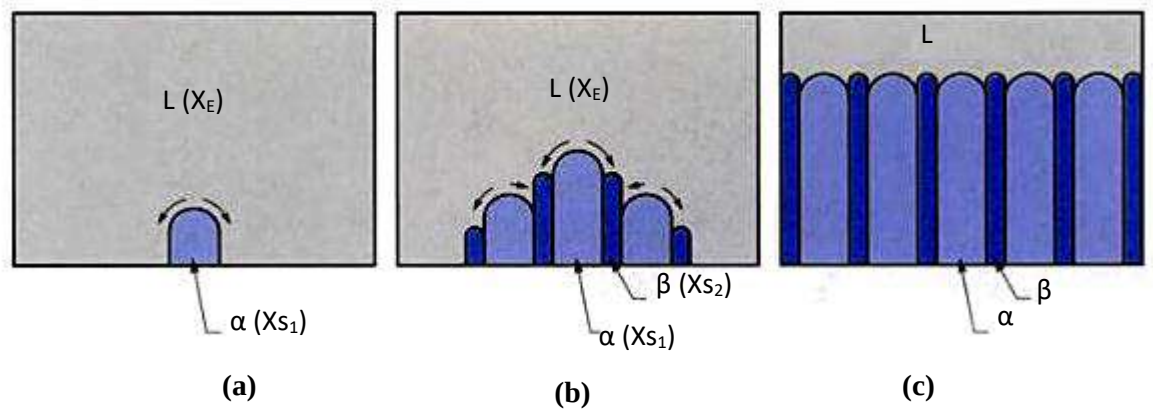

Fig. II-15 : Formation and growth of eutectic constituent :

(a) Formation of a nucleus of the α phase with composition Xs_1 within the liquid of composition X_E . The arrows indicate the rejection of solute in front of the α nucleus.

(b) Lateral growth of the eutectic by formation of the β phase.

(c) Planar growth of the solidification front.

❖ **Peritectic growth**

Alloys with a peritectic phase transition are commonly observed in metals such as steels and copper-based alloys. A peritectic transformation involves the combination of a solid phase and a liquid phase to form a new single solid phase.

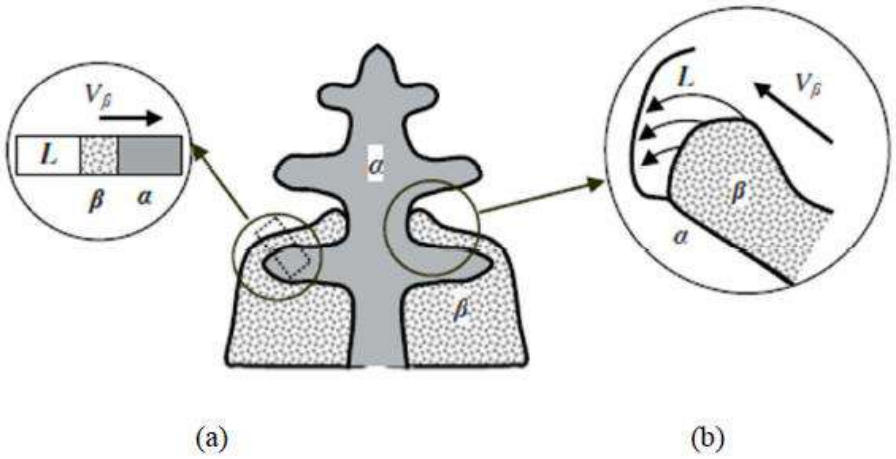

Fig. II-16-: Peritectic growth mechanism:
(a) Peritectic transformation
(b) The peritectic reaction

III-4. Solidification structures

During the development of an alloy, the material is melted to a liquid state and then cast into a mold to obtain a shaped piece. In the case of static casting in an ingot mold, the macroscopic structure of the alloy depends on both the nucleation rate and the rate of heat exchange (determined by the nature and thickness of the ingot mold wall). If we consider a cross-section at the mid-height of the ingot mold, typically three distinct crystallization zones can be observed (Fig. II-14):

❖ ***Chill zone of equiaxed crystals (coating zone):*** When molten metal comes into contact with a mold significantly cooler than its liquidus temperature, it undergoes rapid cooling and nucleation occurs immediately (quenched from high temperature to ambient). The substantial supercooling in this zone facilitates the initial formation of solid nuclei through heterogeneous nucleation (aided by the mold walls), with a high density of nuclei preventing each other from further growth.

- ***Basaltic zone (columnar zone):*** Once the coating zone is established, the temperature gradient within the liquid decreases. Dendritic growth of grains continues, but those with dendrites aligned parallel to the heat flux grow more rapidly. In the basaltic zone, grains exhibit nearly uniform orientation and cross-sectional area. The length of basaltic grains can extend several centimeters, with this zone being thicker than the first zone.

- ***Equiaxial zone:*** Towards the end of solidification, the evolution from the basaltic zone is constrained by the nucleation of numerous crystals within the remaining supercooled liquid. This nucleation is heterogeneous and frequently occurs on dendrite remnants. In this zone, grains are randomly oriented and grow uniformly in all directions.

We can observe that not all of these zones are necessarily present in a foundry piece. In addition to structural heterogeneity, there is chemical heterogeneity observed at the center of the ingot: elements with lower melting points segregate towards the center, known as the major segregation phenomenon.

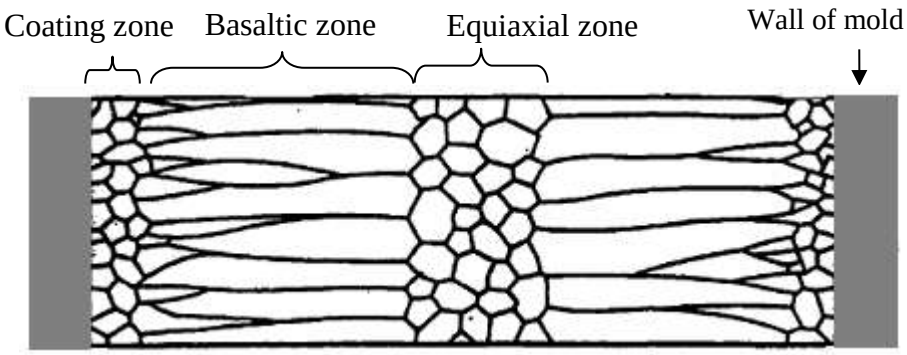

Fig. II-14- : Schematic representation of the different zones formed during solidification.

Practice exercises

Exercise 1:

Show, using a phase diagram, that due to slow diffusion in the solid state, the actual solidification of a binary alloy occurs at a lower temperature than predicted by the equilibrium diagram.

What are the consequences for the dendritic microstructure?

Exercise 2:

Determine the critical free enthalpy of germination ΔG^* for a spherical germ of critical size.

Exercise 3:

Calculate the dimensions and the free enthalpy of the critical germ formed during solidification of a pure metallic material. ΔG_v called the free enthalpy per unit volume and γ the interface energy.

Inclusions are very frequently added to reduce the size of the metallic grains. Germination then occurs in contact with a substrate.

- What is the type of nucleation in this case?
- Remake the calculations of dimensions and critical germ free enthalpy.
- Under what conditions is nucleation easier?

Exercise 4:

1- Explain why, under a given pressure, a pure substance is solid at low temperatures and liquid at high temperatures.
2- We consider a section of an ingot represented in Figure II-15-(a)-. Describe what you observe in this figure.
3- Figure II-15-(b)- shows a section of a commercially pure copper ingot. Compare the two figures (a) and (b) and highlight the differences between them.

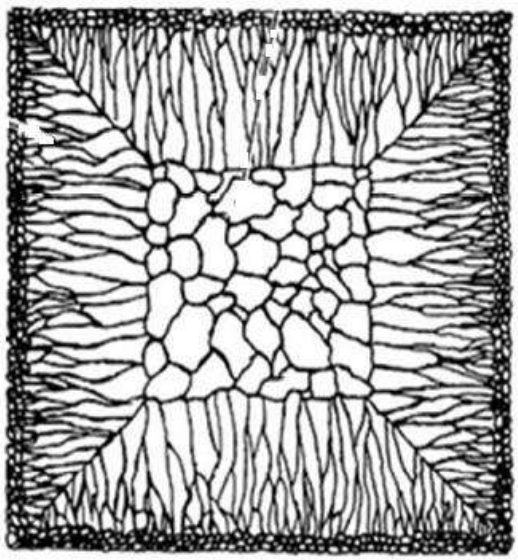

-(a)- Section of an ingot *(Amarican Society for Metals, Metals Handbook, Volume 8: Metallography, Structures and Phase Diagrams, 8th Edition, 1973).*

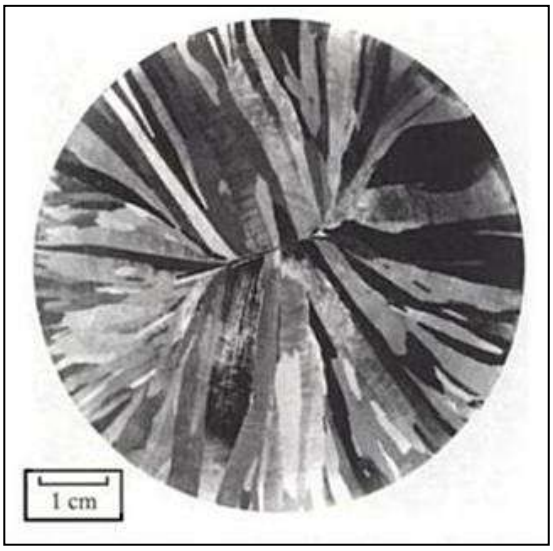

-(b)- Section of a commercially pure copper ingot *(J.P. Bailon, J.M. Dorlot, Des matériaux, presses internationales polytechnique de Montérial, 3eme édition, 2000).*

Fig. II-15

Answers

Answers for Exercise 1

The issue highlighted in this exercise is *minor segregation*.

Consider the binary alloy A-B with composition C_0 (Fig. II-16-). If this alloy is cooled under equilibrium conditions (i.e., with a very slow cooling rate), the point representing the overall composition of the solid follows the solidus curve from S_0 to S_f. In such cases, the time required for the solid's composition to uniformly homogenize through solute diffusion would be extensive.

As a result, the global composition of the solid is shown in Fig. II-16, positioned to the left of the ideal solidus line. Solute B was rejected from the center of the solid grains toward the boundaries (grain boundaries). This variation in composition is referred to as *minor segregation*: it is the accumulation of solute atoms at the grain boundaries of a material.

N.B. For more details, refer to the section in this chapter titled "Solid Growth in the Case of Alloys (Solidification of a Single-Phase Alloy under Non-Equilibrium Conditions).

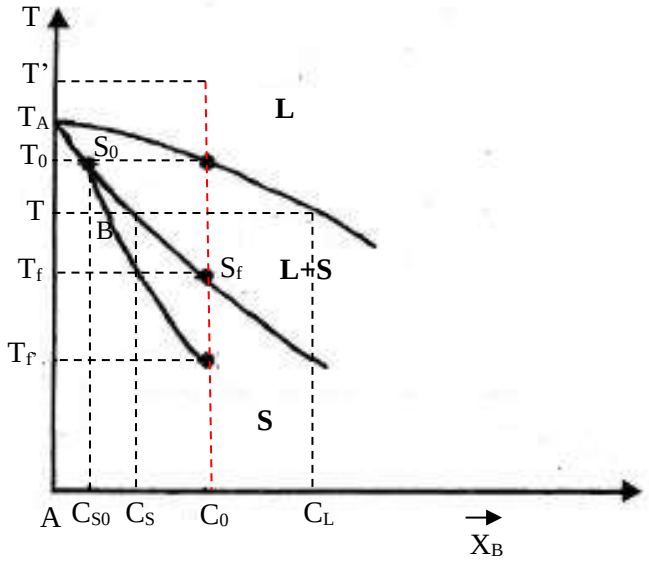

Fig. II-16-: Part of the phase diagram illustrates the deviation from equilibrium during the solidification of a single-phase binary alloy.

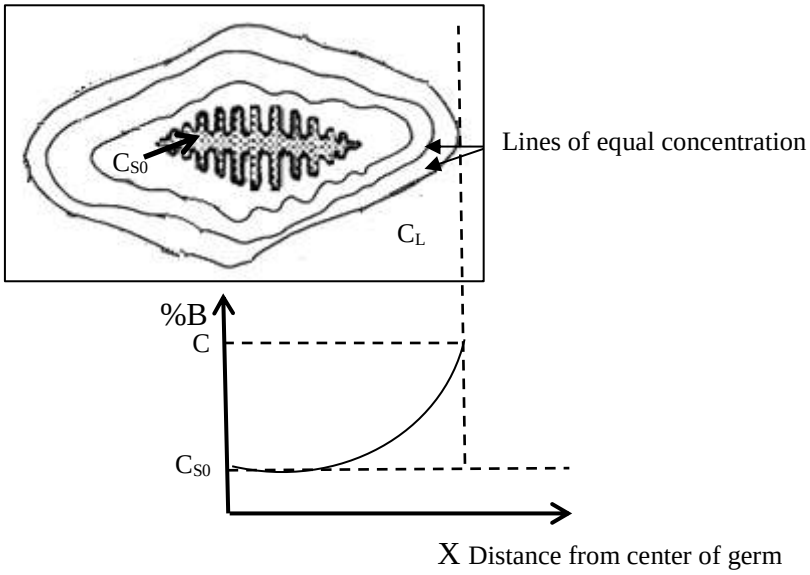

Fig. II-17-: Lines of equal concentration in a single-phase alloy exhibiting minor segregation.

Answers for Exercise 2

ΔG_g^{f*} corresponds to a critical size r = r*,

The derivative of $\Delta G_g^{f} = 0$ for the value r*:

$$\frac{d\Delta G_g^f}{dr} = 0 \qquad \text{(II-15)}$$

$$-\Delta G_v 4\pi r^2 + \gamma_{s\text{-}l} 8\pi r = 0$$

$$r^* = \frac{2\gamma T_F}{L\Delta T}$$

The critical value of the free energy is:

$$\Delta G_g^{f*} = \frac{16\pi\gamma^3 T_F^2}{3L^2\Delta T^2}$$

Answers for Exercise 3

1. Assuming the germ is spherical in shape:

   $$r^* = \frac{2\gamma T_F}{L\Delta T}$$

   $$\Delta G(r^*) = \frac{16\pi\gamma^3 T_F^2}{3\Delta G_v^2}$$

2. Addition of inclusions ⇒ heterogeneous germination

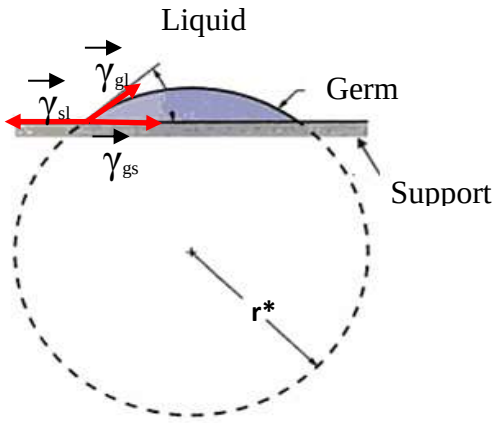

Fig. II-18- : Heterogeneous germination on a solid support.

To calculate the free energy of heterogeneous nucleation it is necessary to to consider the following:

- The volume contribution associated with solidification $V_g\Delta G_v$
- The removal of an interface between the particle and the liquid, with energy γ_{sl}
- The formation of the interfaces between the particle and the solid, and the solid and the liquid, with energies γ_{gs} and γ_{gl} respectively

$$\Delta G_{het} = V_g \Delta G_v + A_{gl}\gamma_{gl} + A_{gs}\gamma_{gs} - A_{sl}\gamma_{sl}$$

Where: $\vec{\gamma}_{sl} + \vec{\gamma}_{gl} + \vec{\gamma}_{gs} = 0$

By projection on the axis of the support:

$$\gamma_{sl} = \gamma_{gl} \cos\theta + \gamma_{gs}$$

- To calculate the volume of the spherical cap, we compute the surface integral of disks with radius r′ along the z-axis over the entire height of the cap (i.e. between z = rcosθ and z=r)

$$V_g = \int_{r\cos\theta}^{r} \pi r'^2 (z) dz$$

$$V_g = \pi r^3 \left[\frac{(2+\cos\theta)(1-\cos\theta)}{3}\right]$$

- The contact surface between the solid and the support can be determined very easily:

$$A_{gs} = \pi r^2 sin^2\theta$$

- To calculate the surface area between the solid and the liquid, you need to use a curvilinear integral:

$$A_{gl} = 2\pi r^2 (1 - \cos\theta)$$

Thus, the total change in the free energy of germ formation (ΔG_g^f) is given by :

$$\Delta G_{het} = \Delta G_{hom}\, f(\theta)$$

Where:

$$f(\theta) = \frac{(2+\cos\theta)(1-\cos\theta)^2}{4}$$

In our case, we are interested in $\Delta G(r^*)$, which represents the energy barrier to form a critical nucleus with radius r* where $r^*_{het} = r^*_{homg} = r^*$.

So: $\Delta G^*_{het} = \Delta G^*_{hom} * f(\theta)$

- $\Delta G_{hete}^* < \Delta G_{homg}^* \Rightarrow$ Heterogeneous nucleation is easier than homogeneous nucleation.

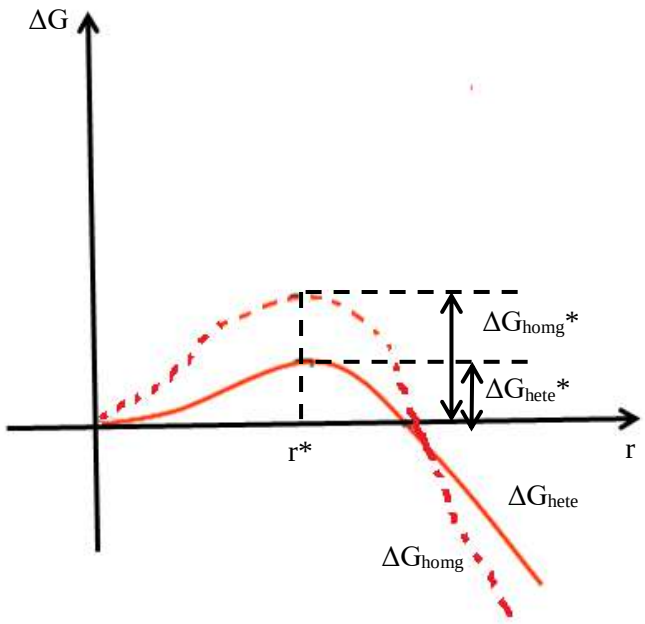

Answers for Exercise 4

1- $\Delta G = G_s - G_L = \frac{-L(T_f - T)}{T_f}$

For solidification to occur (i.e., for the formation of a solid phase), ΔG must be less than 0. Therefore when $T >> T_f \Rightarrow \Delta G > 0 \Rightarrow G_s - G_L > 0$

This means $G_s > G_L \Rightarrow$ indicating that the liquid phase is stable, and vice versa

2. For a description of the ingot and its three different crystallization zones, refer to the section titled "Solidification Structures" in the course material.
3. The difference between the two figures is the absence of an equiaxed zone in the copper ingot

Chapter

III

General classification of phase transformations and issues related to new phase nucleation.

III-1. Introduction

Phase transformations occur when temperature, pressure, or the chemical composition of the system (i.e., the number and type of components) change. Phase transformations driven by temperature variations are particularly significant, including phenomena such as precipitation and ordering in solid solutions.

A phase transformation, whether complete or partial (stopping at an intermediate stage), is crucial for achieving optimal material properties. These properties are influenced not only by the composition and characteristics of the phases but also by the alloy's microstructure. This includes factors such as the size, morphology, dispersion, and distribution of the phases, as well as the basic crystallographic structure or grain substructure. The purpose of certain heat treatment processes is precisely to develop the desired microstructure.

In general, the temperature of the final heat treatment operation is higher than the temperature at which the material will be used. As a result, the material retains its structure and properties for as long as possible.

The study of phase transformations is challenging because the mechanisms and kinetics of phase transformations of the same type (such as allotropic transformations, precipitation, or ordering in solid solutions) can vary significantly.

The analysis of phase transformations in alloys requires considering a combination of various mechanisms that may occur either sequentially or simultaneously.

The theory of phase transformations in the solid state relies on the same principles established in the study of crystallization processes. However, two specific factors must also be considered when dealing with transformations in a crystalline medium:

- ***Elastic energy factor***

During the formation of a new phase in a crystalline medium, the change in the system's free energy (ΔG) must account for not only the volume energy variation $V.\Delta Gv$ and the interface energy $A\gamma$, but also the energy associated with the elastic stress field. The elastic energy factor, together with the interface energy, influences the morphology, orientation, and distribution of the new phase particles during their formation and growth.

- **Factor limiting the mobility of atoms through diffusion in the crystal and the potential for cooperative movement of all atoms:**

Limiting the mobility of atoms allows for the achievement of metastable and even absolutely unstable states using conventional techniques such as temperature and pressure.

A sudden change in pressure over a wide range (several tens or hundreds of atmospheres) at low temperatures, or a high cooling rate under conditions of limited atomic mobility, can achieve extremely high supercooling. This, in turn, significantly alters the course of the phase transformation.

The cooperative movement of atoms, or its weak development, leads to a type of phase transformation known as martensitic transformation. The kinetics of martensitic transformations differ significantly from those of other phase transformations.

III-2. General classification of phase transformations

The classification of phase transformations can be based on comparing the crystallographic structure and chemical composition of the phases in the initial state with those produced by the transformation. In this context, the transformation occurs through the formation of one or several new phases, which differ in:

- **The crystalline structure**, which refers to the arrangement of atoms in the lattice (e.g., allotropic transformations in metals and alloys, ordering).
- **The chemical composition**, while maintaining the same atomic lattice coordination (e.g., demixing of a solid solution).
- **Structure and composition** (e.g., precipitation from supersaturated solid solutions).

If a phase transition is accompanied by an abrupt change in a property, then, considering the requirement for thermodynamic stability, the variation in the thermodynamic potential of the system must be infinitesimally small near the transition point. This can occur in two cases:

- When an infinitesimally small amount of the new phase appears, with a distinct difference in properties compared to the initial phase.
- When there is an infinitesimally small variation in any property throughout the entire volume.

The formation of a new phase with different properties leads to the development of surface energy. Therefore, very small domains of the new phase are not favorable. This type of transition is known as a first-order phase transition.

If the phase transition occurs through a gradual variation in internal parameters (e.g., concentration distribution, atomic displacement, or other aspects of the atomic structure), such that at the transition point the difference between the parameters of each phase is infinitesimally small, the transition is classified as a *second-order phase transition*. In this type of transition, metastable states are, in principle, not possible.

III-3. New phase nucleation problems

The need for supercooling to form a new phase arises not only from the energy required to create the interface between the old and new phases but also from overcoming the elastic resistance of the medium.

A more detailed analysis of first-order phase transitions reveals that, under certain conditions, the system's transition through intermediate states towards equilibrium (considering factors such as the continuous variation in the degree of differentiation of constituents or homogeneous shear during lattice deformation) can result in an increase in free energy. This potential barrier can be conceptualized as the formation of critical nuclei through fluctuations.

In Figure III-1, we show the variation in the free energy of the system as a function of a given parameter X for a first-order transformation (a) and a second-order transformation (b).

The origin of the calculation is set at the free energy level of the initial phase β. The diagram shown in this figure is suitable, for example, for the thermodynamic analysis of the precipitation process in a supersaturated solid solution. In this context, the vertical axis represents the change in the free energy of the system, while the horizontal axis represents the composition of the solid solution.

- In the domain of stable existence (e.g., at temperatures T_1 and T_2 for the high-temperature phase β), the phase remains stable with respect to both weak and strong fluctuations in the parameter X (the composition).

- At the phase transition point ($T_3 = T_0$), equilibrium between the phases is characterized by the equality of their free energies (or thermodynamic potentials) despite differences in specified structural parameters (x′ and x″).
- For $T<T_3$, the initial phase is unstable with respect to large variations in the parameter X. Cooling reduces the energy barrier associated with changes in the atomic structure, leading to the transformation of the β phase into the α phase.
- Up to the temperature $T>T_5$, the system remains stable with respect to small fluctuations in the parameter x.
- At $T_c = T_5$, there is a loss of stability of the initial system with respect to infinitesimally small variations in the parameter X. This temperature Tc is referred to as the absolute temperature at which the stability of the initial phase is lost.

In the case of second-order phase transitions, the parameter X can represent, for example, the degree of order in order-disorder transformations. In such transitions, each intermediate structure has a lower free energy throughout the volume, and no metastable states are present.

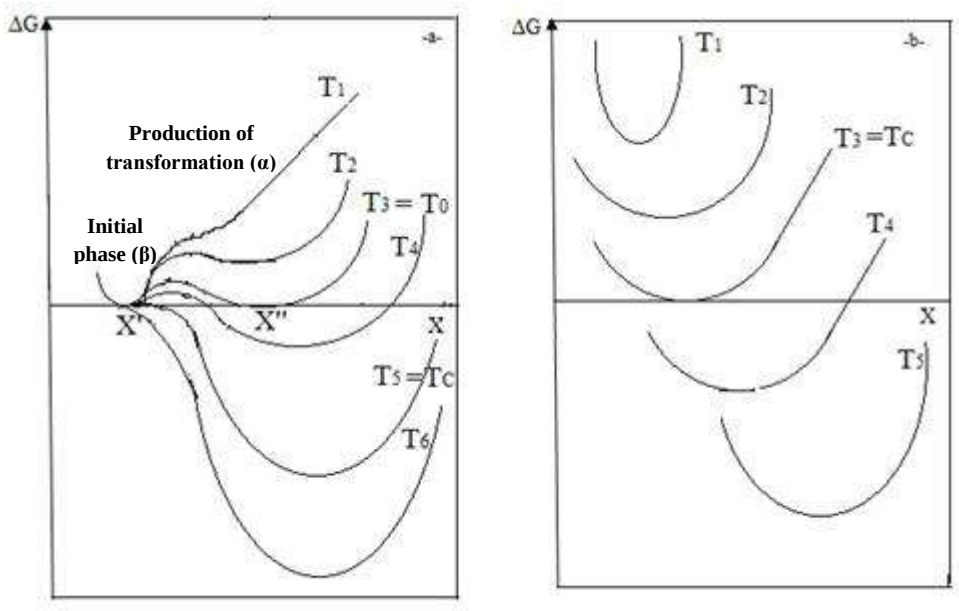

Fig. III-1- : Variation of the Gibbs free energy (ΔG) as a function of a thermodynamic parameter for two systems: one exhibiting a first-order transition (a) and the other exhibiting a second-order transition (b).

Chapter

IV

Kinetics of Phase Transformations in Solid Materials and Alloys

IV-1. Introduction

There are two types of phase transformations, depending on the mode of substance transfer from the initial phase (parent phase):

Firstly, the most common type in practice involves uncoordinated atomic movements. This process leads to the destruction of the lattice structure of the original phase and the reconstruction of the lattice structure of the new phase. Phase transformations of this nature involve mechanisms for transferring substances within a solid medium, specifically diffusion. When the phase change is accompanied by a change in chemical composition, atoms move over distances that are significantly larger than the interatomic distances.

The second type involves crystallographic changes without a change in chemical composition. These transformations involve movements of atoms over short distances. The displacements are coordinated (known as *shear structures*), meaning each atom retains its neighboring atoms. An example is the martensitic transformation in steels, which produces stainless steel blades that maintain their sharpness for an extended period due to their hardness.

It is essential to study the kinetics of transformations before examining the different types of solid-state transformations in alloys.

IV-2. General characteristics of solid-state transformations

The general characteristics of phase transformation kinetics can be summarized as follows:

a. The initiation of reactions is challenging, leading to significant delays in time or temperature, depending on whether the reaction is conducted at a constant or variable temperature.

b. The initiation of reactions is influenced by defects in the crystal lattice and, consequently, by factors that alter the number and nature of these defects (such as hardening).

c. The subsequent evolution of reactions is often governed by the diffusion of lattice species within the matrix. Therefore, the effect of temperature on the reaction rate primarily results from its impact on the diffusion coefficients.

These characteristics are common to most solid-state transformations that involve a change in the number of phases, which are known as first-order transformations. However, it is

challenging to draw a clear distinction between first-order and second-order transformations, as the appearance or disappearance of a phase in a solid system can sometimes occur gradually, both thermodynamically and kinetically.

IV-3. Initiation of reactions proceeding by nucleation and growth

Among the transformations that can occur in metals or alloys in the solid state, a particularly important category is those in which a new phase forms within an initially homogeneous single-phase medium. From a purely chemical perspective, this situation can arise from various types of reactions, including:

- *Precipitation of an intermetallic compound in a supersaturated solid solution during a decrease in temperature***:** An example of this type of reaction is the precipitation of the compound Al_3Mg_2 from a solid solution of Al-Mg, which is homogeneous at high temperatures, upon slow cooling.

  Magnesium-rich solid solution→ Solid solution poor in magnesium + Al_3Mg_2

- *Allotropic transformation* of a pure metal through a sudden transition between stability domains: An example of this type of transformation is the cooling-induced change in iron from its phase γ (Feγ, face-centered cubic or FCC) to its phase α (Feα, body-centered cubic or BCC).
- The *eutectoid transformation* of a solid solution results in the formation of two new phases rather than just one. A well-known example of this process is the formation of the eutectoid: α + Fe_3C, within a homogeneous solid solution of 0.8% carbon in γ iron below 727°C. The transformation can be represented as:

  Solid solution $\gamma \leftrightarrow \alpha + Fe_3C$

From a morphological perspective, these different transformations begin in a similar manner. The alloy is initially heated to a high temperature where it exists as a single homogeneous phase. Upon cooling to a temperature where this phase becomes unstable, small crystalline particles of the new phase start to appear in a dispersed state. These particles grow at the expense of the matrix until, in the case of an allotropic transformation, they completely replace it.

In the case of precipitation within a supersaturated solution, the particles cease to grow once the solution reaches its new equilibrium state. This process is typically divided into two successive stages: nucleation and growth.

IV-4. Classical theory of nucleation

The theory to be developed focuses on how the stability and growth potential of a nucleus of the new phase evolve in relation to its size.

Nucleation is the phenomenon by which a new phase begins to form within the parent phase. There are two types of nucleation: homogeneous and heterogeneous. Homogeneous nucleation theoretically occurs only in a perfect crystal, where the locations of precipitate formation are indeterminate and randomly distributed within the matrix. In contrast, heterogeneous nucleation occurs at crystal defects or surfaces, which serve as preferential sites for the formation of new phases.

IV-4-1. Homogeneous nucleation

When a supersaturated solid solution (the parent phase) is allowed to evolve, concentration fluctuations occur, leading to the formation of clusters of solute at a temperature where the parent phase becomes unstable. The formation of a cluster with radius r (the new phase) alters the energy of the system. The nucleus of the new phase becomes stable only when it reaches a certain critical volume, which can be evaluated as follows:

- The free enthalpy of the initial nucleus must be less than 0 for the nucleus to be stable.
- The change in the free enthalpy of the system is the sum of three contributions:

  1- If ΔGv is the change in free energy per unit volume at temperatures where the new phase is stable, then the formation of a volume V of this phase results in a decrease in free energy by $V\Delta G_v$ (noted with a negative sign in the expression for ΔG). It is important to note that ΔG_v is zero at the equilibrium temperature Te.

  2- The creation of an interface with a total surface area A results in an increase in the free energy of the nucleus by $A\gamma$, where γ is the specific interfacial energy between the parent phase and the new, presumably isotropic phase.

  3- When the volume of the nucleus of the new phase differs from the volume initially occupied by the parent phase (which is generally the case), the free energy of the nucleus increases by an amount proportional to V, due to a stress energy per unit volume in the new phase, denoted as ΔG_c .

The total change in free energy associated with the formation of a nucleus with volume V is therefore expressed as:

$$\Delta G = -V\Delta G_v + A\gamma + V\Delta G_c = -V\,(\Delta G_v - \Delta G_c) + A\gamma \qquad \text{(IV-1)}$$

Assuming that the interface energy is independent of orientation and that the germ is spherical with a radius r, the previous equation simplifies to:

$$\Delta G(r) = -\frac{4}{3}\pi r^3 * (\Delta G_v - \Delta G_c) + \gamma * (4\pi r^2) \qquad \text{(IV-2)}$$

The variation in the free energy of nucleus formation thus depends on its size r (see Figure IV-1).

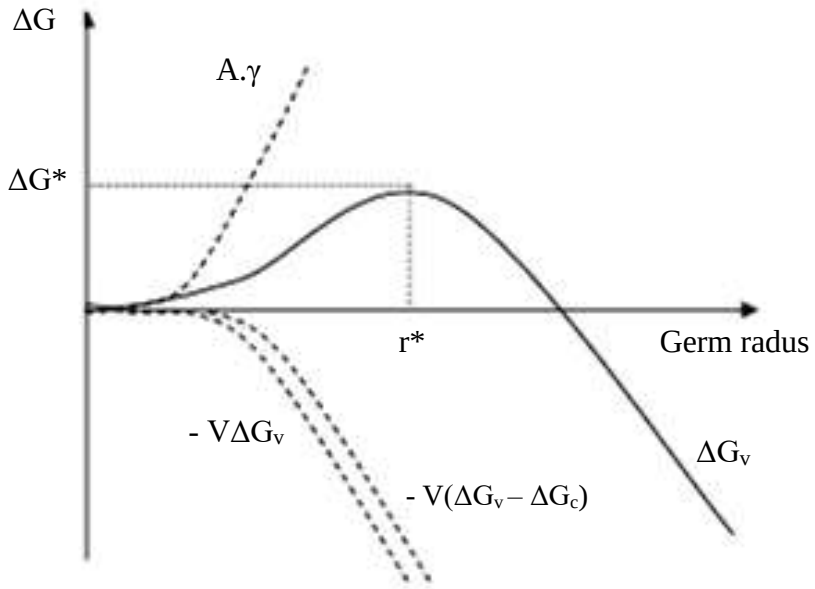

Fig. IV-1 : Evolution of the free energy of spherical nucleus formation as a function of its radius r.

We observe that if the size of the germs is small, the interface energy is dominant, making the germs unstable and causing them to spontaneously disintegrate within the matrix. Conversely, if the germ size is sufficiently large, the driving force becomes dominant, and the germs can evolve and become stable. Thus, there is a critical germ size threshold beyond which germination can occur and transformation can begin. By differentiating the equation for ΔG, we can determine the critical germ size r*:

$$r^* = \frac{2\gamma}{(\Delta G_v - \Delta G_c)} \qquad \text{(IV-3)}$$

This yields the value of the activation free energy barrier for the formation of a critical germ:

$$\Delta G^* = \frac{16\pi\gamma^3}{3\,(\Delta G_v - \Delta G_c)} \quad \text{(IV-4)}$$

- **Homogeneous nucleation rate**

Statistically, the number of germs larger than the critical size is given by:

$$N^* = N_0 exp\left(-\frac{\Delta G^*}{KT}\right) \quad \text{(IV-5)}$$

N_0, being the number of atoms in the matrix per unit volume.

The greater the number of atoms with sufficient energy to overcome the energy barrier, the higher the probability of germ formation. This means that the germination rate is proportional to exp $exp\left(-\frac{\Delta G^*}{KT}\right)$ and to the diffusion rate of the atoms to the germs $exp\left(-\frac{\Delta G_D}{KT}\right)$.

In general, the germination rate can be expressed as:

$$V_{homo} = WN_0 exp\left(-\frac{\Delta G_D}{KT}\right) exp\left(-\frac{\Delta G^*}{KT}\right) \quad \text{(IV-6)}$$

Where W is a factor that accounts for the vibrational frequency of the atoms.

IV-4-2. Heterogeneous nucleation

Nucleation, whether in a solid or a liquid, is often heterogeneous. Favorable germination sites include structural defects such as dislocations, grain boundaries, inclusions, free surfaces, and vacancies under supersaturation. These sites are in a non-equilibrium state, resulting in atoms in the immediate vicinity being in a higher energy state, which increases the system's free energy. If the formation of a germ of the new phase leads to the elimination of a defect, the free energy of the entire system decreases by an amount equal to the defect's free energy, ΔG_d. Thus, the defect energy plays a similar role to that of the energy per unit volume, serving as a driving force. Consequently, the expression for the variation in free energy associated with the formation of a germ of volume V is:

$$\Delta G_{\text{hété}} = -V\,(\Delta G_v - \Delta G_c) + A\gamma - \Delta G_d \quad \text{(IV-7)}$$

An example of this type of germination is *germination on grain boundaries*:

Let θ be the wetting angle of the particle on the grain boundary (see Figure IV-2 (a)), and r its radius of curvature (assuming a double spherical calotte geometry). If $\gamma_{\alpha\alpha}$ is the interfacial energy and $\gamma_{\alpha\beta}$ is the interface energy between the two phases, α (the parent phase) and β (the new phase), then the free enthalpy of creating the germ in heterogeneous germination is derived from that obtained in homogeneous nucleation.

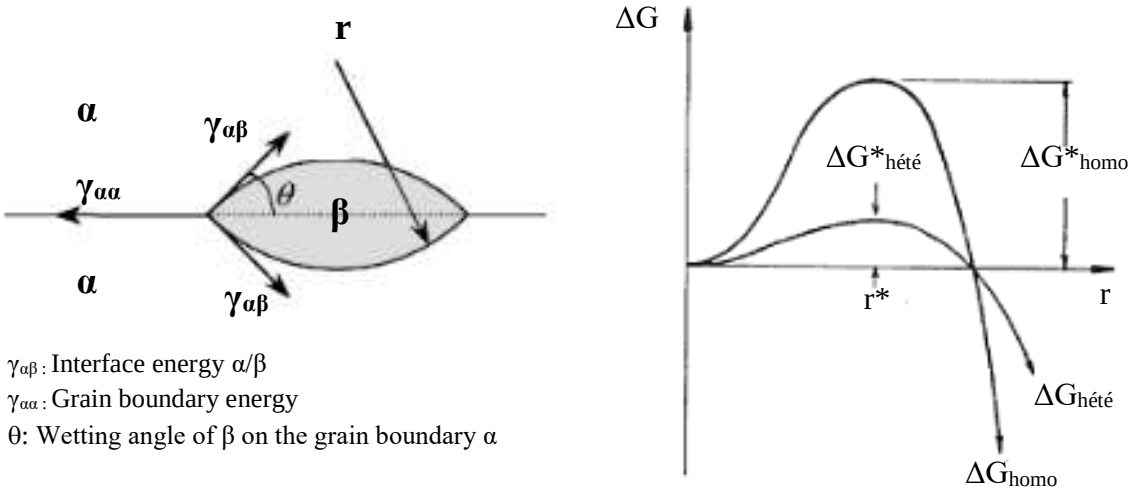

$\gamma_{\alpha\beta}$: Interface energy α/β
$\gamma_{\alpha\alpha}$: Grain boundary energy
θ: Wetting angle of β on the grain boundary α

-a- -b-

Fig. IV-2: Heterogeneous nucleation: (a) schematic representation and (b) reduction in the energy barrier to nucleation, while the critical radius remains unchanged.

- **Heterogeneous nucleation rate**

Nucleation occurs more rapidly at heterogeneities. However, the impact of these heterogeneities on the germination rate and the transformation of the alloy depends on their concentration. In homogeneous germination, every atom serves as a potential germination site. In contrast, for germination at grain boundaries, only the atoms located at the grain boundaries can participate in the process. If the concentration of germs at heterogeneous sites per unit volume is C_1, the rate of heterogeneous germination is given by the following relationship:

$$V_{hetro} = WC_1 exp\left(-\frac{\Delta G_D}{KT}\right) exp\left(\frac{\Delta G^*}{KT}\right) \quad \text{(IV-8)}$$

IV-5. Description of the overall behavior of phase transformations according to Avrami's theory:

Solid-state phase transformations that proceed via a nucleation mechanism generally follow the transformation law proposed by Avrami. The Avrami treatment provides an equation that allows for the calculation of the extent of phase transformation as a function of time.

The formation and growth of a new β phase within an initial α phase can be envisioned as follows:

- Initially, at time t_0, a germ appears within the parent phase α. This germ represents the nascent β phase. The time required for the formation of these germs is referred to as the incubation period.
- In the next stage, the germs grow at the expense of the α phase, contributing to the progress of the transformation (see Fig. IV-3). At time t_f, the transformation ceases when the initial phase is entirely converted into the new phase β. The growth of the new phase may not proceed uniformly in all directions.

The growth of the new phase proceeds freely during the initial stages of the transformation. However, this behavior changes once a certain conversion rate is reached, at which point the growing phases begin to contact each other. Taking this characteristic into account and based on the principles of nucleation and growth, we derive a general equation that describes the conversion rate (volume fraction f) as a function of the transformation time:

$$f = 1 - \exp(-K t)^n \qquad \text{(IV-9)}$$

This is Avrami's equation, where n varies from 1 to 4 depending on the type of transformation, and K is a function of the nucleation and growth processes, which are strongly dependent on temperature. By knowing K as a function of temperature, one can calculate the time required to achieve a specified conversion rate (e.g., 1%, 50%, 90%) at a given temperature.

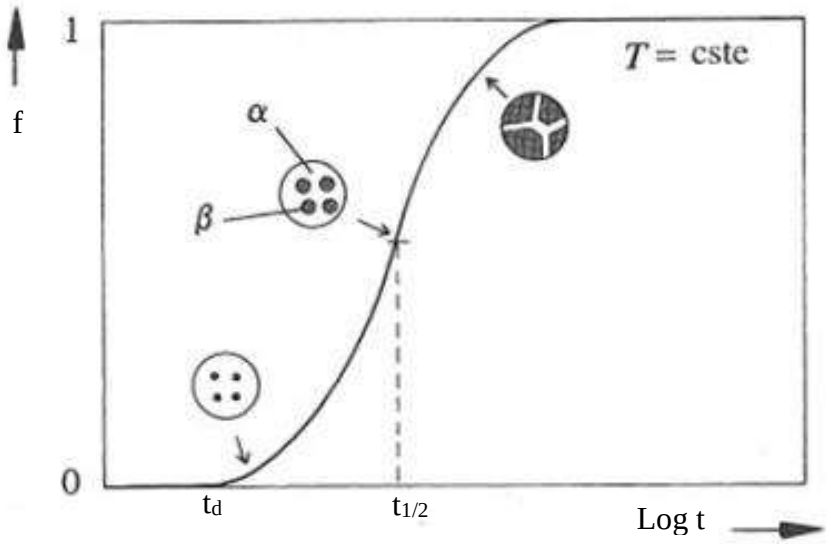

Fig. IV-3- : Isothermal variation of the volume fraction f of the transformed phase as a function of the logarithm of time t according to the Avrami equation. Here, f represents the fraction of the β phase transformed at time t, while (1−f) denotes the fraction of the untransformed α phase.

IV-6. Diagrams TTT (Transformation/Time/Temperature)

From Avrami's expression, we can plot the transformation fraction (f) curves as a function of time and temperature, creating TTT (Time-Temperature-Transformation) diagrams. Typically, two conversion rates are selected, which are determined experimentally and characterize the start (e.g., 1% conversion) and end (e.g., 99% conversion) of the reaction. This is illustrated in Figure IV-4-(a). The figure shows how to determine the values of t_d and t_f at a temperature $T=T_1$ within the transformation interval. Figure IV-4-(b) establishes the relationship between the TTT diagram and the isotherm at temperature $T=T_1$. These TTT diagrams help in determining the appropriate heat treatment needed to achieve a specific structural state in a material. Although TTT diagrams can theoretically be obtained for any phase transformation, they are challenging to determine experimentally for the crystallization of metals and metal alloys due to the rapid nature of the transformation.

Reading a TTT diagram is straightforward. For example, consider selecting a temperature $T_l<T_e$ and analyzing the progress of the transformation. After rapidly cooling (quenching) the material from $T>T_e$ down to T_l (solid line in Figure IV-4 (a)), the material is held at a constant temperature T_l. The transformation effectively begins at time $t=t_d$. The transformation proceeds initially at an increasing rate because the rate of transformation is proportional to the volume

transformed, as illustrated in Figure IV-4 (b). Subsequently, the transformation rate gradually decreases as the growing grains start to interact with each other.

Practically, the transformation stops when the transformed volume reaches 99% (at $t=t_f$). The dashed curve in Figure IV-4-(a) represents the end of the isothermal transformation as a function of the transformation temperature.

A typical example of a solid-solid transformation illustrated by TTT diagrams is the eutectoid transformation in steels containing 0.8% mass. C. This transformation occurs from austenite to form ferrite and iron carbides (cementite) (see Fig. IV-5).

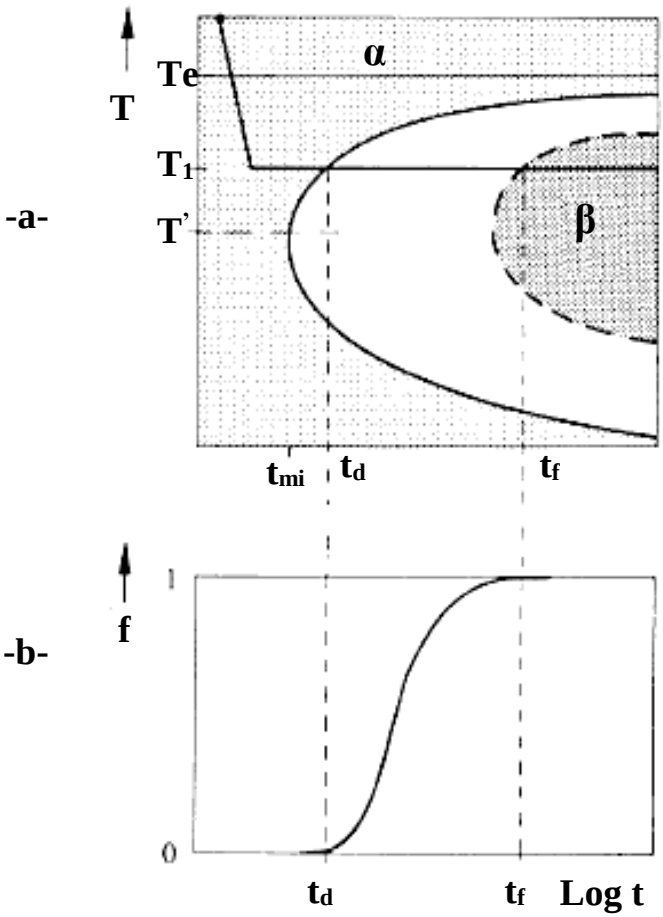

Fig. IV-4: Schematic appearance of the TTT diagram of a phase transformation: (a) Phase transformation curves as a function of time and temperature for two values of the conversion rate, characterizing the start (1% conversion, t_d) and the end (99% conversion, t_f) of the reaction. t_{min} represents the minimum time required for the transformation to commence. (b) The relationship between the TTT diagram and the transformation isotherm at temperature $T=T_1$.

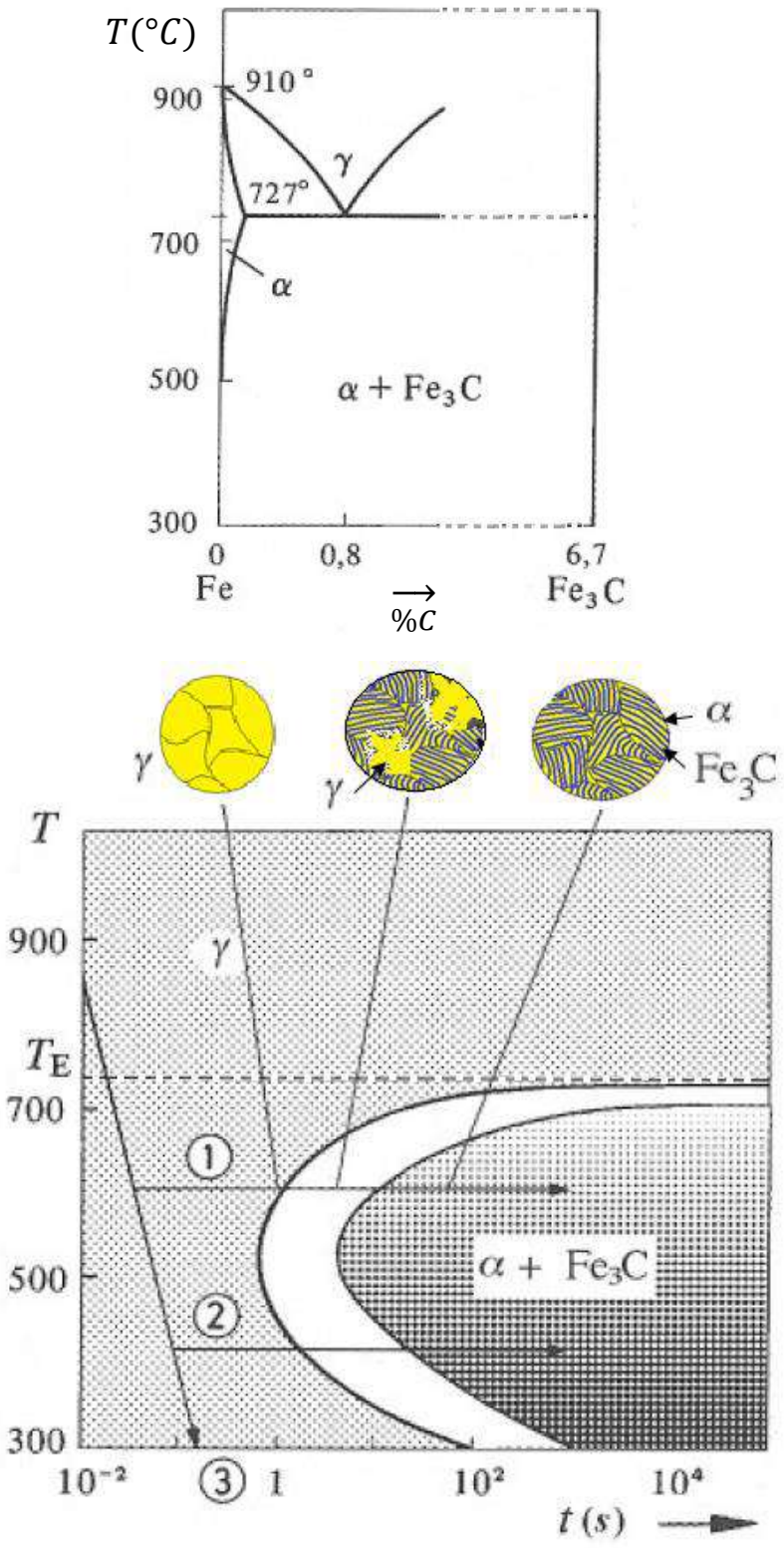

Fig. IV-5- : Part of the Fe-Fe₃C phase diagram (a) and the TTT diagram for the eutectoid transformation in this system (b).

IV-7. Spinodal decomposition theory

The previous theory attributed the delay in germination to the positive energy required for the creation of interfaces, which was considered the source of the barrier. However, an alternative analysis of the phenomenon has been known for some years, and we will briefly describe it.

IV-7-1. Definition of Spinodal decomposition

Spinodal decomposition is a phase transformation phenomenon that occurs when a continuous solid solution is cooled below a critical temperature.

Figure IV-6(a) shows the phase equilibrium diagram of the A-B binary system. Above the critical temperature and below the melting temperature, this system exists as a continuous solid solution, α.

Below T_c, an isothermal section of the diagram at temperature T′ reveals three distinct zones based on the value of x (the composition of element B).

- ✓ a single-phase zone consisting of an A-rich phase α_1 for $0 < x < x_1$,
- ✓ a two-phase zone comprising both phases for $x_1 < x < x_4$,
- ✓ a single-phase zone consisting of a B-rich phase, α_2, for $x_4 < x < 1$.

The phenomenon of isomorphic demixing in the continuous solid solution for $x_1 < x < x_4$ is illustrated in Figure IV-6(b). This figure shows the variation of the molar free enthalpy of the system as a function of composition at temperature T′.

For the two solid solutions to be in equilibrium with each other, the chemical potential of component A must be the same in both solid solutions, α_1 and α_2. The same applies to the chemical potential of component B. The rule of the common tangent to the free molar enthalpy curve of the phase allows us to determine the compositions of the solid solution α_1 saturated with B (x_1) and the solid solution α_2 saturated with A (x_4) in equilibrium with each other.

The range of points x_1 and x_4, obtained at different temperatures, defines a curve on the equilibrium diagram that serves as the boundary between the single-phase regions and the two-phase region. The area where the two solid solutions, α_1 and α_2, coexist is referred to as the *miscibility gap*.

In addition to its three domains, the molar free enthalpy curve of the continuous solid solution has two points of inflection, x_2 and x_3, which become significant when examining the mechanism of transformation from a single-phase system to a two-phase system.

In the region between the two inflection points, x_2 and x_3, where $\partial^2G/\partial X^2<0$, the single-phase solid solution is unstable and undergoes spinodal decomposition. In the composition ranges x_2-x_1 and x_4-x_3, the single-phase solid solution is metastable and will decompose into two solid solutions through a nucleation and growth mechanism, given sufficient activation energy.

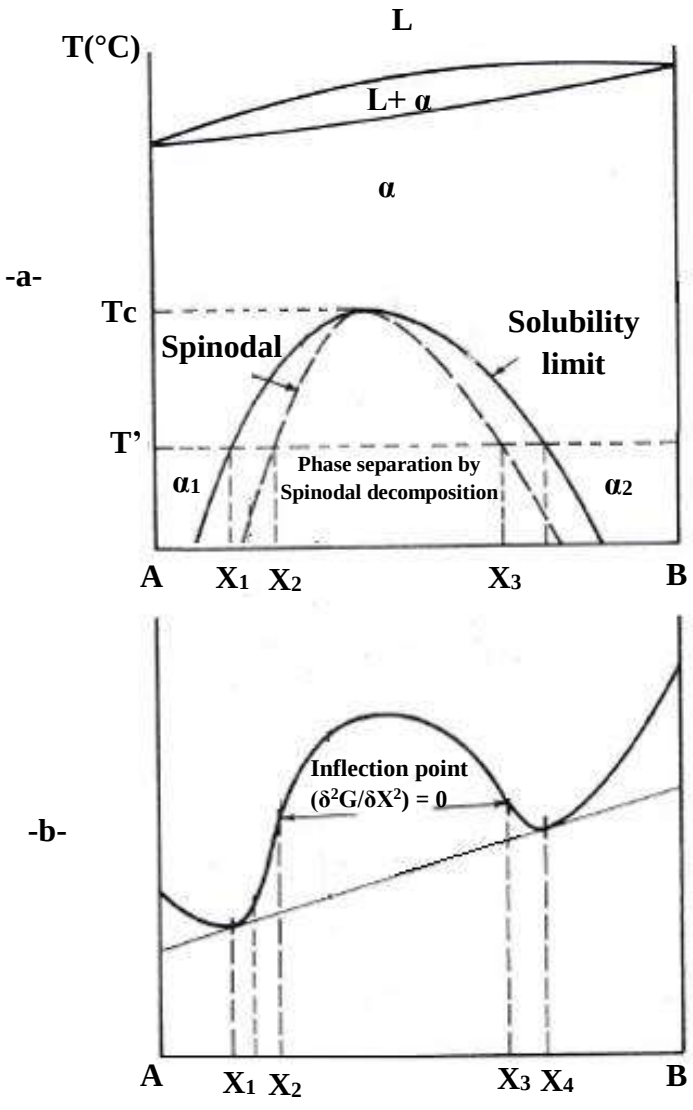

Fig.IV-6: (a) Phase diagram of a binary system showing a miscibility gap.
(b) Variation of the free enthalpy of a solid solution at temperature T′.

IV-7-2. Mode of decomposition

To explain the mode of decomposition, we refer to the molar free enthalpy curve of the single-phase binary system at temperature T, for an average concentration X_i of element B, which is within the spinodal decomposition region (see Fig. IV-7).

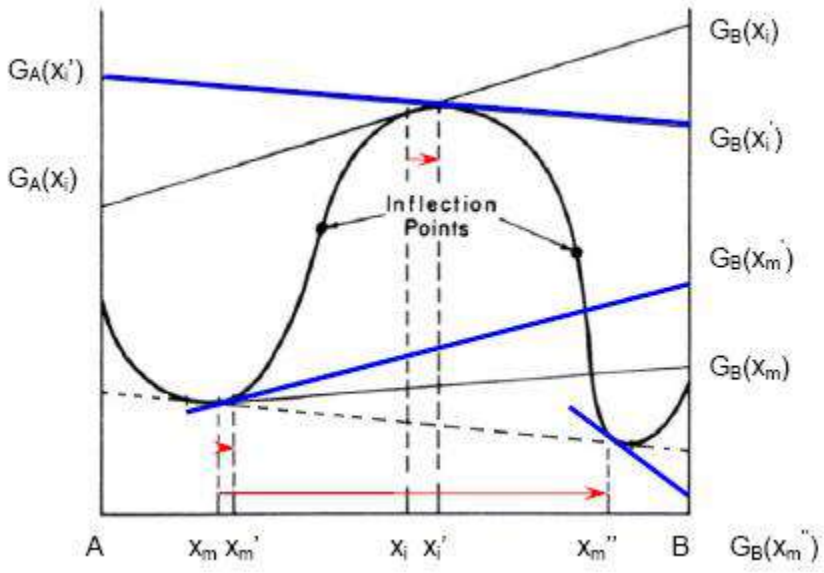

Fig. IV-7: Variation of the chemical potential as a function of composition within the miscibility range.

At a point in the solid solution, consider the emergence of a small fluctuation in composition, shifting from X_i to X_i', which locally generates a composition gradient. This concentration gradient of element B is associated with a gradient in chemical potential, which induces a flow of matter B in the direction of decreasing chemical potential.

In Figure IV-7, the material with composition X_i has chemical potentials $G_A(Xi)$ and $G_B(Xi)$ for constituents A and B, respectively. The material with the average composition X_i' has chemical potentials $G_A(Xi')$ and $G_B(Xi')$.

In the domain of spinodal decomposition, a fluctuation in concentration from X_i to X_i' (an increase in the concentration of B) leads to a decrease in the chemical potential of component B (and an increase in the chemical potential of component A). According to Gibbs' phase rule, the B constituents adjacent to the area of composition fluctuation will diffuse into this region, which is an unusual direction of increasing concentrations, while the A constituents will move away from it. This results in regions of the material that become increasingly enriched in B and others that become increasingly depleted in B (see Fig. IV-8 (a), Stage II). This self-propagating phenomenon leads to spinodal decomposition (see Fig. IV-8 (a), Stage III).

In the metastable range at temperature T, the decomposition mechanism differs from that of spinodal decomposition. A small fluctuation in composition (transition from X_m to $X_m + dX_m$) (see Fig. IV-7 and Fig. IV-8(b), Stage I) induces a change in chemical potential from $G_B(X_m)$ to $G_B(X_m')$, with $G_B(X_m') > G_B(X_m)$. Matter flow is then directed in the usual manner, towards decreasing concentrations (see Fig. IV-7 and Fig. IV-8(b), Stage II). Consequently, this composition fluctuation eventually diminishes (see Fig. IV-7 and Fig. IV-8(b), Stage III).

In the metastable domain, for a large fluctuation in composition, such as from X_m to X_m'', where $G_B(X_m'')$ is lower than $G_B(X_m)$, the composition fluctuation will increase. This leads to the nucleation and growth of two solid solutions with compositions X_1 and X_4 (see Fig. IV-7 and Fig. IV-8(c)).

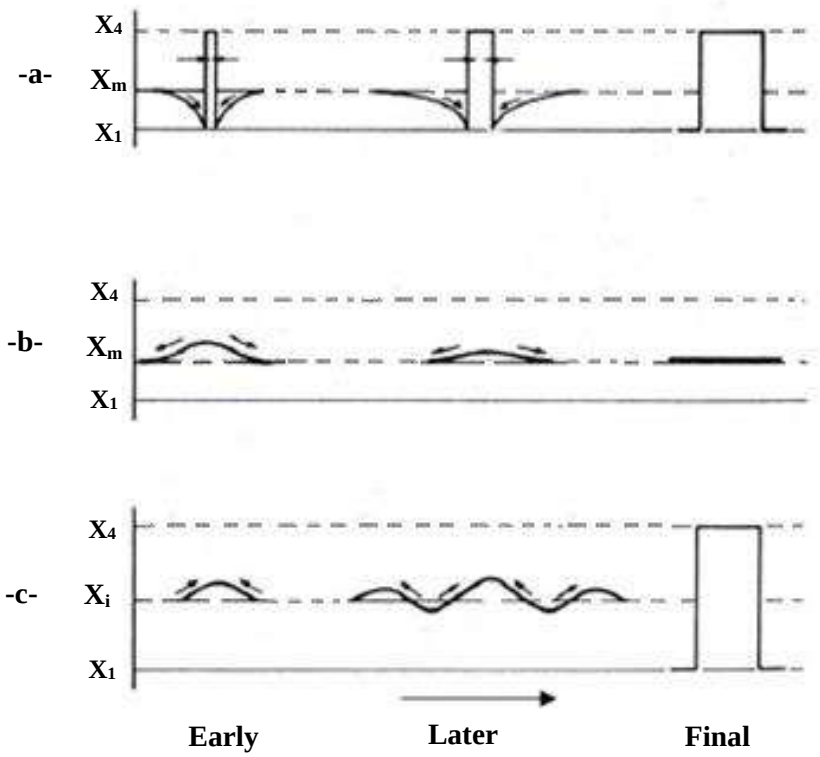

Fig. IV-8: (a) Progression of a small fluctuation within the Spinodal decomposition region,
(b) Disappearance of a small fluctuation in the metastable phase,
(c) Nucleation and growth of a large fluctuation in the metastable phase.

IV-8. Limitations of Previous Theories

In the discussion of the preceding theories, several factors of significant importance were neglected. This limitation notably affects the validity of the quantitative conclusions that

someone unfamiliar with the complexities of solid-state reaction kinetics might draw from the previous discussion. Therefore, it is particularly instructive to identify these simplifications and investigate how they may influence the mechanisms of transformations in each specific case.

It should be noted that the two approaches are only apparently contradictory. While the first approach emphasizes the critical role of interfacial energy, the second approach simplifies by neglecting it. However, it is possible to incorporate this energy into Spinodal theory by translating the Spinodal curve downward from its simplified form. The difference between these two curves, which can vary with temperature, represents the elastic deformation energy resulting from the parameter differences between enriched and depleted regions.

It should be noted that while classical theory introduces the concept of interfacial energy from the outset, it neglects the fact that this energy can vary significantly for the same pair of associated phases due to several factors, including:

- The morphology of the dispersed phase within the original matrix,
- The orientation relationship between the two adjacent crystal lattices,
- Constraints resulting from volume changes during processing.

Practice exercises

Exercise 1:

Consider the nucleation of a new phase β in the form of a sphere with radius rrr within an infinite matrix of another phase α. If nucleation occurs at grain boundaries, as shown in Figure 1,

- What is the type of Nucleation in this case?
- Provide the equation for calculating the free enthalpy of nucleation in this case, assuming that the interfacial energy (γ) of the α phase is isotropic and equal to that of the β phase.
- Calculate the critical radius value r*.
- Calculate the wettability angle of the β phase particle on the grain boundary (θ) if $\gamma_{\alpha/\beta}$= 500 and $\gamma_{\alpha/\alpha}$= 600 mJ/m^2
- Evaluate the f(θ) factor for this germ.

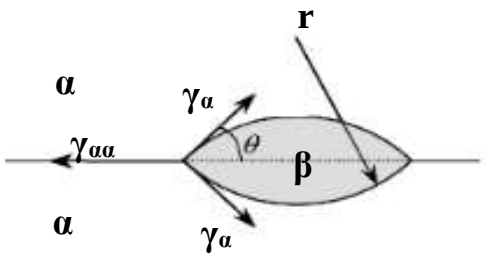

Fig. IV-9-

Exercise 2:

The isothermal transformation diagram in Fig. 2 pertains to a eutectoid steel, with phases labeled as A (austenite), B (bainite), P (pearlite), and M (martensite).

- Determine the final microstructure of a small sample subjected to the following time-temperature treatments. In each case, the initial temperature of the sample was 845°C and was held long enough for the sample to achieve a complete and homogeneous austenitic structure.

(a) Rapid cooling to 350°C, holding at this temperature for 104 seconds, then rapid cooling to room temperature.

(b) Rapid cooling to 250°C, holding at this temperature for 100 seconds, then rapid cooling to room temperature.

(c) Rapid cooling to 650°C, holding at this temperature for 20 seconds, then rapid cooling to 400°C, holding at this temperature for 103 seconds, followed by rapid cooling to room temperature.

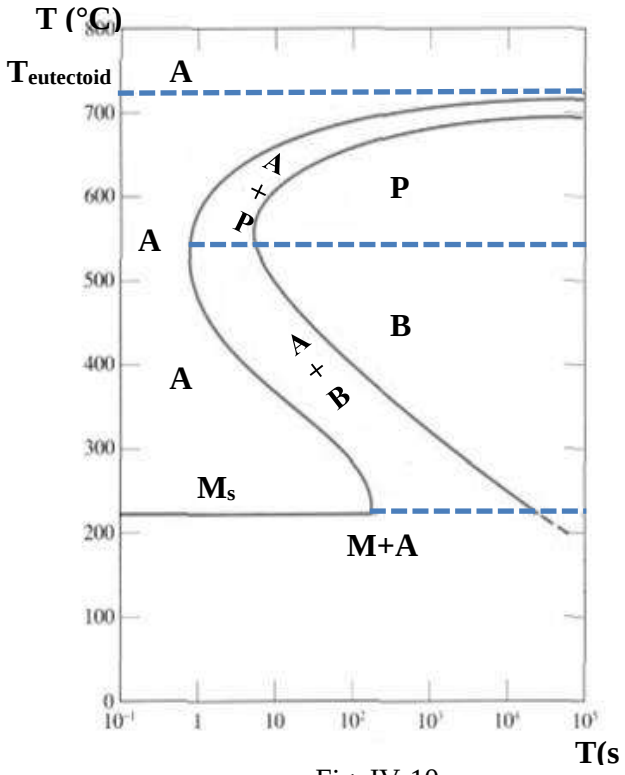

Fig. IV-10-

Exercise 3:

Solid-state phase transformation kinetics that proceed by a nucleation mechanism generally follow a transformation law proposed by Avrami. The Avrami treatment provides an equation that allows the calculation of the degree of phase transformation as a function of time.

1. If f_1 and f_2 are the fractions recrystallized at a given temperature at times t_1 and t_2, respectively, derive a relation for nnn in the Avrami equation.
2. For copper, the fraction recrystallized at 135°C is given in the following table:

Recrystallized fraction	t (s)
0.10	300
0.50	540

- Determine n and K in the Avrami equation

Answers

Answers for Exercise 1

- heterogeneous nucleation
- $\Delta G_{hete} = -V(\Delta G_v - \Delta G_s) + A\gamma - \Delta G_d$

In this exercise there are two spherical caps:

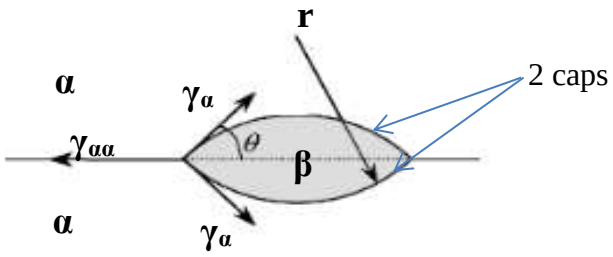

$\Delta G_{hete} = -2V(\Delta G_v - \Delta G_s) + 2A\gamma_{\alpha\beta} - A_{\alpha\alpha}\gamma_{\alpha\alpha}$

$\gamma_{\alpha\alpha} = 2\cos\theta\gamma_{\alpha\beta}$

$\Delta G_{hete} = (-V(\Delta G_v - \Delta G_s) + 2A\gamma_{\alpha\beta})(\frac{2-3cos\theta+\cos^3\theta}{2})$

$\Delta G_{hete} = \Delta G_{homg}(\frac{2-3cos\theta+\cos^3\theta}{2})$

$f(\theta) = (\frac{2-3cos\theta+\cos^3\theta}{2})$

$$r^* = \frac{2\gamma_{\alpha\beta}}{(\Delta G_v - \Delta G_s)}$$

$$\frac{\Delta G^*_{hete}}{\Delta G^*_{homg}} = f(\theta)$$

The grain boundary ability of decreased ΔG^*_{hete} depends on the angle $\theta \leftrightarrow \frac{\gamma_{\alpha\alpha}}{2\gamma_{\alpha\beta}}$

Si $\gamma_{\alpha\beta}$=500 mJ/m^2 et $\gamma_{\alpha\alpha} = 600$ mJ/m^2

The wettability angle θ\thetaθ is : θ = 33,56°

f(θ) = 0.208

Answers for Exercise 2

The temperature change curves versus time for the three treatments are shown in Fig. IV-11-

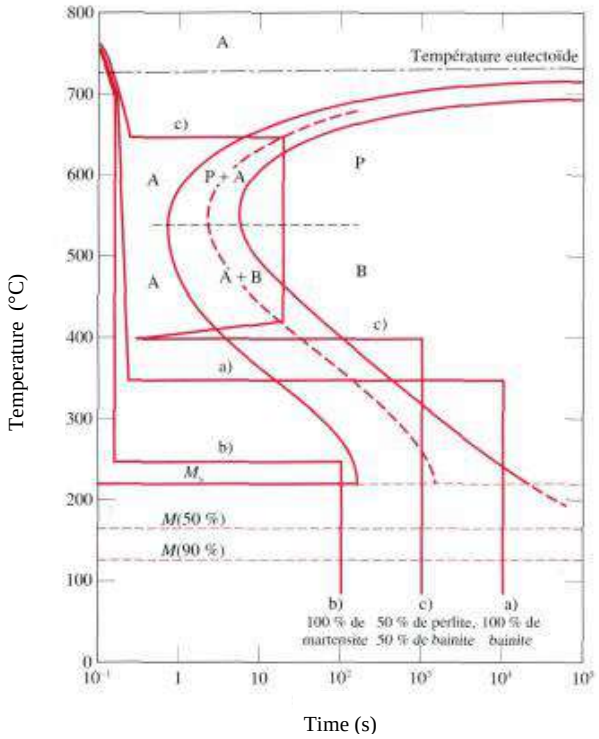

Fig. IV-11-

a) At 350°C, the transformation of austenite into bainite is isothermal. It begins after about ten seconds and ends approximately 500 seconds later. Therefore, after the 104 seconds specified in the problem, the sample contains only bainite. This means that no further transformation is possible, even if the subsequent rapid cooling curve crosses into the region of the diagram corresponding to martensite.
b) At 250°C, the transformation to bainite begins after approximately 150 seconds. This means that after 100 seconds, the sample still contains only austenite. Once cooling lowers the sample temperature to about 215°C or below, the instantaneous transformation of austenite to martensite begins and progresses. As a result, when the sample reaches room temperature, the final microstructure consists solely of martensite.
c) In the case of the isothermal curve at 650°C, pearlite formation begins after approximately 7 seconds. After 20 seconds, about 50% of the austenite initially present in the sample has transformed into pearlite. The vertical line represents the rapid cooling to 400°C, during which the amount of austenite transforming into pearlite or bainite is very small or even zero,

despite the cooling curve passing through the regions of the diagram corresponding to pearlite and bainite. At 400°C, the elapsed time measurement is reset to zero. After 10 seconds, the austenite that was still present in the sample (about 50%) has completely transformed into bainite. Since no austenite remains in the sample, any further transformation is impossible during the rapid cooling to room temperature. The final microstructure thus consists of pearlite and bainite in equal proportions, with 50% of each.

Answers for Exercise 3

1. $f = 1 - e^{-(Kt)^n}$

$$nln\left(\frac{t_2}{t_1}\right) = ln\left(\frac{ln(1-f_2)}{ln(1-f_1)}\right)$$

$$n = \frac{n\left(\frac{ln(1-f_2)}{ln(1-f_1)}\right)}{ln\left(\frac{t_2}{t_1}\right)}$$

2. Determination of n and K:

$$lnln\left(\frac{1}{(1-f)}\right) = nlnt + lnK$$

Solving gives n=3.22

K= $1.11 \times 10^{-9}.s^{-3.22}$

Chapter

V

Role of elastic strain energy and Interfacial energy

V-1. Introduction

During a first-order phase transformation, a heterogeneous state appears, even though the initial and final states are single-phase. After the formation of the new phase nucleus, the transformation is manifested by the movement of the interface boundary between the two phases. The energy level of the interface boundary and its properties are determined by the atomic structure of the boundary (including the degree of disorder) and the difference in chemical composition between the adjacent phases. It is evident that the greater the difference in the atomic structure of the phases (including differences in interatomic distances and coordination) and the nature of the atoms, the higher the interface energy will be.

V-2. Total coherent, semi-coherent, and incoherent

In crystals, different phases can be distinguished by the crystallographic directions along which interatomic directions are coincident. Examples of complete coincidence (in all three directions) in the arrangement of atoms include the formation of ordered domains or when a phase arises from a solid solution, which is isomorphic to the matrix but differs in composition. In such cases, we can speak of total coherence between the lattice of the new phase and the old phase (see Figure V-1-a).

Differences in specific volumes (atomic radii and interatomic distances) lead to elastic deformation. Lattice mismatch (ε) during the growth of the new phase crystal can result in the formation of dislocations, which reduce this elastic deformation (see Figure V-1-b).

$$\varepsilon = \frac{(a_p - a_M)}{a_M} \qquad \text{(V-1-)}$$

a_p: is the lattice parameter of the precipitated phase
a_M: is the lattice parameter of the matrix

The formation of a coherent interface is influenced by the energy gain, which depends on the degree of lattice mismatch between adjacent phases (see Fig. V-1-a). In most phases, each atom has an optimal arrangement of nearest neighbors that results in low energy. However, at the interface, there is typically a change in composition, causing each atom to interact with incorrect neighbors across the interface. This mismatch increases the energy of the interface atoms and contributes to the overall interface energy, denoted as γ_{ch}. For a coherent interface, this is the primary contribution, i.e.:

$$\gamma_{(coherent)} = \gamma_{ch} \qquad \text{(V-2-)}$$

In general, coherent interfacial energies can be up to about 200 mJ/m². When the atomic spacing at the interface is not identical, coherence can still be maintained by applying stress to one or both lattices, as illustrated in Fig. V-1-(a). The resulting lattice distortions are referred to as coherency strains.

The strains associated with a coherent interface increase the total energy of the system. When the atomic mismatch or interfacial area becomes sufficiently large, it becomes energetically more favorable to replace the coherent interface with a semi-coherent interface, as shown in Fig. V-1-(b).

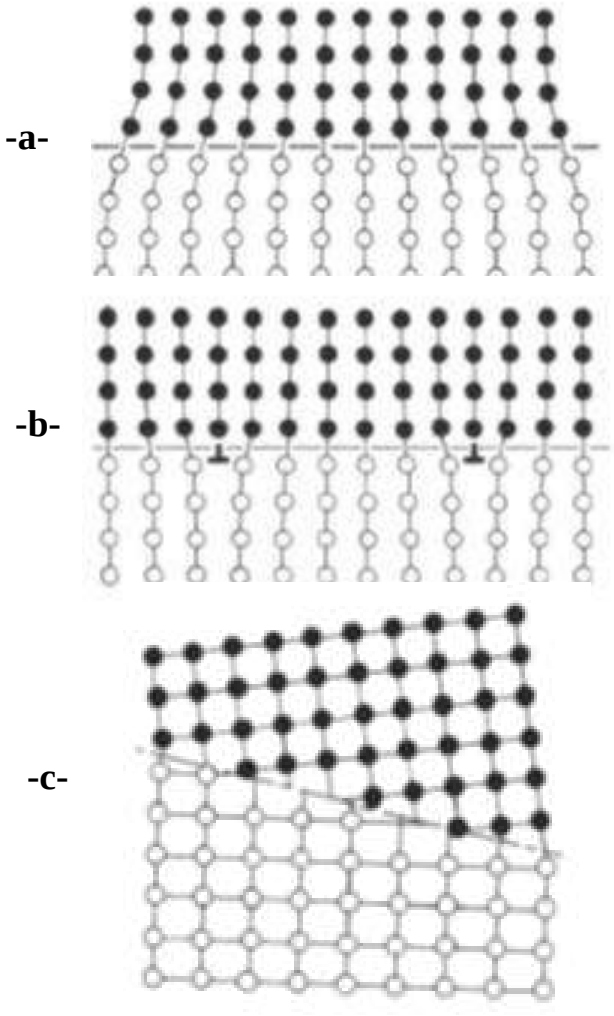

Fig. V-1-: Interfaces: (a) coherent (with a slight offset leading to coherence constraints in adjacent lattices), (b) semi-coherent, (c) incoherent

If d_α and d_β are the unconstrained interplanar spacings of the corresponding planes in the α and β phases, respectively (see Fig. V-2), the misfit between the two lattices is defined by:

$$\delta = \frac{d_\beta - d_\alpha}{d_\alpha} \qquad \text{(V-3-)}$$

It can be shown that, in one dimension, the lattice misfit can be fully compensated without generating a long-range strain field by introducing a set of edge dislocations with a distance D between them, given by:

$$D = \frac{d_\beta}{\delta} \qquad \text{(V-4-)}$$

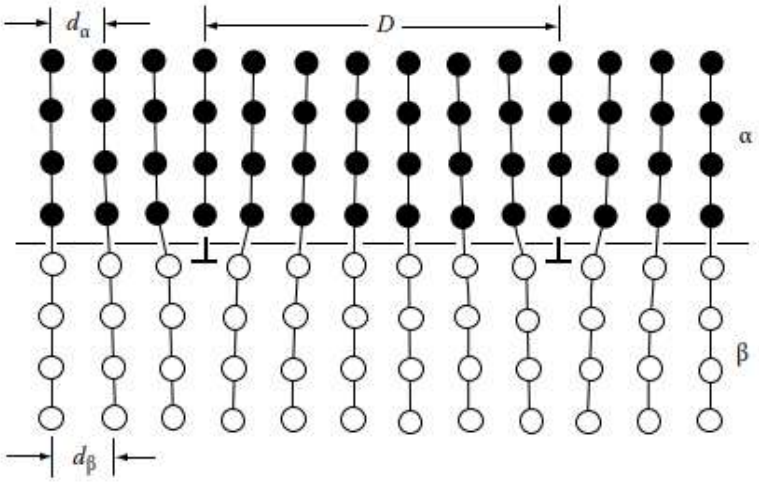

Fig. V-2-: Semi-coherent interface: The misfit parallel to the interface is compensated by a series of edge dislocations.

For small d,

$$D \cong \frac{b}{\delta} \qquad \text{(V-5-)}$$

Where b is the dislocation Burgers vector:

$$b = \frac{(d_\alpha + d_\beta)}{2} \qquad \text{(V-6-)}$$

The interfacial energy of a semi-coherent interface can be approximately viewed as the sum of two components: (a) a chemical contribution, γ_{ch}, similar to that of a fully coherent

interface, and (b) a structural term, γ_{st}, which represents the additional energy due to structural distortions caused by dislocations, i.e.:

$$\gamma_{\text{(semi-coherent)}} = \gamma_{ch} + \gamma_{st} \qquad \text{(V-7-)}$$

Equation (V-4) shows that as the shift δ increases, the spacing between dislocations decreases. For small values of δ, the structural contribution to the interfacial energy is approximately proportional to the dislocation density at the interface, i.e., for small δ, $\gamma_{st} \propto \delta$.

As the spacing between dislocations decreases, the associated strain fields increasingly overlap and cancel each other out. The energies of semi-coherent interfaces generally range from 200 to 500 mJ/m².

The introduction of additional dislocations disrupts the partial coherence, resulting in a completely incoherent interface (see Fig. V-1-c).

In general, incoherent interfaces occur when two randomly oriented crystals are joined along any interface plane, as shown in Figure V-1-c. However, they can also arise between crystals with an orientation relationship if the interface structure differs between the two crystals.

As the particles reach a sufficiently large size, lattice coherence is lost. The decrease in elastic energy is associated with the formation of accommodation dislocations at the grain boundaries.

Complete relaxation of elastic stresses is achieved once a sufficient number of dislocations have formed, such that the distance between them is:

$$l = \frac{b}{\varepsilon} \qquad \text{(V-8-)}$$

Where b is the Burger vector of the dislocations,

The mechanisms for the formation of dislocations can vary between different particles:

- Formation of prismatic loops around the particles within the matrix.
- Creation of dislocation loops inside the precipitates through the condensation of point defects.
- Generation of accommodation dislocations at the interface itself.

- Attraction of pre-existing dislocations from the matrix to the interface.

V-3- Characteristics of the phases formed by precipitation

The concepts of order, orientation relations, and coherence are crucial for describing the characteristics and properties of precipitates within a matrix.

A phase is considered *ordered* if its constituent atoms are arranged according to the geometric pattern of the crystallographic structure, with each crystallographic site occupied by a specific type of atom. This is known as long-range order. If there are fluctuations or deviations in the chemical assignment, the compound exhibits only short-range order. In the extreme case where atoms are arranged randomly on the crystallographic lattice, the phase is termed *disordered*.

Ordered precipitates typically consist of defined stoichiometric compounds with a restricted range of chemical compositions, which is characteristic of most equilibrium compounds. Metastable precipitates, which form during aging or tempering treatments, are often ordered.

Another important characteristic of structural precipitation is the nearly systematic presence of preferential crystallographic orientation relations between the matrix and the precipitates. These relations arise either from homogeneous precipitation or from heterogeneous precipitation on dislocations, sub-grain boundaries, or specific grain boundaries or phases within the matrix. This is particularly evident in epitaxial relations, where there is a parallel alignment between the crystallographic planes or directions of the matrix and those of the precipitates.

Finally, precipitates are considered coherent if there is geometric continuity between the crystallographic lattices of the matrix and the precipitates in all crystallographic directions. In this case, only the atomic arrangement within the lattice is altered (see Fig. V-3-a).

In aluminum alloys, coherent precipitation is the initial stage of homogeneous precipitation, occurring either during or after the formation of GP (Guinier-Preston) zones. Coherent precipitates are typically very small, generally up to 5 nm in size, unless the deviation from coherence is minimal. For GP zones, this deviation is relatively small, ranging from 0.1% to 1%.

When the coherence misfit is too high, dislocations become geometrically necessary at the precipitate-matrix interfaces to accommodate the elastic distortions. This mechanism is observed in precipitates with a significant coherence misfit, which is common in heterogeneous precipitation induced by crystallographic defects and can also result from the excessive growth of initially coherent precipitates. In such cases, the orientation relationships are semi-coherent, meaning that the lattice of the matrix and the precipitates are coherent only along a few specific planes or crystallographic directions (see Fig. V-3-b).

Finally, precipitates are considered incoherent if there is no specific crystallographic orientation relationship between the lattice of the matrix and that of the precipitate (see Fig. V-3-c). This represents the final stage of precipitation, typically resulting in equilibrium phases. An example of an incoherent precipitate is the θ ($CuAl_2$) phase in Al-Cu alloys. Although there is an orientation relationship between the θ precipitate and the aluminum matrix, this is likely due to the fact that θ forms from the θ' phase, rather than indicating that θ is semi-coherent with the matrix.

- **Precipitation at grain boundaries**

Particular situations arise when a second-phase particle is located at a grain boundary, as it requires considering the formation of interfaces with two differently oriented grains. Three possibilities can then occur (see Fig. V-4): (1) the precipitate may have incoherent interfaces with both grains, (2) it may have a coherent or semi-coherent interface with one grain and an incoherent interface with the other, or (3) it may have a coherent or semi-coherent interface with both grains. The first two cases are commonly encountered, while the third possibility is less likely.

The minimization of interfacial energy in these cases results in planar or slightly curved semi-coherent or coherent interfaces, and somewhat curved incoherent interfaces. An example of a grain boundary precipitate is shown in Fig. V-5.

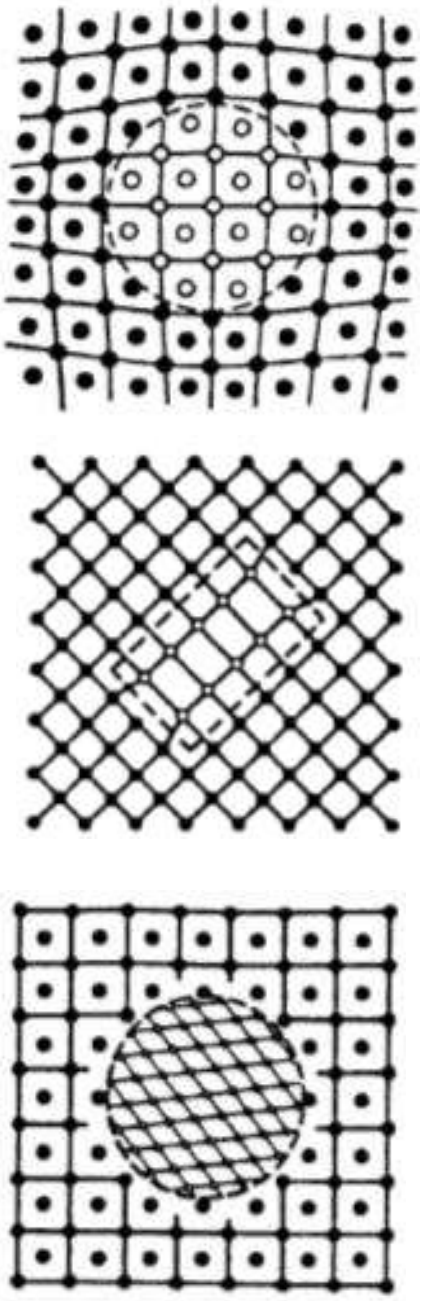

-a-

-b-

-c-

Fig. V-3- : (a) Coherent precipitate with lattice distortion due to volume variation

(b) Semi-coherent precipitate

(c) Incoherent precipitate

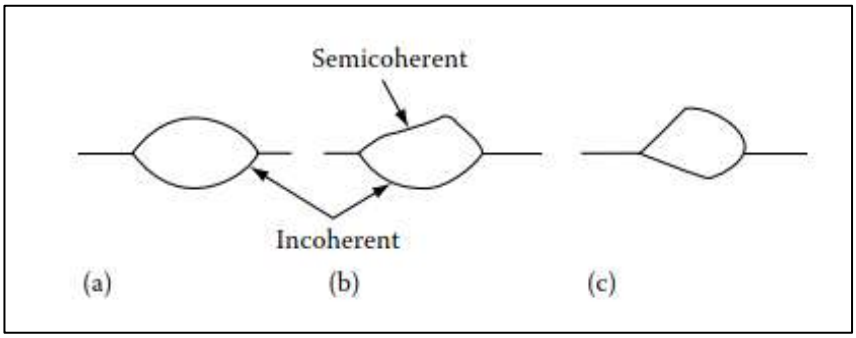

Fig. V-4-: Possible morphologies for grain boundary precipitates include:

- *Incoherent interfaces*: Slightly curved
- *Coherent or semi-coherent interfaces*: Planar

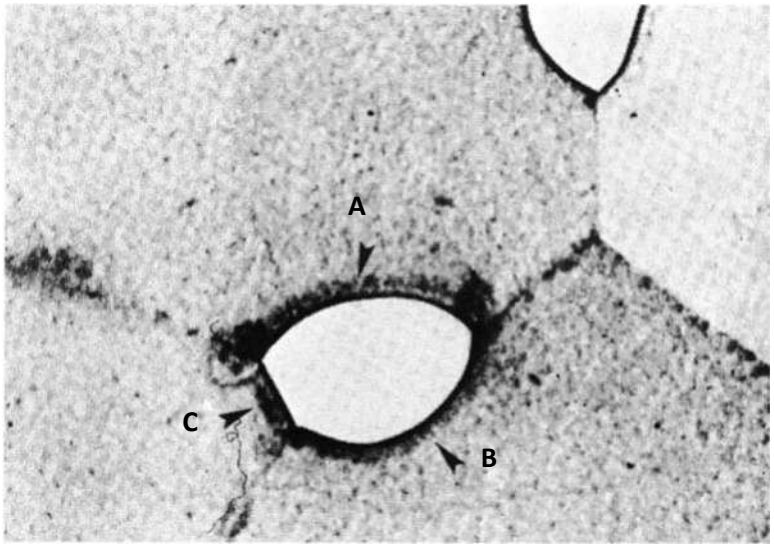

Fig. V-5-: A precipitate at a grain boundary triple point in an α-β Cu-In alloy, where interfaces A and B are incoherent, while interface C is semi-coherent (×310) *(After G.A. Chadwick, Metallography of Phase Transformations, Butterworths, London, 1972.)*

V-4- Misfit Strain effects

When a misfit is present, the formation of coherent interfaces increases the free energy of the system due to the elastic strain fields that develop. If this elastic strain energy is denoted as ΔGs, the equilibrium condition is given by:

$$\sum A_i \gamma_i + \Delta G_s = minimum \qquad \text{(V-9-)}$$

The origin of coherence constraints for a misfitting precipitate is illustrated in Fig. V-6. If the circled matrix volume in Figure V-6-(a) is sheared and the matrix atoms are replaced by

smaller atoms, the sheared volume will experience a uniform negative expansion strain toward an inclusion with a smaller lattice parameter, as shown in Figure V-6-(b). To achieve a fully coherent precipitate, the matrix and the inclusion must be subjected to equal and opposite strains, as depicted in Fig. V-6-(c).

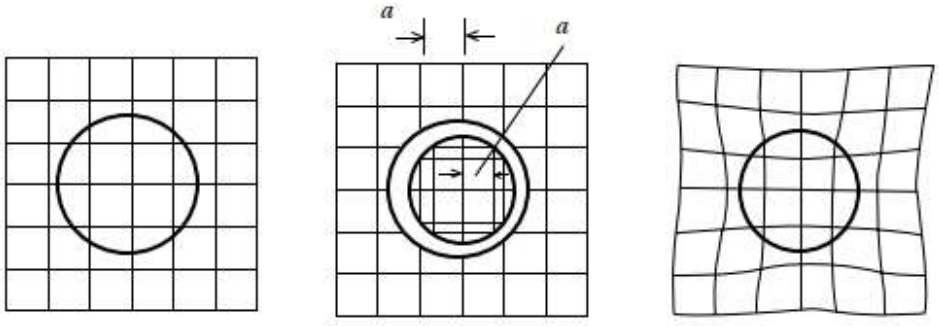

Fig. V-6-: The origin of coherence constraints.

If the lattice parameters of the unconstrained precipitate and the matrix are a_β and a_α, respectively, the unconstrained misfit δ is defined by:

$$\delta = \frac{a_\beta - a_\alpha}{a_\alpha} \qquad \text{(V-10-)}$$

However, the constraints that maintain coherency at the interfaces deform the lattice of the precipitate. For a spherical inclusion, this distortion is purely hydrostatic, meaning it is uniform in all directions, resulting in a new lattice parameter a_β'. The misfit with this constraint, denoted as ε, is defined by:

$$\varepsilon = \frac{a'_\beta - a_\alpha}{a_\alpha} \qquad \text{(V-11-)}$$

If the elastic moduli of the matrix and the inclusion are equal and the Poisson's ratio is 1/3, then ε and δ:

$$\varepsilon = \frac{2}{3}\delta \qquad \text{(V-12-)}$$

In practice, the inclusion typically has elastic constants different from those of the matrix; however, ε generally falls within the interval: $0.5\,\delta < \varepsilon < \delta$.

When the precipitate is a thin disk, the in-situ misfit is not uniform in all directions. Instead, it is relatively large perpendicular to the disk and nearly zero within the plane of the broad faces, as shown in Figure V-7.

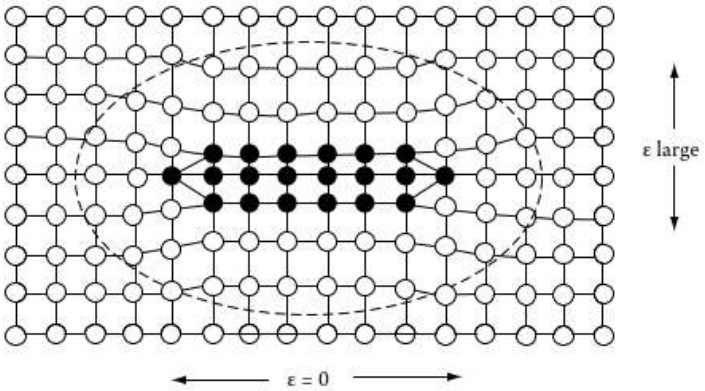

Fig. V-7-: For a coherent thin disk, the misfit is minimal parallel to the plane of the disk, with the maximum misfit occurring perpendicular to the disk.

In general, the total elastic energy depends on the shape and the elastic properties of both the matrix and the inclusion. However, if the matrix is elastically isotropic and the precipitate and matrix have equal elastic moduli, the total elastic strain energy ΔGs is independent of the precipitate's shape. Assuming a Poisson's ratio υ =1/3, it is given by:

$$\Delta G_s \cong 4\mu\delta^2 V \qquad \text{(V-13-)}$$

Where μ is the shear modulus of the matrix and V is the volume of the unstressed precipitate in the matrix. Therefore, the coherence strains generate an elastic strain energy that is proportional to the volume of the precipitate and increases with the square of the lattice misfit (δ^2).

When the inclusion is incoherent with the matrix, there is no effort to align the two lattices, and the lattice sites are not maintained across the interface. In such cases, there are no coherence constraints. However, misfit strains can still occur if the inclusion is not the correct size for the space it occupies (see Fig. V-8). In this scenario, the lattice shift δ\deltaδ is not significant, and it is more appropriate to consider the volume shift Δ, defined by:

$$\Delta = \frac{\Delta V}{V} \qquad \text{(V-14-)}$$

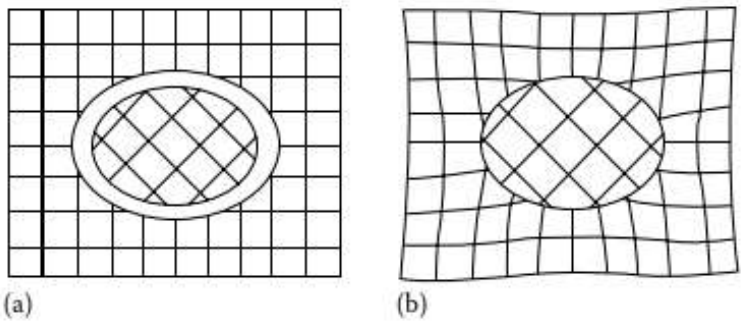

Fig. V-8-: The origin of misfit strain for incoherent inclusion

Nabarro provides the elastic strain energy for a homogeneous, incompressible inclusion in an isotropic matrix as:

$$\Delta G_s = \frac{2}{3}\mu\Delta^2 V f\left(\frac{c}{a}\right) \qquad \text{(V-15-)}$$

Where μ is the shear modulus of the matrix.

Thus, the elastic strain energy is proportional to Δ^2. The function f (c/a) accounts for shape effects and is illustrated in Fig. V-9. For a given volume, a sphere (c/a=1) has the highest strain energy, while a thin, flattened spheroid (c/a→0) has very low strain energy. A needle-like shape (c/a→∞) has strain energy between the two extremes. Therefore, the equilibrium shape of an incoherent inclusion will be an oblate spheroid with a c/a value that balances the competing effects of interfacial energy and strain energy. When Δ is small, the effects of interfacial energy should dominate, leading the inclusion to be approximately spherical.

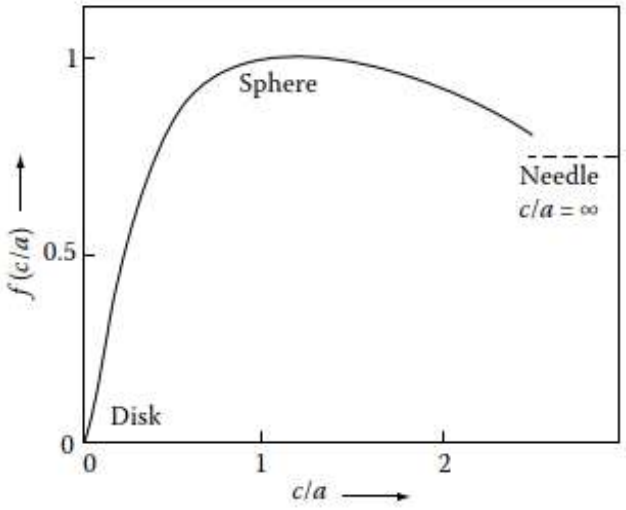

Fig. V-9- : The variation of f(c/a). *(After F.R.N. Nabarro, Proceedings of the Royal Society A, 175 (1940) 519.)*

V-5- Loss of coherence

Precipitates with coherent interfaces exhibit low interfacial energy, but they are associated with coherent strain energy in the presence of misfit. Conversely, if the same precipitate has non-coherent interfaces, it will exhibit higher interfacial energy. Now, consider which state yields the lowest total energy for a spherical precipitate with misfit δ and radius r.

The free energy of a crystal containing a fully coherent spherical precipitate includes contributions from:

- The coherence strain energy, described by the following equation,
- The interfacial chemical energy γ_{ch}.

The sum of these two terms is given by:

$$\Delta G_{coh} = 4\mu\delta^2 \frac{4}{3}\pi r^3 + 4\pi r^2 \gamma_{ch} \qquad \text{(V-16-)}$$

If the same precipitate has incoherent or semi-coherent interfaces, there will be no mismatch energy, but there will be an additional structural contribution to the interfacial energy γ_{st}. The total energy in this case is given by:

$$\Delta G_{non-coh} = 0 + 4\pi r^2(\gamma_{ch} + \gamma_{st}) \qquad \text{(V-17-)}$$

For a given δ, $\Delta G_{(coherent)}$ and $\Delta G_{(non\text{-}coherent)}$ vary with r as shown in Fig. V-10. When small, the coherent state provides the lowest total energy, while for large precipitates, it is more favorable for them to be semi-coherent or incoherent (depending on the magnitude of δ). At the critical radius (r_{crit}); $\Delta G_{(coherent)} = \Delta G_{(non\text{-}coherent)}$, giving:

$$r_{crit} = \frac{3\gamma_{st}}{4\pi\delta^2} \qquad \text{(V-18-)}$$

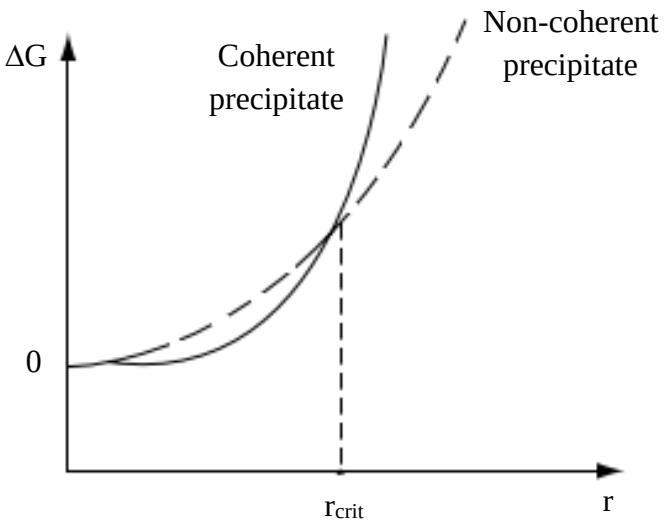

Fig. V-10-: Total energy of the matrix plus precipitate as a function of the radius of the precipitate, for both coherent and non-coherent spherical precipitates (semi-coherent or incoherent).

- **Characteristics of the phases formed during precipitation and their modulated structure**

These structures are formed, for example, during the demixing of solid solutions. In binary alloys such as Ni-Al, Ni-Ti, Ni-Au, and ternary alloys like Cu-Ni-Fe and Fe-Ni-Al, two new isomorphic phases with different compositions are formed. The dependence of the lattice parameter on the concentration follows Vegard's law:

$$a = a_0(1 + q_0 C) \qquad \text{(V-19-)}$$

Where:

a_0 is the lattice parameter of one of the constituents.

q_0 is the expansion coefficient of the lattice.

C is the concentration of the 2nd component.

Differences in composition and thus in lattice parameters inevitably lead to the imposition of constraints. It can be demonstrated that, in terms of elastic energy, the formation of complexes consisting of alternating lamellae, enriched and depleted in one of the elements, is more favorable than the formation of separate phases in the form of independent discs.

Practice exercises

Exercise 1:

Mg can dissolve in Al to form a substitutional solid solution. However, Mg atoms are larger than Al atoms, and therefore each Mg atom distorts the surrounding Al lattice, creating a stress field that effectively exists around each Mg atom.

- Show the strain energy in kJ mol^{-1} and eV $atom^{-1}$.
- What hypotheses are implicit in this calculation?

We give: The shear modulus of μ_{Al} = 25GPa, r_{Al} = 1,43 Å, r_{Mg} = 1,60 Å.

Exercise 2:

Figure -1- shows the various phases, both stable and metastable, present in the Al-4 at.% Cu alloy. These phases are presented in the figure, not necessarily in the chronological order of their formation.

- Characterize the interfaces for each phase and indicate which phases are expected to germinate most easily. Deduce the hardening precipitation sequence in Al-Cu alloys.

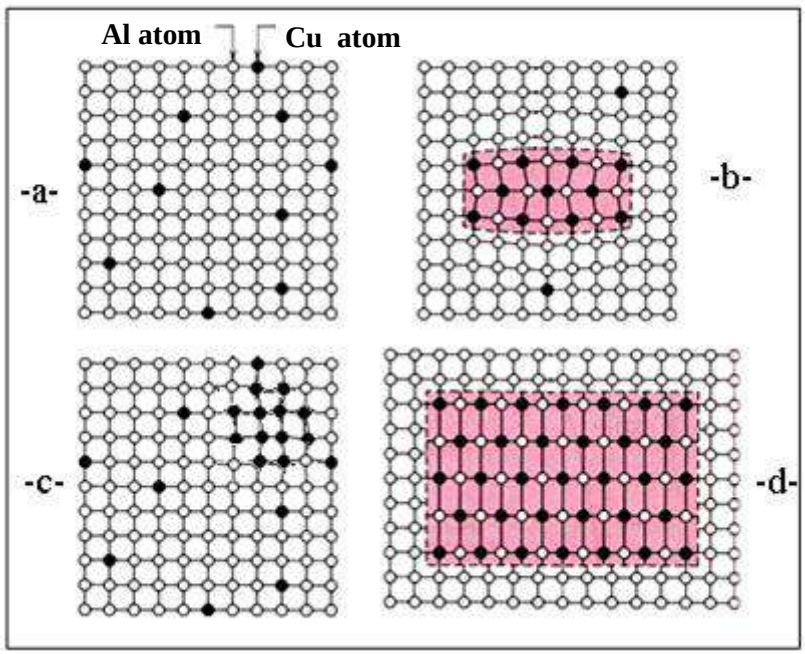

Figure 1

Exercise 3:

1. A coherent interface between a precipitate and a matrix is characterized by an interfacial energy γ_{ch}.
- What precipitate shape minimizes this surface contribution?
2. In reality, the lattice parameters of precipitates are not perfectly equal to the lattice parameter of the matrix, resulting in semi-coherent interfaces.
- What is the free energy associated with the presence of a spherical precipitate?
3. If the same precipitate has an incoherent (or semi-coherent) interface,
- What occurs?
- What is the free energy associated with the presence of this precipitate in this case?
4. For a given misfit δ, illustrate the variation of ΔG_{coh} and ΔG_{incoh}.
- What do you observe?

Answers

Answers for Exercise 1

$\Delta G_s \cong 4\mu\delta^2 V$

δ=0.119

V=1.225x10^{-29} m^3

μ_{Al} = 25 GPa=25x10^9 Nm^{-2}

ΔG_s = 10.5 kj.mol^{-1} = 0.1 eV.atom^{-1}

It is also implicitly assumed that individual Mg atoms are sufficiently spaced apart so that each atom can be considered isolated, i.e., in a dilute solution. The use of Equation 3.39 also relies on the assumption that the matrix surrounding a single atom behaves as a continuum.

Answers for Exercise 2

- GP zones are coherent with the matrix (fig. -3-c-).
- θ’ precipitates are semi-coherent with the matrix (fig. -3-b-).
- θ precipitates are incoherent with the matrix (fig. -3-d-).

- The precipitation sequence:

$\alpha \rightarrow \alpha_1 + GP \rightarrow \alpha_2 + \theta'' \rightarrow \alpha_3 + \theta' \rightarrow \alpha_4 + \theta$

Answers for Exercise 3

1- The shape that minimizes this surface contribution is a sphere.

2- Elastic deformation is necessary to accommodate the atoms at the interface, resulting in additional energy due to this deformation.

The free energy associated with the presence of a coherent spherical precipitate consists of two contributions:

- the deformation energy: $\Delta G_{st} = 4/3\pi r^3 * 4\mu\delta^2$
- the interface energy: $\Delta G_{ch} = 4\pi r^2\gamma_{ch}$

$$\mathbf{\Delta G_{coh} = 4/3\pi r^3 * 4\mu\delta^2 + 4\pi r^2\gamma_{ch}}$$

In this case, the precipitate is much less deformed, making its deformation energy negligible. However, a second term, γ_{st}, is added to the interface energy, which then becomes:

$$\Delta G_{ch} = 4\pi r^2(\gamma_{ch} + \gamma_{st})$$

hus, the total free energy for an incoherent precipitate is: $\mathbf{\Delta G_{incoh} = 4\pi r^2(\gamma_{ch} + \gamma_{st})}$

3-

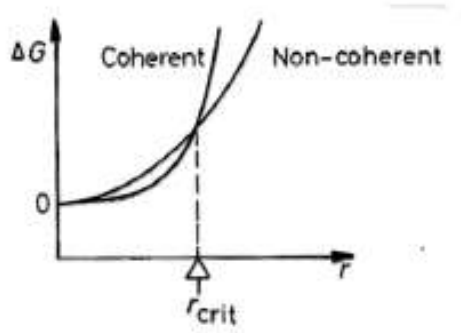

It is observed that a small precipitate is more favorably coherent, while a larger precipitate tends to be incoherent.

Chapter

VI

Mechanisms of crystal growth during diffusionless transformations

VI-1. Introduction

Phase transformations in the solid state can be categorized into two main types:

- *Diffusional Transformations*

These transformations involve the formation of a new phase through the breaking of atomic bonds in the initial phase and the subsequent redistribution of atoms within the solid. During diffusional transformations, atoms move over relatively long distances and their movement is essential for the process. In this type of transformation, diffusion is a crucial mechanism.

- *Diffusionless Transformations*

Also known as *athermal transformations*, diffusionless transformations do not require the diffusion of atoms over long distances but involve the displacement of a large number of atoms over short distances. In these transformations, there is no change in chemical composition, and they generally propagate independently of time. It should be noted that displacive transformations can occur during very rapid cooling.

In steels, phase transformations during cooling from the austenitic phase are of two types: diffusional transformations, which generally lead to the formation of ferrite and carbides, and displacive or martensitic transformations. The physical mechanism involved in the formation of these new phases depends on the temperature at which the transformation begins, which is a function of the cooling rate. Figure VI-1 illustrates the mechanisms of displacive and diffusional transformations.

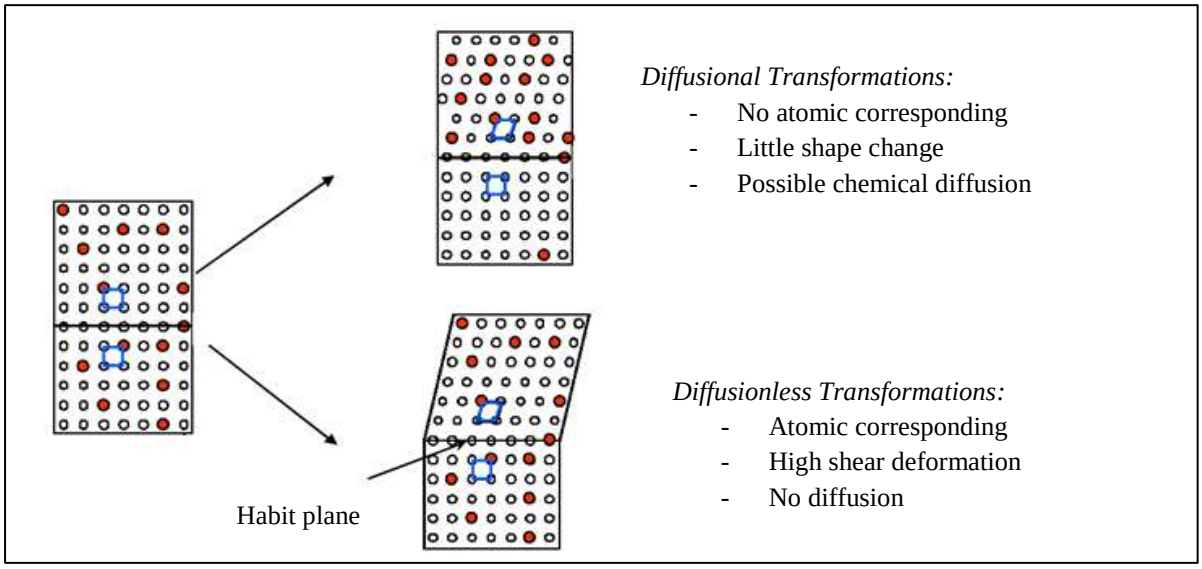

Fig. VI-1- : Illustration of the mechanisms of displacive and diffusional transformation.

VI-2. Normal transformation

The solid-state transformation kinetics are considered normal if the time and temperature dependencies of the transformation rate $V_{tr} = f(T, t)$ match those observed during the study of the crystallization process. During a decrease in temperature (for reactions that occur upon cooling), the rate of transformation initially increases and then decreases:

- The increase in the transformation rate is attributed to the ease of nucleation and the acceleration of growth as supercooling increases.
- The subsequent decrease in the transformation rate with further supercooling is explained by the reduced mobility of atoms as the temperature drops.

VI-3. Martensitic transformation

The term *martensite*, named after the physicist A. Martens, refers to the product formed by the quenching of carbon steel from the high-temperature phase known as "austenite." The term has since been extended to describe products formed through similar mechanisms, even if these products have structures quite different from those of steels (such as certain metal alloys). The structure of the martensite phase results from a transformation of the crystallographic lattice that occurs in the absence of atomic diffusion. This transformation is known as martensitic transformation.

The martensitic transformation is a first-order transformation that occurs without diffusion, through the shearing of entire groups of atoms. This process is externally manifested by the appearance of an acicular microrelief on the surface of a metal cut. As such, the martensitic transformation is classified as a displacive phase transformation in the solid state. During these transformations, atoms maintain their relative positions, with each atom retaining the same neighbors and not moving more than an interatomic distance. The progression of the transformation is driven by the movement of the interfaces between the phases, at a rate limited by the speed of sound in the material. In martensitic transformations, lattice distortion (deformation) is more significant than atomic rearrangement.

Martensitic transformation induces transformation strain. Specifically, directly above each martensite wafer, the metal surface exhibits tilting, and any straight line drawn on the surface of the austenite will show bending as it passes through the martensite crystallites after transformation (see Figure VI-2-(a) and VI-2-(b)). The measured transformation strain is a

plane-invariant strain characterized by a large shear component and a small expansion directed normal to the invariant plane. The rate of transformation is described by:

$$Y = 1 - exp[-\alpha M_s - T] \qquad \text{(VI-1-)}$$

α: coefficient and $T < T_{Ms}$

The M_f point designates the temperature below which martensite no longer forms. While M_f cannot be precisely determined, it is often approximated as $M_f = M_s - 215°C$. Martensite is carbon-saturated compared to equilibrium ferrite; it is a solid solution of carbon within a centered quadratic Q.C lattice of the ferrite, where c/a=1+0.045 x (% Carbon) by mass (Fig. VI-3-).

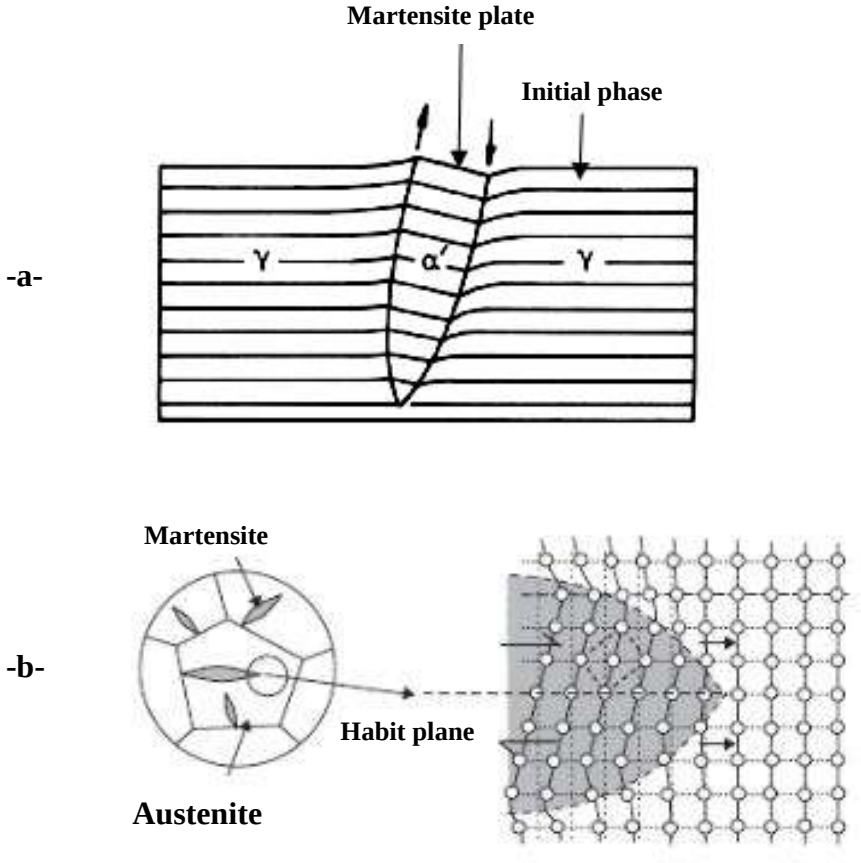

Fig. VI-2-: (a) Formation of Martensite α' from initial phase γ

(b) Simplified schematic representation of the martensitic transformation mechanism in iron.

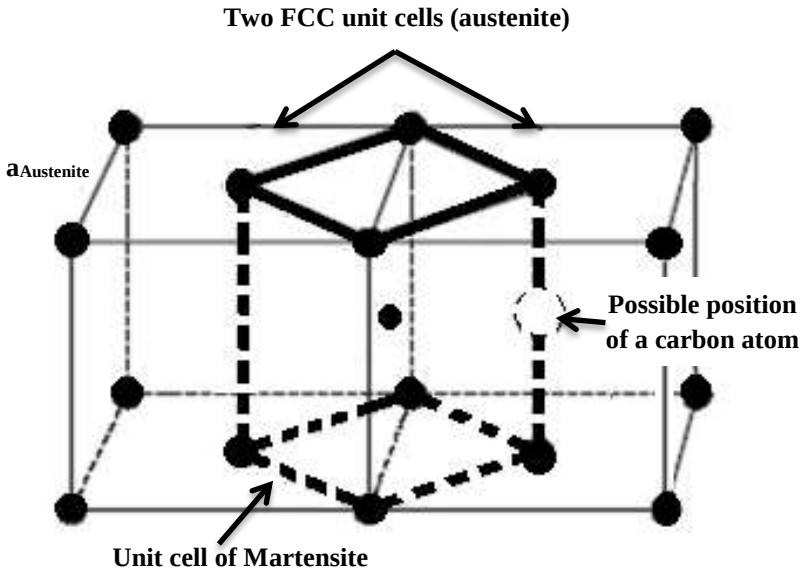

Fig. VI-3-: Schematic representation of the unit cell of martensite

❖ **Habit plane (adjoining plan)**

The interface between the initial phase and the martensite, on the macroscopic scale, is known as the invariant plane, also referred to as the *habit plane* or the adjoining plane. An invariant plane is characterized by two key conservation properties: its orientation remains unchanged by the transformation, and the relative atomic positions within this plane are preserved (i.e., distances and angles are conserved).

VI-3-1. General characteristics of martensitic transformation

The martensitic transformation has the following main characteristics:

1. It is a solid-state phase change resulting from homogeneous crystal lattice deformation. This deformation is not due to atomic diffusion but rather to a collective and cooperative movement of atoms over distances relatively small compared to the lattice parameters.
2. The transformation occurs almost instantaneously, with a rate comparable to the speed of sound in the solid.
3. The martensitic transformation results in changes to both the shape (shear) and volume of the specimen. For shape memory alloys, the volume change is minimal, while the shear is significant.
4. To minimize the energy between the formed martensite and the remaining austenite, martensite domains typically take the shape of flattened platelets. Martensite forms

preferentially on specific crystallographic planes, known as the limit plane, adjunction plane, or habit plane. These planes are associated with the shear of martensite. The domains formed generally exhibit a flattened platelet shape.

Figure VI-4 illustrates the various forms of martensite in steels as an example.

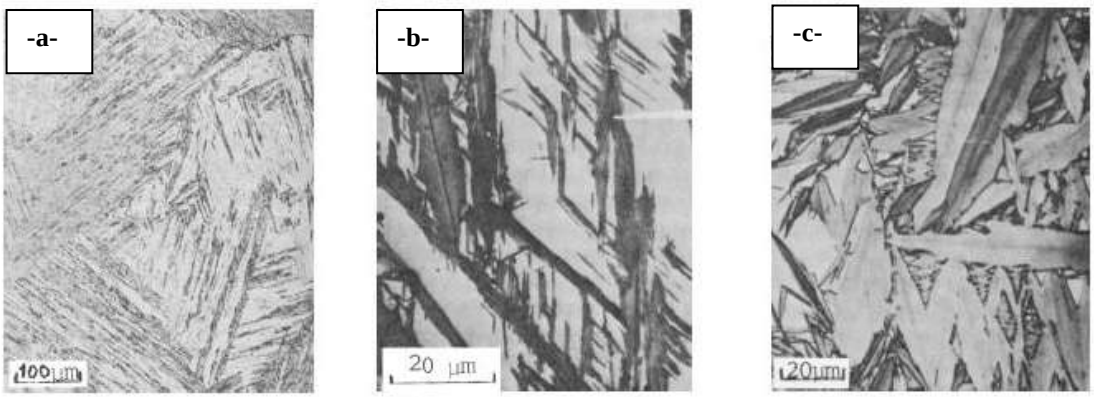

Fig. VI-4- : Different martensite morphologies in iron alloys: (a) low C (lath), (b) medium C (plate), (c) Fe–Ni (plate). *(D. A. Porter, K. E. Eastorting. Phase transformation in metals end alloys, second edition, Chapman et Hall, London, (1992))*

VI-3-2. Thermodynamic aspect of martensitic transformation

Before delving into the details of the martensitic transformation from a thermodynamic perspective, we will define the key characteristics, including the transformation temperatures and the extent of the transformation. The transition from the initial phase to the martensitic phase, and vice versa, is temperature-dependent. Critical temperatures characterizing the transformation process are defined as follows:

M_s: The start temperature of the direct transformation (austenite → martensite).
M_f: The end temperature of the direct transformation.

The direct martensitic transformation during cooling (austenite → martensite) begins at the temperature M_s (martensite start) and becomes complete at the temperature M_f (martensite finish). Since the transformation occurs without diffusion, the initial phase and the martensitic phase differ only in their crystallographic structures. Thus, the system can be considered as consisting of two solid phases with different crystallographic structures but identical chemical compositions.

The study of the variation in free enthalpy of these two phases, excluding deformation energies and surface energies, is illustrated in Figure VI-5. This can be expressed by the following relation:

$$\Delta G_{A\rightarrow M} = G_A - G_M \qquad \text{(VI-2-)}$$

G_M: the free energy of martensite

G_A: the free energy of austenite

In Figure VI-4, which presents Gibbs free energy as a function of temperature, it is evident that the martensitic transformation occurs when the free energy of martensite (G_M) is lower than the free energy of austenite (G_A), i.e., at temperatures below the critical temperature T_0. At T_0, the difference in the chemical free energy, $\Delta G_{A\rightarrow M}$, between the two phases becomes zero, establishing a thermodynamic equilibrium such that:

$$\Delta G_{A\rightarrow M} = G_A - G_M = 0 \qquad at\ T = T_0 \qquad \text{(VI-3-)}$$

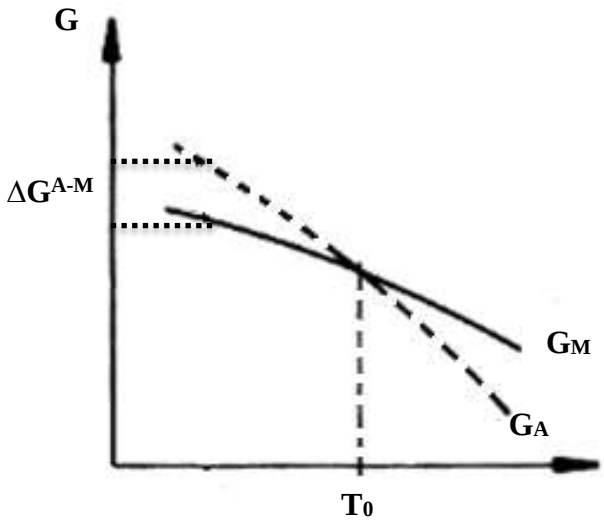

Fig. VI -4- : Gibbs energy of austenite and martensite as a function of temperature

However, in reality, the two phases are not entirely independent of each other; the martensitic transformation occurs through a mechanism of nucleation and growth. This implies the presence of interface energy between the two phases. The energy required to move this

interface contributes to the overall energy balance, creating an energy barrier that influences the progression of the transformation.

VI-4. Massive transformation

The martensitic mechanism assumes the absence of atomic redistribution, indicating a non-diffusional nature of the transformation in solid solutions. However, in complex component alloys, transformations can also occur without the redistribution of components between phases. This type of transformation is referred to as massive.

The immediate result of such a transformation is a single-phase state. In classic cases, during normal kinetics, the grains appear as massive blocks without distinct shapes or clear lines of separation. This characteristic led to the term "massive transformations."

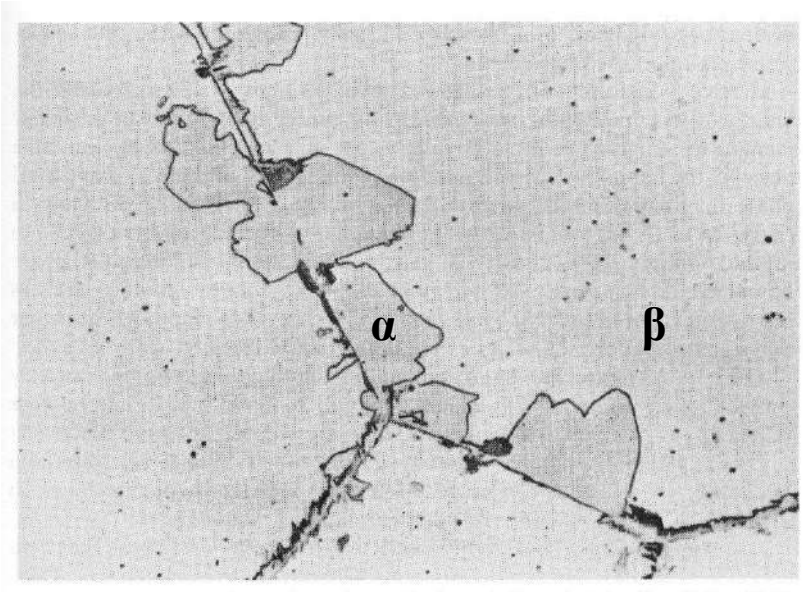

Fig. VI- 5- : Formation of the α phase by massive transformation at the grain boundaries of the β phase in the Cu-38.7% Zn alloy, quenched from 850°C. *(D. Hull, K. Garwood, the mechanism of phase transformations in metals, institue of metals. London (1956)*

The following table outlines the differences between the two types of transformations: diffusional and diffusionless.

Displacive transformation (or martensitic)	**Diffusive transformation**
- Atoms migrate over interatomic distances. - Atoms migrate by bond breaking and local rearrangement. - Atoms move individually and are not necessarily cooperative. - The rate of transformation is influenced by temperature and is typically governed by diffusion kinetics. - The transformed volume depends on both temperature and time. - The composition can change due to atomic diffusion. - The transformed phase may not always maintain crystallographic relationships with the initial phase.	- Atoms migrate over distances ranging from 1 to 10^6 interatomic distances. - Atoms move from site to site through activated thermal diffusion. - Atom movement is random. - The rate of transformation strongly depends on temperature and typically cannot occur below 0.3 to 0.4 T_f (where T_f is the melting point). - The transformed volume depends on both time and temperature. - Diffusion allows for composition changes in alloys. - There may be some crystallographic relationships between the phases.

Practice exercises

Exercise 1:

Calculate the volume percentage change resulting from martensite formation in a 1% C steel.

Exercise 2:

Sketch a diagram demonstrating the Bain model of homogeneous deformation during martensitic transformation of FCC → BCC. Supposing that a_γ = 3.56 Å, a_α = 2.86 Å and the ratio c/a = 1.1

- Calculate the maximum movements of atoms during the martensitic transformation.

Answers

Answers for Exercise 1

c/a=1+0.0467 × (% carbon)

Answers for Exercise 2

Diagram of the Bain deformation:

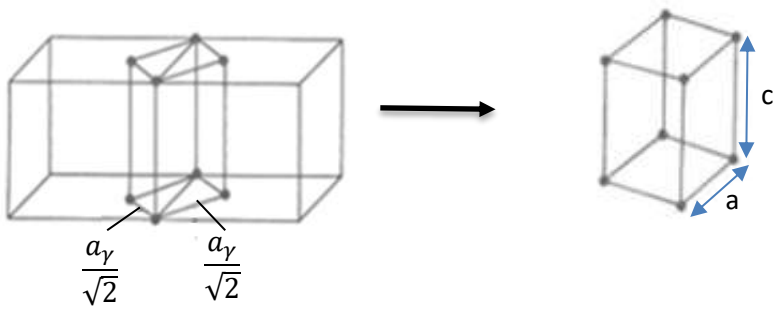

Austenite Martensite

Movements of atoms can be calculated as follows:

c/a = 1.1 and a_α = 2.86 Å, so c_α = 3.15 Å

$\frac{a_\gamma}{\sqrt{2}}$ = 2.52 Å

Movement of atoms along the vertical direction is: 3.56 – 3.15 = 0.41 Å

Movement of atoms along the horizontal direction is: 2.86 – 2.52 = 0.34 Å

Chapter

VII

Types of diffusional transformations

VII-1. Introduction

One of the solid-state phase transformations that is of particular interest to researchers today is the precipitation reaction. This reaction occurs in certain materials during heat treatment (such as tempering or aging) and imparts the material with its working properties.

Precipitation processes from supersaturated solid solutions, which involve diffusion phenomena, are generally classified into two main categories: discontinuous and continuous precipitation. In practice, homogeneous precipitation is rare; nucleation almost always begins on heterogeneities in the initial phase, which lower the free enthalpy of nucleation by reducing either surface energy, strain energy, or both. These heterogeneities can include impurities, inclusions, dislocations, surfaces, or grain boundaries. It is well established that the presence of lattice defects promotes nucleation, even under conditions where it would be unlikely to occur without these defects. Consequently, precipitate crystallites often form on these defects before those resulting from homogeneous precipitation. During discontinuous precipitation, the initial supersaturated phase, which maintains a constant solute concentration, coexists with the precipitation products. These products correspond to equilibrium phases with compositions determined by equilibrium at the given temperature. Thus, a concentration discontinuity exists at the interfaces between regions that have undergone the decomposition reaction and those that have not yet undergone it.

VII-2- Definition of precipitation

The precipitation of a supersaturated solid solution is a solid-state transformation that results in an increase in the number of phases. It generally involves the decomposition of the supersaturated solid solution (the initial matrix) into two new phases:

- The depleted matrix
- The precipitated phase

It follows that an alloy, which may be single-phase at a certain temperature, can become two-phase at lower temperatures. The supersaturated homogeneous alloy is relatively soft, with low hardness and elastic limit. However, the precipitation of a second phase induces structural hardening, which increases both the hardness and the elastic limit of the material.

To initiate a precipitation reaction, the following three steps must be carried out:

1. **Homogenization Treatment**: This step eliminates any segregation within the alloy and achieves a homogeneous single-phase system. The homogenization temperature is selected to be above the solubility limit, within the single-phase range.
2. **Quenching**: The homogenized alloy is rapidly cooled to obtain a single non-equilibrium phase known as a supersaturated solid solution. This solution contains more solute than the equilibrium solid solution at this temperature and may also experience additional supersaturation in vacancies.
3. **Aging**: The alloy is then heated to a temperature within the two-phase range, causing the formation of one or more new phases.

Homogenization treatment is used to eliminate any segregation in the alloy and achieve a homogeneous single-phase system. This is done at a temperature above the solubility limit, within the single-phase domain.

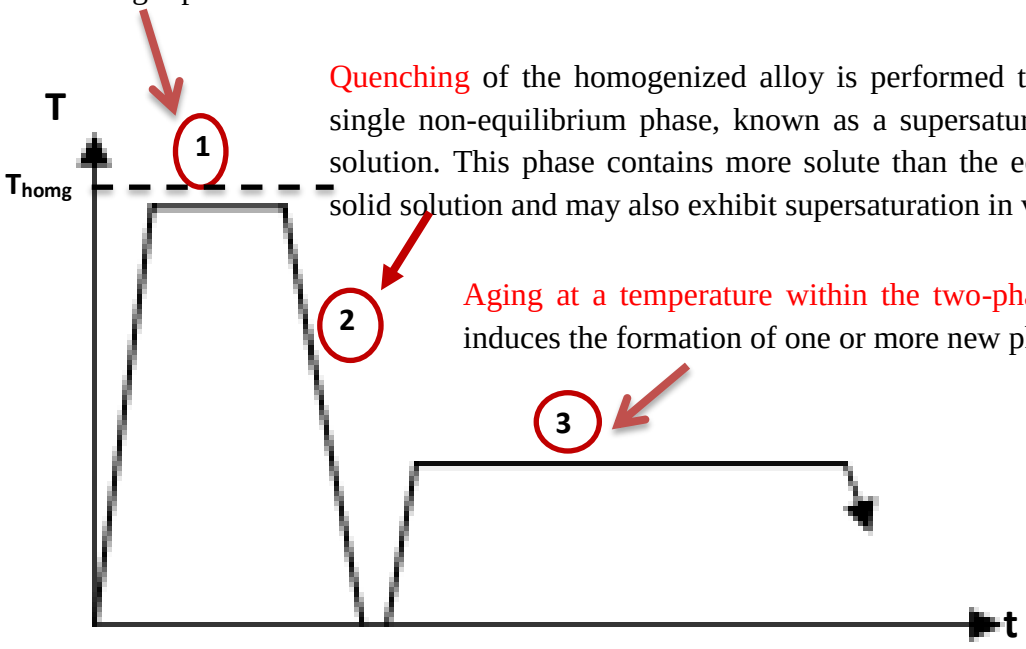

Quenching of the homogenized alloy is performed to obtain a single non-equilibrium phase, known as a supersaturated solid solution. This phase contains more solute than the equilibrium solid solution and may also exhibit supersaturation in vacancies.

Aging at a temperature within the two-phase range induces the formation of one or more new phases.

Fig. VII-1- : Schematic representation of the precipitation steps

There are generally two types of precipitation, as indicated in the introduction:

- **Continuous Precipitation**: In this process, the supersaturated solid solution depletes in a theoretically homogeneous and continuous manner throughout the matrix. The lattice parameter evolves continuously. Occasionally, continuous precipitation occurs

predominantly at grain boundaries and slip planes, in which case it is referred to as localized or heterogeneous precipitation.

- **Discontinuous Precipitation**: This type of precipitation is characterized by the formation of two distinct regions during the transformation:
    - One region where the transformation is complete.
    - Another region where the solid solution remains supersaturated.

The transformation typically starts at the grain boundaries, leading to the development of cells, hence the term cellular precipitation. During this process, the lattice parameter changes discontinuously, taking on two distinct values.

VII-3. Characteristics of Precipitation

VII-3-1. Criteria for composition and sequence of heat treatments for alloys

Consider a binary aluminum-element (Al-M) alloy as illustrated in Figure VII-2-. For an alloy with a concentration X_1 (where X_1 is lower than the solubility limit X_S of the solute element M), and at a temperature T_1 that is higher than the solidus temperature T_S, the alloy should be maintained at this temperature for a sufficient duration to achieve thermodynamic equilibrium. This will ensure the complete dissolution of the solute atoms M.

When the alloy is cooled very slowly from temperature T_1 to a temperature below T_S, the solid solution of M in aluminum, which retains its face-centered cubic (FCC) structure (denoted as α), tends to decompose. This decomposition results in the formation of relatively coarse particles of the stable intermetallic compound Al_xM_y within a solid solution of aluminum that is now poor in M atoms. This equilibrium precipitation leads to a structure similar to that obtained during annealing. However, this structure is generally of limited interest for alloy hardening due to the large size of the precipitates (on the micrometer scale) and their relatively low number per unit volume of the alloy. The molar fraction f_m of the precipitates follows the lever rule or the rule of inverse segments.

$$f_m = \frac{BA}{BC} \qquad \text{(VII-1-)}$$

Where BA and BC are defined in figure VII-2-, at temperature T_2.

- The quenching operation involves rapidly cooling the alloy after dissolution to prevent the decomposition of the solid solution and the formation of coarse equilibrium

precipitates. Quenching also traps the numerous vacancies that are stable at high temperatures. Upon quenching to room temperature T_2 (see Figure VII-2-), a supersaturated solid solution is obtained, where the solute atoms M and vacancies are randomly distributed within the face-centered cubic (FCC) lattice of aluminum. This results in a supersaturated solid solution, as illustrated in Figure VII-3-a-.

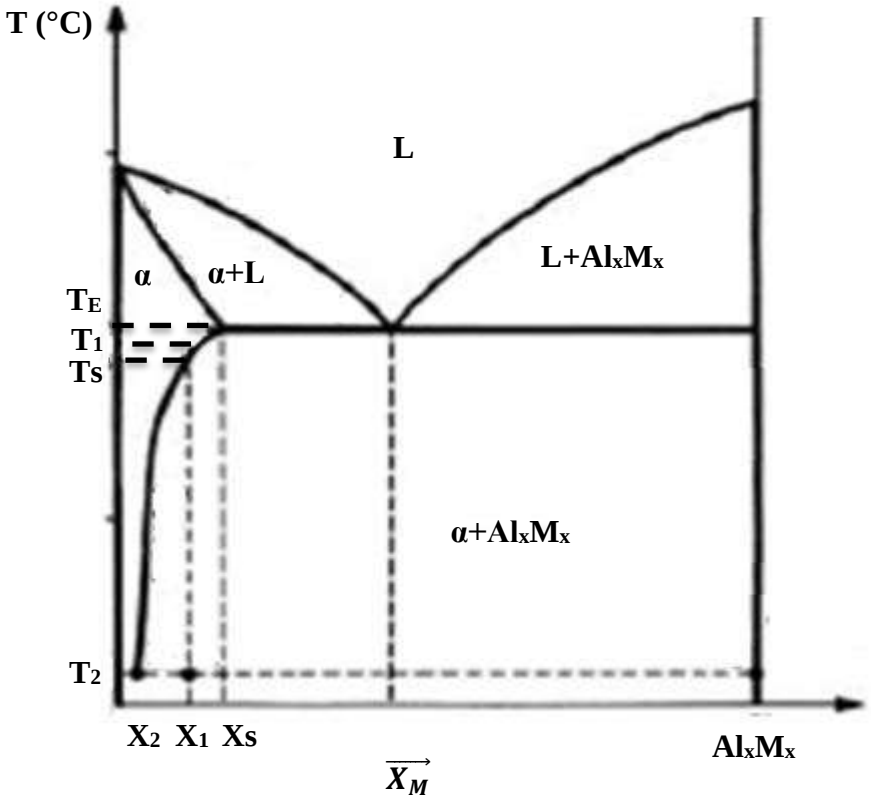

Fig. VII-2- : Principle of heat treatment for hardening aluminum alloys through precipitation in a binary phase diagram.

After dissolution and quenching, hardening through precipitation results from the decomposition of the supersaturated solid solution into its main solute elements. During aging at room temperature or at a low temperature following quenching, the supersaturated solid solution is metastable. This phase, known as natural aging or maturation, involves the gradual and spontaneous hardening of the alloy. The solid solution decomposes to form small clusters of solute atoms, known as *Guinier-Preston (GP) zones*, which occur at a very high density. This process represents the pre-precipitation stage.

These clusters of atoms are always located at the nodes of the aluminum matrix lattice and consist of small segments of crystallographic planes within the aluminum lattice, enriched in solute atoms (see Figure VII-3-b-). The presence of these Guinier-Preston (GP) zones introduces elastic distortions into the matrix lattice. The localized chemical enrichment and the resulting elastic deformations can enhance the precipitation process. In certain cases, structural defects such as dislocations can facilitate this precipitation by promoting higher diffusion rates of solute atoms or accommodating the associated elastic deformations.

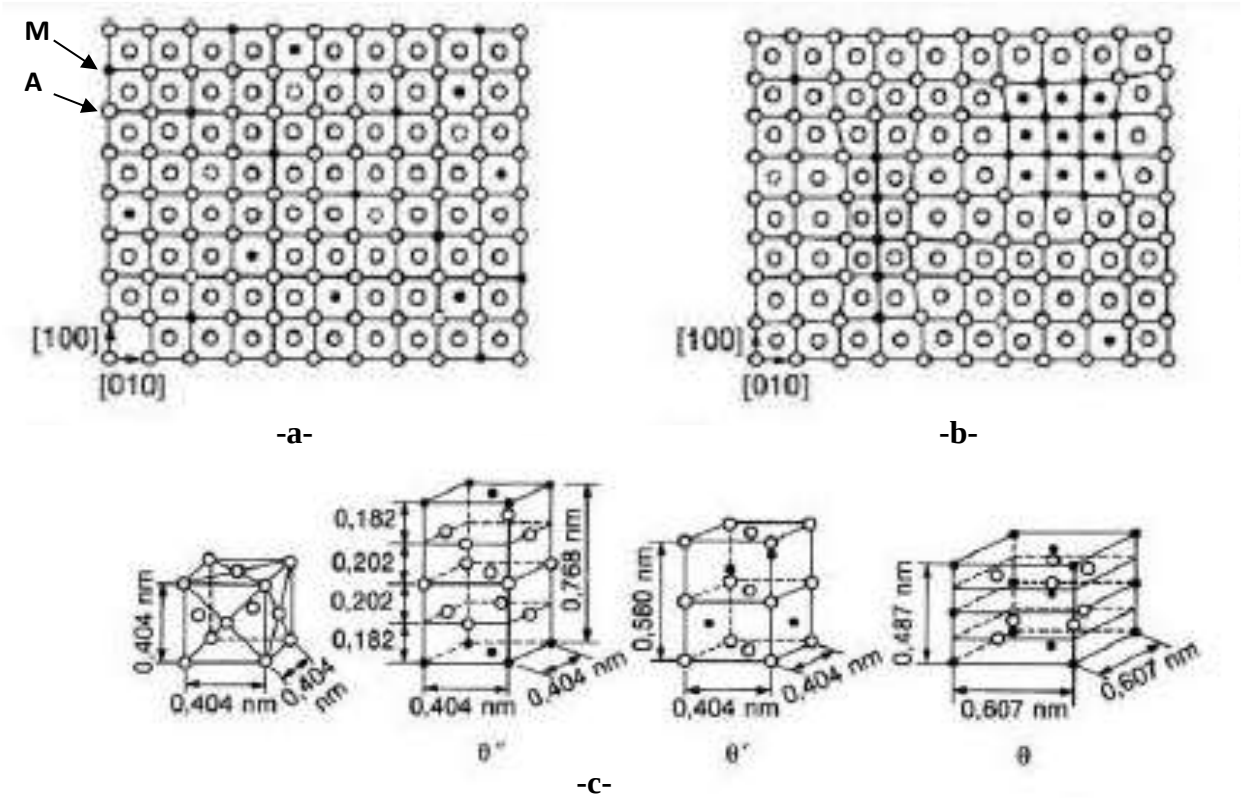

Fig. VII-3- : Different steps of the precipitation sequence of the Al-Cu system (*B. DUBOST et al, Techniques de l'Ingénieur, traité Matériaux métallique, la fiche M240, 1991).*

(a)- α-substitutional solid solution.n

(b) GP zones formation

(c) Lattice structures of the metastable intermetallic compounds θ" and θ', and the equilibrium intermetallic compound θ (Al_2Cu).

Subsequent heating at a moderate temperature (around 100°C), known as tempering, enhances the decomposition of the solid solution. This process involves the dissolution of the previously formed Guinier-Preston (GP) zones and the precipitation of a large number of very fine particles (ranging from 10^{16} to $10^{17}/cm^3$ with an average size between 2 and 50 nm). These precipitates are metastable intermetallic compounds, often referred to as transition precipitates.

They possess their own distinct crystal lattice and chemical composition, as illustrated in Figure VII-3-c-. This stage further hardens the alloy, reaching its maximum mechanical strength.

The precipitation of the equilibrium intermetallic compound in a matrix that is low in solute typically occurs only during an over-tempering treatment. This treatment is conducted at higher temperatures, generally above 160°C, and for a duration longer than that required to achieve the relative maximum hardening. During this stage, the alloy experiences relative softening due to the coalescence of precipitates. The largest of these precipitates, which can reach sizes on the micrometer scale, become visible under optical microscopy at high magnification. The microstructure thus tends to resemble that of the annealed state, which is the most thermodynamically stable. This annealed state is typically achieved after several hours at temperatures between 250 and 400°C.

VII-3-2. Precipitation sequence in quenched aluminum alloys

For thermodynamic and kinetic reasons, the quenching of a supersaturated solid solution almost never leads directly to the precipitation of the equilibrium intermetallic phase. Instead, the hardening of alloys at room temperature and during subsequent tempering generally results from a sequential decomposition of the α-solid solution and a progressive depletion of solute. This process typically follows the schematic steps:

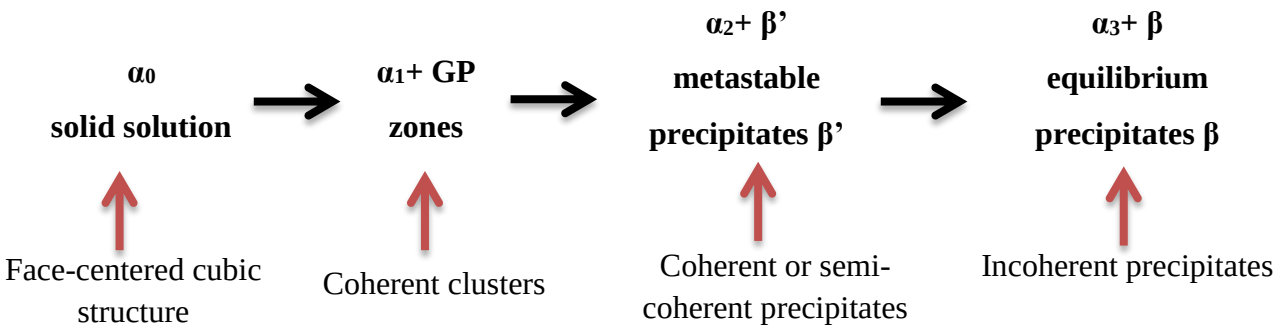

For significant structural hardening, it is crucial to achieve a high density and a homogeneous distribution of clusters and/or metastable precipitates within the matrix.

VII-4. Types of precipitation in metal alloys

VII-4-1. Continuous precipitation

This reaction involves the diffusion of atoms over large distances from the initial phase to the precipitate nuclei, resulting in a gradual modification of the solute composition towards its equilibrium value. An experimental characteristic of this transformation is the continuous variation in the crystal lattice parameter of the matrix until it reaches a limiting value corresponding to the equilibrium state. Precipitation begins with the formation of nuclei at the expense of the Guinier-Preston (G.P) zones, which eventually disappear and give way to metastable or stable phases. The transition from the initial state to the final state typically involves a series of intermediate stages, as outlined in the previous discussion on aluminum alloys.

❖ **Guinier-Preston zones (G.P)**

In 1938, Guinier and Preston proposed the existence of zones enriched with dissolved atoms that form small domains coherent with the matrix. These zones, known as Guinier-Preston (G.P.) zones, are responsible for the initial stage of hardening.

In contrast to the precipitation mechanisms of metastable and stable phases, which typically occur on structural heterogeneities, the formation of Guinier-Preston (G.P.) zones happens homogeneously. This mechanism has been extensively studied in aluminum-based alloys, where it has been established that G.P. zones form at sufficiently low temperatures. Vacancies play a crucial role in this process. After quenching, excess vacancies, which are present at low temperatures and before reaching their equilibrium limit, facilitate the diffusion of solute atoms. These atoms then cluster together rapidly, forming coherent zones with a distinct shape and structure.

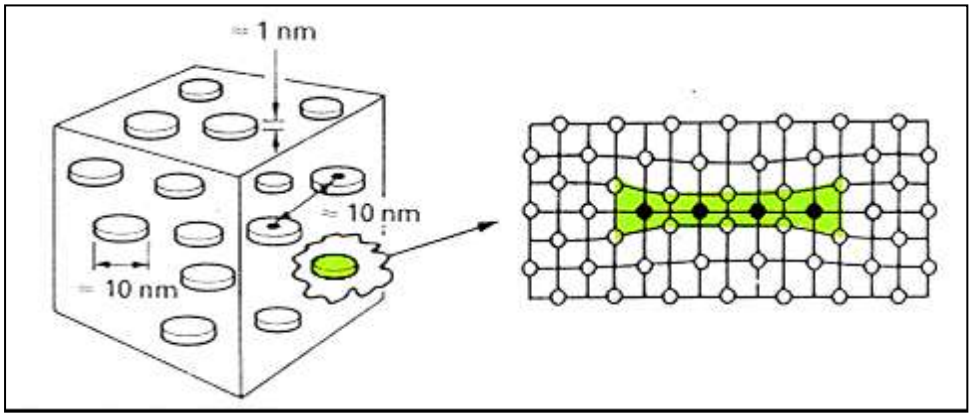

Fig. VII-4- : Guinier-Preston zones (G.P)

Due to their size, these precipitates create localized deformation fields (see Figure VII-5-). Dislocations are either attracted to or repelled by these particles, leading to their bending around the precipitates. To allow dislocation movement, a significant stress must be applied to overcome these elastic interactions. As the dislocation moves through or around a precipitate, it shears the particle, creating an interface of width b (see Figure VII-5-a-). The work required to move the dislocation is equivalent to the change in cohesive forces at this interface. This results in a high yield stress, which can increase with the particle diameter up to a critical size. Beyond this critical diameter, the Orowan mechanism becomes relevant, where circumventing the particle becomes easier than cutting through it (see Figure VII-5-b-).

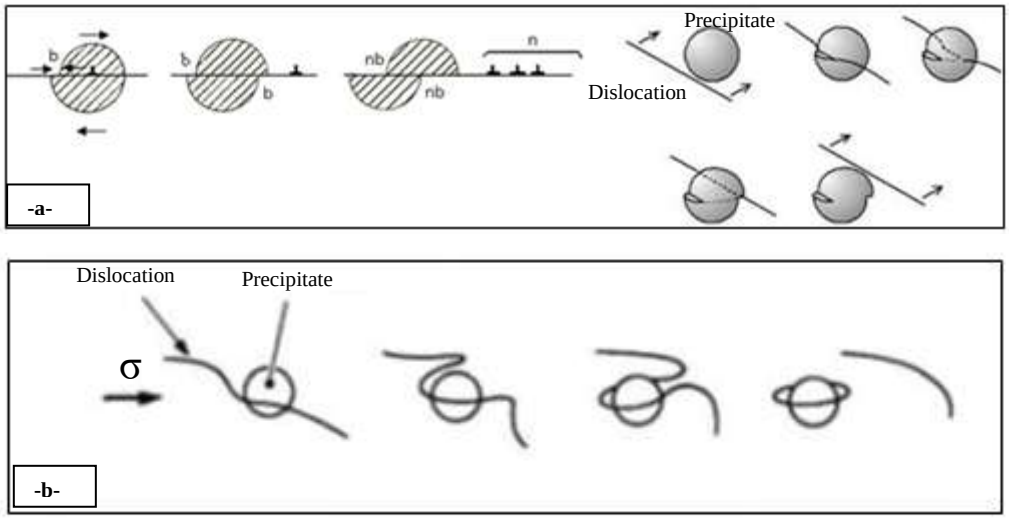

Fig. VII-5- : (a) Shearing of a coherent precipitate.
(b) Dislocation line bends around the precipitate: (Orowan mechanism)

VII-4-2. Discontinuous precipitation

Discontinuous precipitation is a type of discontinuous reaction involving two migrating phase boundaries. This heterogeneous solid-state reaction is diffusion-controlled at the boundaries, which serve as transport pathways for the solute. It typically occurs preferentially at regions with significant crystallographic misorientation. During this process, the supersaturated solid solution α' is replaced by a cellular structure composed of two phases, α and β.

$$\alpha' \longrightarrow \alpha + \beta$$

Where: α': The supersaturated matrix.

α: the same phase as α′ but with a different concentration

β: equilibrium precipitate (of the second phase).

Since Agreew et al. first discovered discontinuous precipitation in Ag-Cu alloys in 1930, our understanding of this reaction has significantly advanced. However, many important questions remain unresolved. It is still unclear which specific mechanism controls the process in a given alloy or why discontinuous precipitation occurs in some alloys and not in others. Additionally, establishing the criteria for this solid-state reaction remains challenging due to the multiple factors that can influence its occurrence.

- ✓ **Different types of discontinuous precipitation**
  - ❖ **Interfacial precipitation**

The precipitation product features a cellular structure with alternating lamellae behind a reaction front that resembles an incoherent grain boundary (see Figure VII-6-). During isothermal annealing, the interlamellar distance generally remains constant. However, Gust et al. have demonstrated that in certain areas, the interlamellar distance of precipitates formed isothermally can vary and follows a Gaussian distribution. In this type of reaction, material transport is facilitated by interfacial diffusion along the reaction front, which is a grain boundary with significant misorientation.

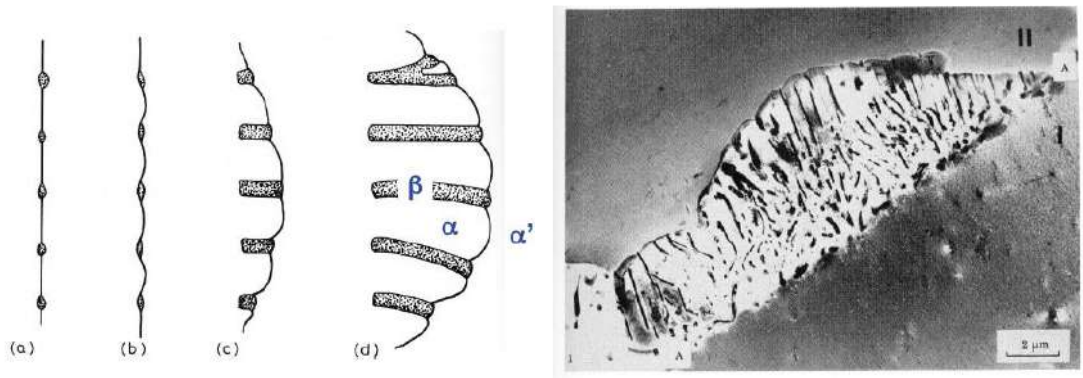

-a- -b-

Fig. VII-6-: (a)- Schematic representation of an interfacial type precipitation reaction

(b)- Cellular precipitation of $Mg_{17}Al_{12}$ in the Mg-9 at. % Al alloy annealed for 1 h at 220°C *(D. A. Porter, K. E. Eastorting. Phase transformation in metals end alloys, second edition, Chapman et Hall, London, (1992)).*

Dislocations play a significant role in the germination and growth of precipitates, as they create preferential regions for precipitation. This second type of precipitation differs from the first type in the following ways:

- The precipitated particles are not lamellar but consist of small platelets with a well-defined crystallographic structure.
- The volume diffusion of the solute element is involved.

Precipitation on dislocations occurs in systems where the specific volumes of the initial matrix and the reaction product are very different. It is assumed that, during the precipitation of the β-phase, the dislocations act as new nucleation sites. This type of precipitation on dislocations is not very common. However, in several solid solutions, both types of precipitation can be observed simultaneously.

❖ **Precipitation at interphase boundaries**

The issue of precipitation at interphase boundaries has been extensively studied theoretically. It is widely accepted that an immobile interphase boundary can provide favorable sites for the nucleation of a new phase, particularly at low temperatures.

In copper-based alloys, only two studies have focused on the investigation of discontinuous precipitation at interphase boundaries. Manna et al. were the first to explore the possibility of inducing discontinuous precipitation from interphase boundaries, similar to that observed at grain boundaries.

In their studies on a Cu-15% mass In alloy, Hamana and Boumerzoug demonstrated that the eutectoid phase can be obtained. Subsequent annealing at 400°C can lead to discontinuous precipitation at the eutectoid/matrix interphase boundaries, similar to what is observed at grain boundaries.

VII-5. Precipitation mechanisms

VII-5-1. Precipitation by germination and growth

According to the classical theory of Gibbs, extended to phase transformations in the solid state by Turnbull and Fischer, germination—the initial stage of precipitation—involves the formation of stable nuclei from the matrix. These nuclei are rich in solute, have a composition significantly different from that of the solid solution, and exhibit a defined interface with the

matrix. Germs can arise from statistical composition fluctuations of sufficient magnitude (on the order of a nanometer) within the solid solution, with very rapid formation kinetics occurring in the presence of vacancies and supersaturation (homogeneous precipitation). Alternatively, they can preferentially form on lattice defects or pre-existing interfaces between different grains or particles (heterogeneous precipitation). The subsequent growth of these germs and precipitates is governed by the diffusion of solute atoms towards them. This diffusion is thermally activated at the tempering temperature, as long as the solid solution remains supersaturated. The proposed mechanisms for precipitation consider both thermodynamic factors and kinetic effects and apply to most precipitation-hardened aluminum alloys.

❖ Thermodynamics of germination

Thermodynamically, germination is only possible after dissolution and quenching if it results in a reduction in the overall free energy of the system, which initially consists of the homogeneous solid solution. This quantity, the Gibbs free energy, first includes the chemical term of the molar free energy associated with germ formation, followed by thermodynamic barriers that oppose the formation of these germs. Figure VII-7 illustrates the free energy curves for the formation of different phases as a function of the concentration X of the added element at the high temperature (T_H) and the low tempering temperature (T_B). In this figure, the phase equilibrium diagram of the system is derived from the minimization of its free energy across the entire range of considered temperatures.

- The curve G(α) shows the variation in the molar Gibbs free energy of the solid solution α\alphaα as a function of solute concentration, as well as that of the GP zones, since the latter share the same crystalline structure as the matrix. This curve exhibits double concavity, with an absolute minimum near the solute concentration at equilibrium X_s (at low values of X) and a relative minimum close to the average solute concentration around the GP zones (at higher values of X).
- G(β′) and G(β) represent the respective free energy curves for the metastable phase β′ (transition precipitate) and the equilibrium phase β (stable phase) as a function of the concentration X of the added element M.

Any mode of decomposition of low amplitude into two phases represented by A and B (at temperature T_H) is thermodynamically impossible within the domain where the curvature of G(x) is positive (Fig. VII-7-b). This is because such decomposition would result in an increase in the system's free energy. The only thermodynamically favorable decomposition of the initial solid solution that decreases the system's free energy is demixing into a highly dilute solid solution (close to the equilibrium concentration) and clusters rich in solute atoms. These clusters can consist of GP zones (with a concentration beyond the second inflection point J_1 or J_2 on the G(α) curve, in the positively curved region) or precipitates of the metastable β′ phase or stable β phase with lower molar free energy. The compositions of the solid solution and the associated GP zones or precipitates are given by the abscissa of the contact points of the tangent common to the two positively curved regions of the G(x) curve (Figs. VII-7-b and VII-7-c).

VII-5-2. Precipitation by Spinodal decomposition

This mode of precipitation, with theory established by Cahn, typically affects alloys with a high volume fraction of precipitates (e.g., copper alloys) but can also explain the structural hardening of certain aluminum alloys in the Al-Zn and Al-Ag systems. On the Gibbs free energy molar curve shown at low temperature in Figure VII-8, the concentration lies between the inflection points I and J (with the curve connecting I to J being the Spinodal curve). Spinodal decomposition is then possible within the domain where the curve G(α) is convex (with negative curvature) and for any temperature where $\partial^2 G(\alpha)/\partial x^2 < 0$.

A continuous and progressive decrease in the chemical free energy of the system, which is thermodynamically favorable, is achieved by the demixing of the initial solid solution into two components: one increasingly poor in solute and the other increasingly rich in solute. The respective concentrations of these phases are given by the abscissas of segment MP, based on the portion of the G(α) curve with negative curvature. Precipitation, which initiates from random fluctuations in the concentration of the solid solution, occurs throughout the grain. Unlike precipitation by germination and growth, there is no energy barrier for nucleation. Initially, the differences in composition are very small, but as the decomposition progresses, these differences increase. The solute migrates towards the precipitates by short-distance diffusion, moving up the concentration gradient until the final composition of the precipitate X_p is reached (Fig. VII-9). This results in a microstructure characterized by an apparently periodic modulation of the distribution of precipitates within the matrix (homogeneous precipitation).

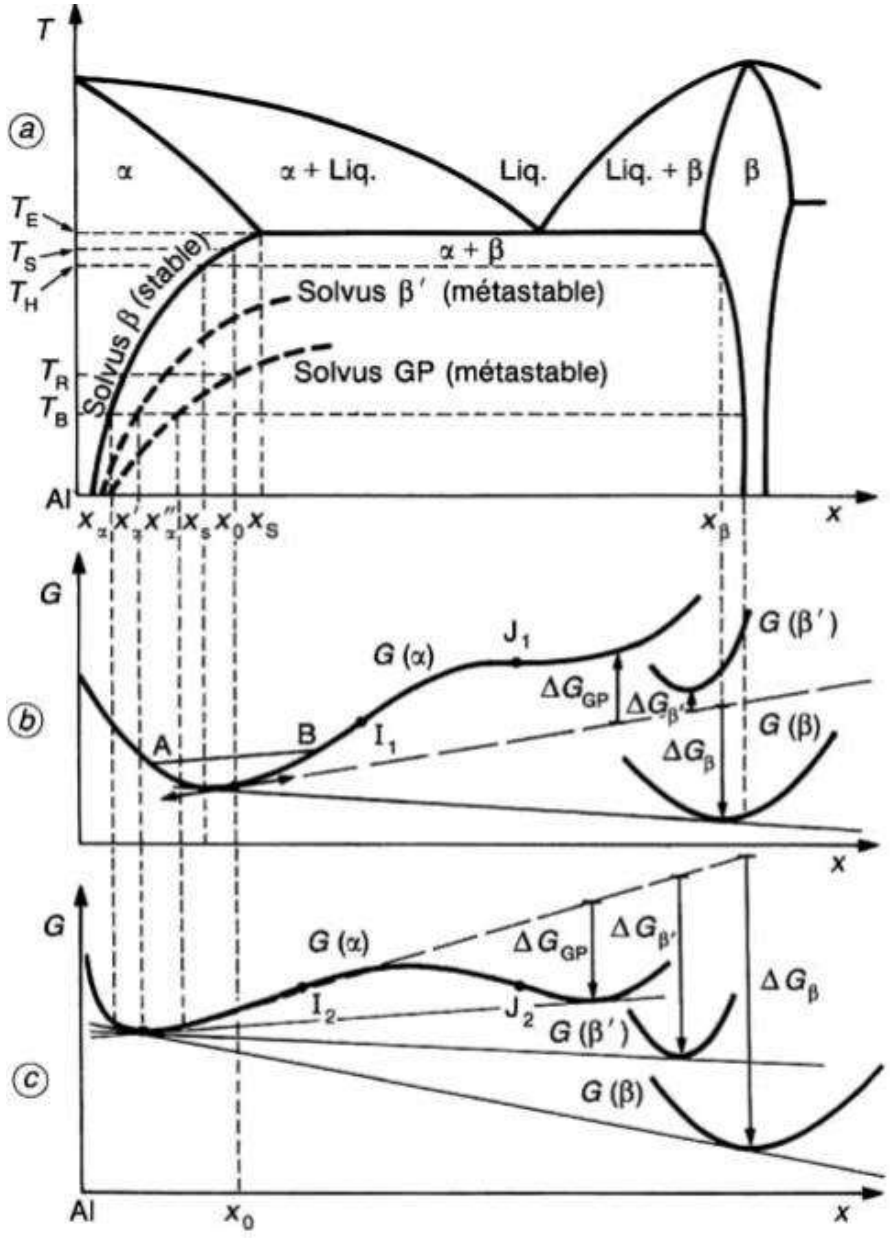

(a) Diagram of equilibrium phases and metastable phases
(b) Molar free energy G at a high temperature T_H
(c) Molar free energy G at low temperature T_B

Fig.VII -7- : Schema for Constructing the Phase Diagram of the Al-M System *(B. Dubost et al, Techniques de l'Ingénieur, traité Matériaux métallique, la fiche M240, 1991).*

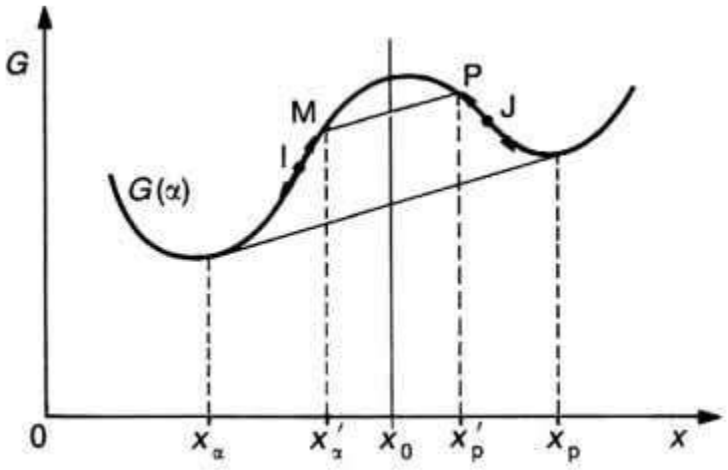

Fig. VII-8- : Free energy curve G at low temperature of an alloy with concentration x_0 *(B. Dubost et al, Techniques de l'Ingénieur, traité Matériaux métallique, la fiche M240, 1991).*

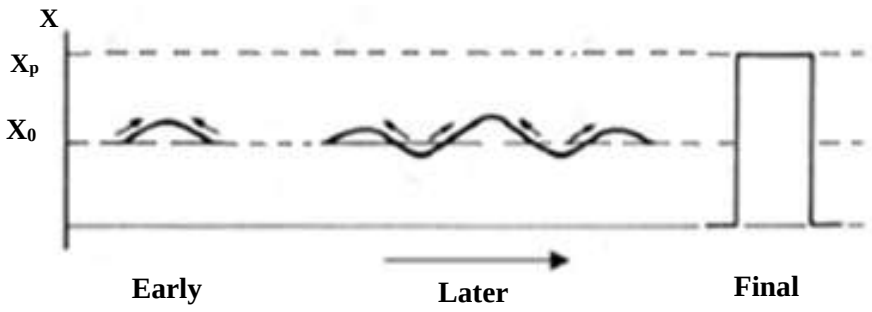

Fig. VII-9- : Evolution of the Solute Concentration Profile xxx in an Alloy Precipitated by Spinodal Decomposition, Depending on the Maturation Stage.

VII-6. Experimental methods for studying structural precipitation

VII-6-1. Metallography

Optical microscopy, due to its limited resolving power, is primarily used to visualize coarse precipitates on samples that have been polished and, if necessary, treated with specific solution reagents (Fig. VII-10). The images obtained reveal attack figures that provide valuable information about the distribution of the coarser phases, such as phases that are insoluble (i.e., phases that do not dissolve during homogenization treatments following alloy fabrication) and precipitates located at grain boundaries.

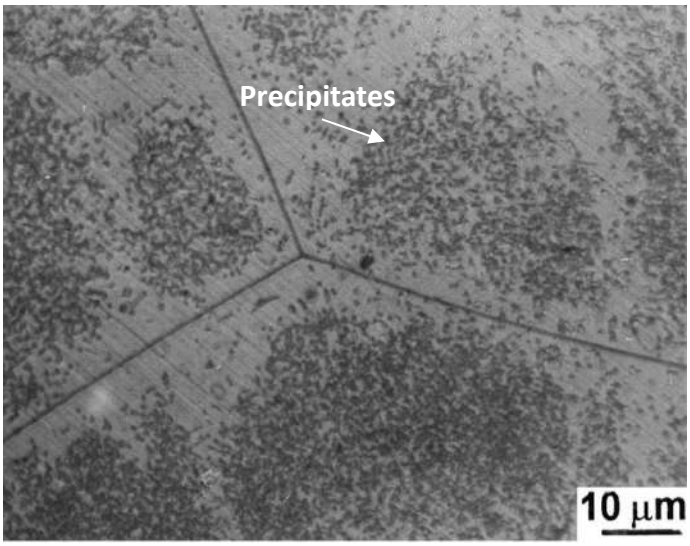

Fig. VII-10-: Microstructure of Al–12 wt.% Mg alloy homogenised 17 h at 430°C, quenched then aged during continuous heating at a rate of 2°C/min to 280°C *(D. Hamana et al., Journal of Alloys and Compounds 320 (2001) 93–102)*

Scanning electron microscopy on polished sections, utilizing the chemical contrast from differences in atomic number seen in backscattered electron imaging, provides similar information with higher spatial resolution while avoiding the need for chemical attack. These techniques can be effectively combined with devices for analyzing image contrasts and morphologies. This allows for quantitative and objective determination of the volume fractions of precipitates, as well as their geometric parameters such as size, shape, and distribution.

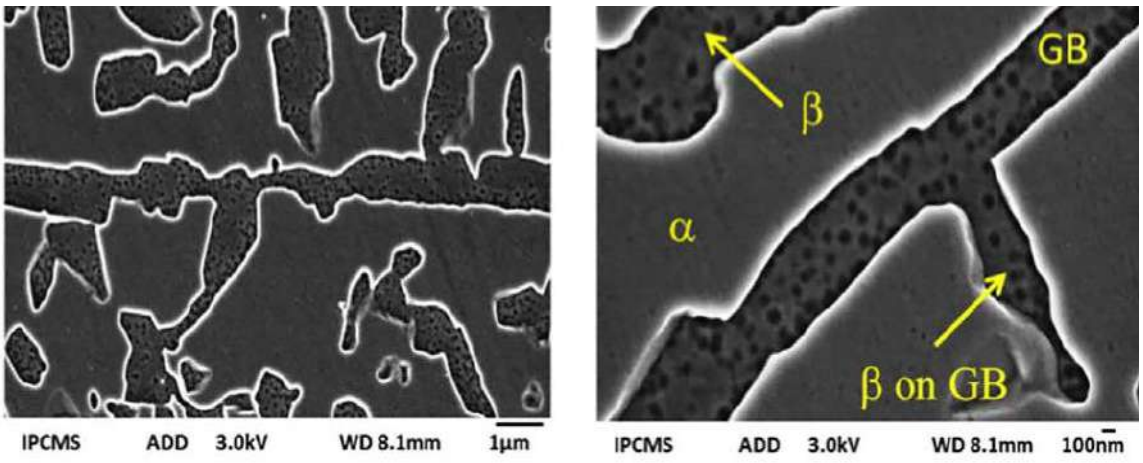

Fig. VII-11-: SEM images of Al-12 wt% Mg alloy homogenized for 17 h at 430 °C quenched and aged for 21 h at 250 °C *(C. Amrane et al., Materials Characterization 134 (2017) 49–54).*

Transmission electron microscopy (TEM) allows for precise characterization of phases in the alloy in terms of crystallographic structure (such as orientation relationships between phases), geometric features (including morphology, size, and distribution of phases at very high magnifications), and chemical composition (main elements). The spatial resolution is sufficient to visualize planes and columns of atoms constituting the microstructure through the interference of diffracted electron beams. Spatial resolution in crystallographic analysis (via electron diffraction) or chemical analysis (through energy-dispersive X-ray spectroscopy or energy analysis of transmitted electrons) can reach a few nanometers. This level of resolution is crucial for characterizing most precipitates in quenched aluminum alloys. However, it may be insufficient for certain cases, such as studying the initial stages of precipitation in Al-Mg-Si, Al-Zn-Mg, and Al-Cu-Mg alloys. TEM, based on electron diffraction, is particularly effective for investigating the orientation relationships of precipitates relative to the matrix and for analyzing structural defects (such as dislocations, lattice distortions, and grain boundaries).

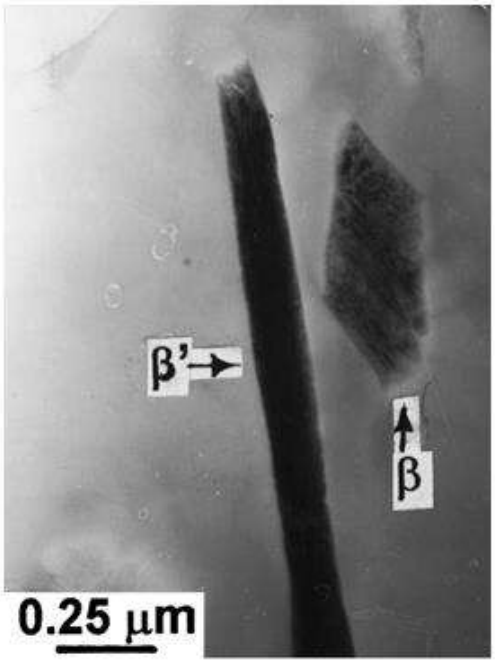

Fig. VII-12-: TEM micrographs of Al–12 wt.% Mg alloy homogenized 17 h at 430°C, quenched and aged 1 h at 250°C illustrating different particles of β' and β phases *(D. Hamana et al., Journal of Alloys and Compounds 320 (2001) 93–102).*

VII-6-2. X-ray and neutron diffraction

The extensive relationships between crystallographic structure and precipitation parameters make diffraction methods (including electron diffraction) essential tools for the microstructural study of metallic alloys. These techniques are employed for crystallographic characterization and, in some cases, for determining the morphology, volume fraction, and size of the precipitates present in the studied system.

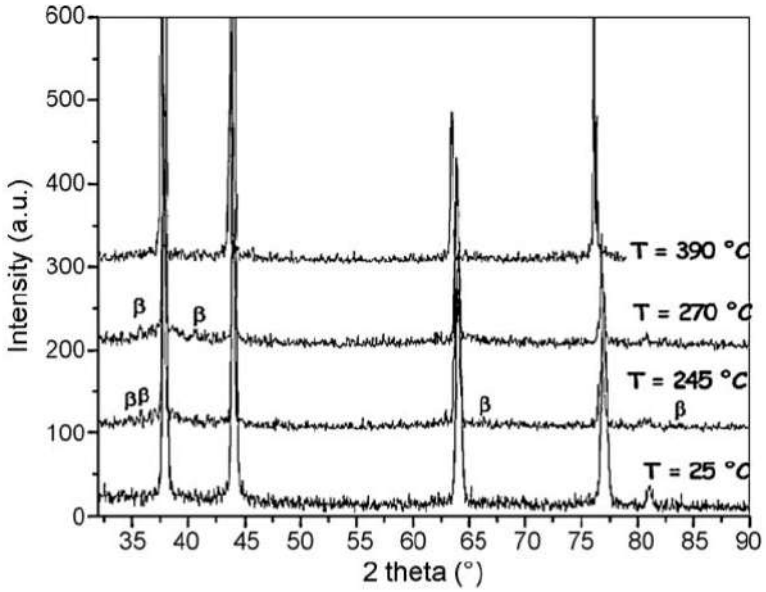

Fig. VII-13-: Sequence of X-ray diffraction patterns recorded during heating at a rate of 2°C/min for an Al–12 wt.% Mg alloy that was homogenized at 430°C for 17 hours, quenched in ice water, and then compressed to reduce its thickness to 16%. *(A. Hayoune and D. Hamana, Materials Science and Engineering A 527 (2010) 7261–7264).*

VII-6-3. Macroscopic physical methods

These methods exploit macroscopic variations in physical properties (such as electrical, thermal, and dimensional) of the material according to its state of structural separation.

Differential Scanning Calorimetry (DSC) is a highly sensitive calorimetric method that allows for the direct measurement of heat released or absorbed by an alloy sample during an exothermic process (such as precipitation) or an endothermic process (such as the dissolution of precipitates or GP zones) caused by a temperature increase at a controlled rate or by a controlled isothermal segment (Fig. VII-14). After calibration, this technique can quantitatively determine the mass fraction of phases formed in the matrix due to homogeneous or

heterogeneous precipitation. DSC also enables accurate determination of phase transformation temperatures, which are also studied using Differential Thermal Analysis (DTA) and are crucial for defining the conditions for alloy dissolution.

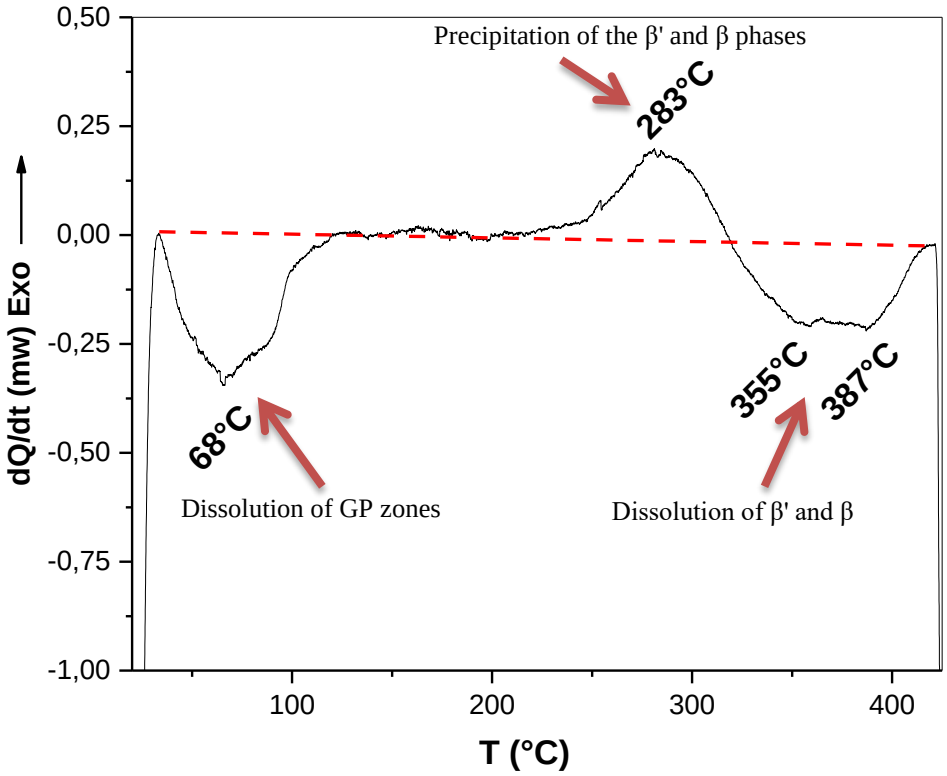

Fig. VII-14-: DSC curves of the Al-12wt. % Mg alloy homogenized then water quenched

Differential dilatometry allows for monitoring the kinetics and phase transformation ranges during heat treatments by measuring dimensional variations (contractions or expansions) induced by the aging or tempering of alloys (Fig. VII-15). However, the effects are generally weaker in industrial light alloys (particularly in ternary systems such as Al-Cu-Mg and Al-Mg-Si) compared to their constituent binary alloys (Al-Cu, Al-Mg, Al-Si). This is due to the compensation of individual effects caused by deviations in atomic radii of different solute atoms relative to the aluminum matrix and the precipitation of various metastable phases.

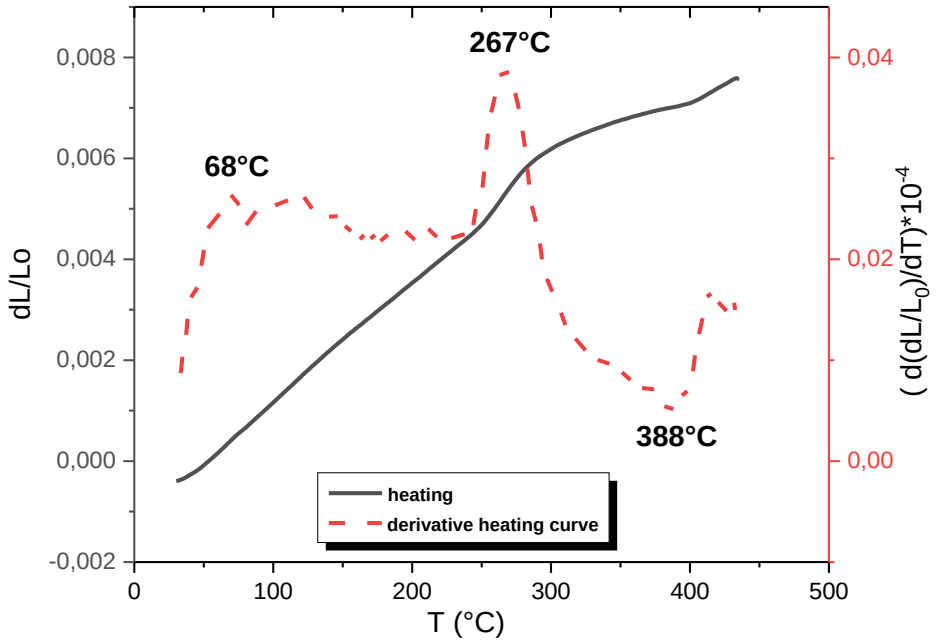

Fig. VII-15-: Derivative heating curve of an Al-12 wt.% Mg alloy that was homogenized for 17 hours at 430°C and then water-quenched.

The electrical conductivity and, conversely, the electrical resistivity are influenced by the progress of the solid solution's decomposition. Solute concentration has a significantly greater impact on these transport properties than the precipitate volume fraction. Measuring surface electrical conductivity and resistivity at room temperature is commonly used in industry as a non-destructive and rapid method for assessing the quenching and tempering state of semi-finished aluminum products, intended respectively for aeronautical and electrical applications. Electrical resistivity initially increases rapidly and then more slowly during maturation due to the formation of GP zones, likely because electron diffusion is affected by the clusters of atoms formed. It subsequently decreases progressively during tempering as the matrix solute is depleted, reaching a minimum value after extensive overaging or annealing. Finally, electrical resistivity is also influenced by the surface area of the precipitates and their shape factor (the ratio of the largest dimension to the smallest dimension).

Practice exercise

The heat treatment sequence used industrially for the Al-12 wt. % Cu alloy is given in Figure 1.

1- What happens during the high temperature plateau?
2- Why do we quench the alloy after the first stage?
3- Is the quenched alloy then in equilibrium?

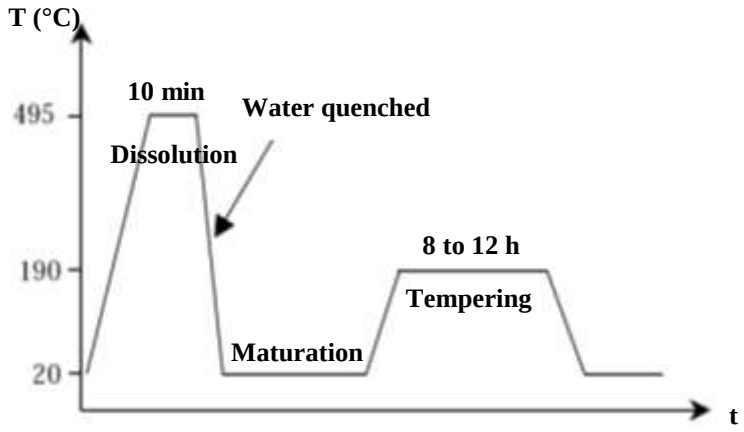

Figure 1

Answers

1. During the high-temperature plateau, the alloy undergoes solution treatment. This process involves heating the alloy to a high temperature where the solute elements (such as copper) dissolve completely into the aluminum matrix. This results in a single-phase solid solution. The purpose of this stage is to homogenize the alloy and dissolve any precipitates or phases present before quenching.

2. The alloy is quenched after the first stage to rapidly cool it and trap the solute elements in a supersaturated solid solution. Quenching prevents the precipitates from forming during cooling, which allows for the subsequent aging process to control the precipitation and enhance the alloy's strength and hardness. This rapid cooling helps to achieve a non-equilibrium state that can be further processed to develop the desired microstructure.

3. No, the quenched alloy is not in equilibrium. After quenching, the alloy is in a non-equilibrium state with a high concentration of solute elements trapped in a supersaturated solid solution. The alloy will undergo a subsequent aging process to allow controlled precipitation of phases and achieve the desired mechanical properties. During this aging process, the solute elements will diffuse and form precipitates, eventually leading to a more stable microstructure.

Annex

Terminologies

Term in English	Term in French	Term in Arabic

A

Abscissa	Abscisse	فاصلة
Acid	Acide	حمض
Actual solution	Solution réel	محلول حقيقي
Activation	Activation	التنشيط
Activation energy	Energie d’activation	طاقة التنشيط
Activation free energy	Energie libre d'activation	الطاقة الحرة لتنشيط (لتحفيز)
Activated state	Etat activé	حالة نشيطة
Addition	Addition	اضافة
Alloying elements	Eléments d'alliage	العناصر المضافة لسبيكة
Allotropic transformation	Transformation allotropique	تحول تآصلي
Alternate	Alterner	تناوب
Annealing	Recuit	تلدين
Atom	Atome	د ر ة
Attractive forces	Forces attractives	قوى جاذبة
Austenite	Austenite	أوستنيت

B

Backscattered	Rétrodiffusé	مرتدة
Bainite	Bainite	بينيت

Barrier	Barrière	حاجز
Beam	Faisceau, rayon	حزمة أشعة
Bending	Pliage	الثني
Binary solution	Solution binaire	ثنائي محلول
Binding force	Force de liaison	قوة الربط
Bond (Chemical bond)	Liaison (Liaison chimique)	رباط (رابطة كميائية)
Braking role	Rôle de freinage	دور المعيقد
Breaking	Rupture	كسر

C

Cap	Calotte	قبعة
Carbon (C)	Carbone (C)	(C)كربون
Casting	Coulée	الصبة
Cast iron	Fonte	الصب، حديد الزهر حديد
Cell	Maille	خلية
Cellular precipitation	Précipitation cellulaire	ترسبات شبكية
Cementite	Cémentite	سيمنتيت
Chemical properties	Propriétés chimiques	خواص كميا ئية
Chimical composition	Composition chimique	تركيب كميائي
Cluster	Amas	كوّمة ، تجمع
Coarse-grain	Gros grains	الحبيبات الخشنة
Coating	Revêtement	تغطية
Coherent	Cohérent	متلاحم، متماسك
Cohesion	Cohésion	تماسك، تلاصق
Cold working	Ecrouissage	على البارد عمل
Collision	Collision	الاصطدام
Composition	Composition	تركيب

Concentration	Concentration	تركيز
Configuration	Configuration	التشكيلة
Continuous	Continue	مستمر
Contraction	Retrait	تقلص، إنكماش
Contrast	Contraste	تباين
Cooling	Refroidissement	تبريد
Cooling rate	Vitesse de refroidissement	سرعة التبريد
Copper	Cuivre	النحاس
Corrosion	Corrosion	تآكل
Cracks	Fissures	الشقوق
Critical nucleus	Germe critique	نوي حرج
Crossing	Traversée	العبور
Crucial	Capital	مهم
Crucible	Creuset	القالب
Crystalline solid state	Etat solide cristallin	الحالة الصلبة البلورية
Curvature	Curvature	إنحناء
Curve	Courbe	منحنى
Cycle	Cycle	الدورة

D

Data	Données	معطيات
Decrease	Diminuer	ينقص
Defects	Défauts	عيوب
Deformation	Déformation	تشويه
Derivation	Dérivation	إشتقاق
Dendrites	Dendrites	تفرعات شجيرية
Dense	Dense	كثيف

Differential scanning calorimetric analysis	Analyse calorimétrique différentielle à balayage	التحليل الحراري التفاضلي
Diffusional transformation	Transformation avec diffusion	تحول بوجود انتشار(تحول انتشاري)
Diffusionless transformation	Transformation sans diffusion	تحول بدون انتشار
Diffusion	Diffusion	إنتشار
Discontinuous	Discontinu	متقطع، غير مستمر
Dislocations	Dislocations	الإنخلاعات
Disorder	Désordre	عشوائية
Displacive transformations	Transformations displacives	تحولات طورية بدون إنتشار
Dissolve	Dissoudre	تذوب
Distortion	Distortion	إلتواء، تشويه
Driving role	Rôle moteur	دور المحرك

E

Elastic deformation	Déformations élastique	تشوه المرونة
Elastic limit	Limite élastique	حد المرونة
Elastic Strain	Elastic Strain	تشوه مرن
Electrical conductivity	Conductivité électrique	موصلة كهربائية
Electrical resistivity	Résistivité électrique	المقاومة الكهربائية
Electrical properties	Propriétés électriques	الخواص الالكترونية
Electrical tension	Tension électrique	جهد كهربائي
Embedding	Enrobage	الاكساء
Embryos	Germe	نوي
Endothermic	Endothermique	ماص للحرارة
Engineering stress	Contrainte conventionnel	اجها د اصطلاحي
Enthalpy	Enthalpie	أنثالبي
Entropy	Entropie	أنتروبي

Equilibrium	Equilibre	توازن
Etching	Attaque	تنميش
Eutectic	Eutectique	أوتكتيك، أصهراني
Excess	Excès	زائد، فائض
Exothermic	Exothermique	ناشر للحرارة
Expansion	Expansion	تمدد
Exploitation	Exploitation (Dilatation)	إستغلال، إستثمار
Extrapolation	Extrapolation	إستكمال

F

Face-centered cubic	Cubique à faces centrées	مكعب متمركز الوجوه
Factor	Facteur	عامل
Failure	Repture	إنكسار, تمزق
Ferrite	Ferrite	فريت
Field	Champ	حقل، مجال
Fine-grain	Grain fin	الحبيبات، الدقيقة
First neighboring	Proche voisin	الجوار الاقرب
Flat	Plat	مستو مسطح
Fluctuation	Fluctuation	تقلب، تبُذل
Fluid	Fluide	مائع
Fraction	Fraction	جزء
Fragile	Fragile	الإنكسار سهل, هش
Free energy	Energie libre	طاقة حرة
Free surfaces	Surface libre	سطح حر
Front	Face	واجهة، أمام

G

Germ	Germe	نوي

Grain	Grain	حبيبة
Grain size	Taille de grain	حجم حبيبات
Grain boundaries	Joints de grains	حدود حبيبات
Growth	Croissance	نمو

H

Hardness	Dureté	صلادة
Hardening	Durcissement	تقسية ، تصليد
Hardening precipitation	Durcissement par précipitation	الإصلاد بالترسّب
Habitat plane	Plan d’habitat	مستوي الإلتحام
Heating	Chauffage	تسخين
Heating rate	Vitesse de chauffage	سرعة التسخين
Heat flow	Transfert de chaleur	تحول حراري
Heat fluxes	Flux de chaleur	تددفق حراري
Heat treatment	Traitement thermique	معالجة حرارية
Heterogeneous	Hétérogène	غير متجانس
Hold	Prise (maintien)	وقفة
Homogeneous	Homogène	متجانس
Homogenized	Homogénéisé	متجانس
Hypereutectoide	Hypereutectoide	فرط اوتيكتيك
Hypoeutectoide	Hypoeutectoide	هبط اوتيكتيك
Hypothesis	Hypothèse	فرضية

I

Ideal solution	Solution idéal	محلول مثالي
Impurity	Impureté	شائبة
Incoherent	Incohérent	غير ملتحم

Inclusions	Inclusions	شوائب
Increase	Augmenter	يزيد
Ingot	Lingot	صبة
Intensive variables	Variables intensives	متغيرات كثيفة
Interaction energy	Energie d'interaction	طاقة التفاعل
Interface	Interface	سطح بيني
Interfacial energy	Energie d’interface	طاقة سطح بيني
Interfacial precipitation	Précipitations interfaciales	ترسبات في سطح بيني
Interference	Interférence	تداخل، تعارض
Interlamellar	Interlamellaire	بين الطبقات
Intermediate	Intermédiaire	متوسط
Intermetallic compound	Composé intermétallique	مركب وسيطي
Internal activation energy	Énergie d'activation interne	طاقة التنشيط الداخلية
Interphase boundary	Joint d’interphase	حد بين الأطوار
Interstitial solution	Solution interstitielle	بيني (محلول إنغراسي)
Insoluble	Insoluble	غير قابل للذوبان
Instantaneous	Instantané	آني، لحظي
Invariant	Invariant	ثابت، لا متغير
Iron	Fer (Fe)	حديد
Iron-based alloy	Alliage à base de fer	سبيكة بنيتها الاساسية الحديد
Isoconversional	Isoconversionelle	متساوي التحول
Isothermal	Isotherme	درجة حرارة ثابته
Isotropic	Isotrope	متماثل الخواص

K

Kinetic	Cinétique	الحركية
kinetic energy	Energie cinétique	الطاقة الحركية

L

Lamellar	Lamellaire	رقائقي
Lamellar structure	Structure lamellaire	البنية الرقائقية
Latent heat	Chaleur latente	حرارة كامنة
Lateral	Latérale	جانبي
Lateral growth	Croissance latérale	النمو الجانبي
Lath structure	Structure en latte	البنية الشرائحية
Layer	Couche	طبقة
Lean	s'appuyer	استند
level	Niveau	مستوى، مسطح
Liquid state	État liquide	حالة سائلة
Loop	Boucle	حلقة
Loss	Perte	فقدان, خسارة

M

Macroscopic	Macroscopique	مشاهدة عيانية، كبيرة
Magnetic properties	Propriétés magnétiques	خواص المغناطيسية
Magnification	Grossissement	تكبير
Martensite	Martensite	مارتنزيت
Matrix	Matrice	مصفوفة
Massive transformation	Transformation massive	تحول بدون انتشار
Maturation (natural ageing)	Maturation (vieillissement naturel)	نضوج (تطبيع في درجة الحرار العاية)
Major segregation	Ségrégation majeure	إنعزال كبير
Mechanical properties	Propriétés mécaniques	خواص ميكانيكية
Mechanism	Mécanisme	آلية, تركيبة
Medium	Moyen	متوسط

Melting	Fusion	إنصهار
Melting-point	Point de fusion	درجة الإنصهار
Melting-pot	Creuset	وعاء الانصهار
Metallography	Métallographie	ميتالوغرافيا
Metallurgy	Métallurgie	علم المعادن
Micrographics	Micrographie	صورة مجهرية
Microscopic	Microscopique	مجهري
Microstructure	Microstructure	بنية مجهرية
Migration	Migration	هجرة
Minor segregation	Segregation mineure	إنعزال طفيف
Minus	Moins	ناقص
Miscibility gap	Lacune de miscibilité	فجوة اللإمتزاج
Mismatch	Décalage	عدم تطابق, إزاحة
Mobility	Mobilité	حركية
Modulation	Modulation	تضمين، تعديل
Mold	Moule	القالب
Molar	Molaire	مولي
Molecular	Moléculaire	جزيئي
Monocrystalline	Monocristallin	أحادي البلورة
Morphology	Morphologie	شكل

N

Nearest neighbor	Plus proche voisin	الجوار الاقرب
Neighboring	Voisin	المجاورة
Needle structure	Structure en aiguille	ابرية البنية
Nucleation	Germination	تنوي
Nucleus	Germe	نوي

O

Offset	Décalage, déporté	إزاحة، مقابلة
Ordered phase	Phase ordonnée	طور مرتب (بنية مرتبة)
Ordering process	Processus de mise en ordre	الترتيب (تشكل الطور المرتب)
Orientation	Orientation	توجيه، إتجاه
Overtempering	Surrevenu	فرط تطبيع

P

Particle	Particule	جسيم، جزيئ
Peritectic	Peritectique	بيريتكيك
Perlite	Perlite	برليت
Phase	Phase	طور
Phase equilibrium diagrams	Diagrammes d'équilibre de phase	بيان اتزان الاطوار
Phase transformation	Transformation de phase	التحول الطوري
Phase transition	Transition de phase	التحول الطوري
Physical properties	Propriétés physiques	الفزيائية الخواص
Planar growth	Croissance planaire	نمو مستو
Platelet	Plaquette	صفيحة
Plastic deformation	Déformations plastiques	لدن تشوه
Polishing	Polissage	صقل
Polycrystalline	Polycristallin	متعدد البلورات
Portion	Partie	جزء
Potential energy	Energie potentielle	الطاقة الكامنة
Potential interaction energy	Energie potentielle d'interaction	طاقة التفاعل الكامنة
Precipitation	Precipitation	ترسيب

Pressure	Pression	ضغط
Primitive cell	Maille élémentaire (primitive)	خلية أولية
Probability	Probabilité	احتمالا
Property	Propriété	خاصية, ملكية
Proportion	Proportion	نسبة
Protuberance	Protubérance	نتوء، حدبة
Pure	Pur	نقي

Q

Quenching	Trempe	سقاية ، تبريد سريع

R

Radius	Rayon	نصف قطر
Random	Aléatoire	عشوائي
Rate	Vitesse	سرعة
Reaction	Reaction	التفاعل
Reagent	Réactif	كاشف
Regular solution	Solution régulier	منتظم محلول
Repulsive forces	Forces répulsives	قوى تافرية
Rod (rod form)	Tige (forme de tige)	قضيب (شكل قضيب)
Rolling	Laminage	،درفلة دلفنة
Roughness	Rugosité	خشونة

S

Scale	Echelle	سلم ، مقياس
Scanning	Balayage	المسح
Segregation	Ségrégation	إنعزال

Semi-coherent	Semi-cohérentes	نصف ملتحم
Sequence	Séquence	تسلسل
Shift	Modification, changement	إنتقال، تغيّر
Shrinkage	Retrait	إنكماش
Size	Taille	تحديد حجم
Solidification	Solidification	تجميد
Solid solution	Solution solide	محلول جامد
Solid state	Etat solide	الحالة الصلبة
Solidus	Solidus	منحنى الجامد
Solubility	Solubilité	ذوبانية
Solution	Solution	محلول
Solubility	Solubilité	ذوبانية
Solubility limit	Limite de solubilité	حد الذوبانية
Specimen	Echantillon	عينة
Spectrum	Spectre	طيف
Spherical cap	Calotte sphérique	غطاء (قبعة) كروي
Stacking faults	Défauts d'empilement	عيوب التكديس
Stainless steel	Acier inoxydable	فولاذ غير قابل للصدأ
State	Etat	حالة
Steel	Acier	فولاذ
Strength	Résistance mécanique	مقاومة ميكانيكية
Stress	Contrainte	إجهاد
Structural transformation	Transformation structurale	التحول البنيوي
Structure	Structure	البنية
Structure defects	Défauts de structure	عيوب البنية
Substitution solution	Solution de substitution	إحلالي محلول
Substrate	Substrat	مادة تستعمل كاساس او قوام
Supercooling (undercooling)	Surfusion	فرط التبريد

Superficial	Superficielle	سطحي
Supersaturated solution	Solution sursaturée	محلول مشبع
Support	Support	سند، دعامة
Sursaturation	Sursaturation	التشبع
System	Système	جملة

T

Tempering	Revenu	تطبيع
Thermal activation	Activation thermique	التنشيط الحراري
Thermal analysis	Analyse thermique	تحليل حراري
Thermal vibration	Vibration thermique	الاهتزاز الحراري
Thickness	Epaisseur	سمك
Transient state	Etat transitoire	حالة زائلة ، حالة عابرة
Transition state	Etat de transition	الحالة الانتقالية
True stress	Contrainte vraie	إجهاد حقيقي
Trunk	Tronc	جذع

U

Unit	Unité	وحدة
Unit cell	Maille élémentaire	خلية أولية
Unit volume	Unité de volume (volume unitaire)	وحدة الحجم

V

Vacancy	Lacunes	الفجوات
Value	Valeur	القيمة

Vaporization	Vaporisation	تبخر

W

Walls	Parois	حواف (جدران)
Walls of the mold	Parois du moule	جدران القالب
Water	Eau	الماء
Well-defined	Bien défini	محددة جيدا (محددة بدقة)
Wetting angle	Angle de mouillage	زاوية الترطيب

References

References

(1) L. Borel, D. Favrat, Thermodynamique et énergétique, presses polytechnique et universitaires romandes, nouvelle édition, 2005.

(2) P. Papon, J. Leblond, P. H. E. Meijer, Physique des transitions de phases concept et applications, cours avec des exercices corrigés, Dunod, France, 2000.

(3) J. Burke, La cinétique des changements de phase dans les métaux, Masson Et Cie Edideurs, Paris, 1969

(4) J. Benard, A. Michel, J. Philibert, J. Talbot, Métallurgie Générale, Masson et C^{ie}, Editeurs, Paris VI, 1969.

(5) L. Guillet, P. Poupeau, transformations à l'état solide des métaux et alliages métalliques, Dunod, Paris, 1973.

(6) B. Chalmers, métallurgie physique, Dunod, Paris, 1963.

(7) D. A. Porter, K. E. Eastorting, Phase transformation in metals end alloys, second edition, Chapman et Hall, London, 1992.

(8) J. P. Mercier, G. Zambelli, W. Kurz, Introduction à la science des matériaux, 3ème édition, Lausanne, 1985.

(9) A. Françoise ; G. Lorenzon, J. M. Haudin, Matériaux pour l'ingénieur, Presses des MINES, 2006.

(10) B. Dubost, P. Sainfort, Durcissement par précipitation, des alliages d'aluminium, Techniques de l'Ingénieur, traité Matériaux métallique, la fiche M240, 1991.

(11) D. Hamana, M. Bouchear, M. Betrouche, A. Derafaa, N.Ya. Rokhmanov, Comparative study of formation and transformation of transition phases in Al–12 wt.% Mg alloy, Journal of Alloys and Compounds 320 (2001) 93–102

(12) C. Amrane, D. Hamana, I. S. Golovin, Internal friction sensitivity to precipitation in Al-12 wt% Mg alloy, Materials Characterization 134 (2017) 49–54

(13) A. Hayoune, D. Hamana, A dilatometric and high-temperature X-ray diffraction study of cold deformation effect on the interaction between precipitation, recovery and recrystallization reactions in Al–12 wt.% Mg alloy, Materials Science and Engineering A 527 (2010) 7261–7264

(14) J. Lévy, Introduction à la métallurgie générale, Éditeur : Presses des mines, Paris, 1999.

(15) J. Lévy, Introduction à la métallurgie générale, Éditeur : Les Presses de l'école des mines de Paris, (2002).

(16) J. P. Mercier, G. Zambelli, W. Kurz, Introduction à la Sciences des matériaux, 3ème édition, Lausanne, 1985.

(17) Z. Laarouk, Introduction à la Métallurgie, Université Mentouri Constantine, polycopié édité, Algérie, 2001.

(18) Y. Quréré, Physique des Matériaux, Edition marketing, 1988.

(19) P. Haasen, Physical Metallurgy, Cambridge University Press**,** 1978.

(20) J. Barralis, G. Maeder, Précis de Métallurgie, 1995.

(21) P. W. Atkins, Éléments de chimie physique, Bruxelles, 1998

(22) H. Fredriksson, G. Nylén, Metal Science, 16, 283-294, 1982.

(23) J-M. Dorlot, J-P. Bailon et J. Masounav, Des materiaux, Ecole Polytechnique de Montreal, Canada, 1986.

(24) B. Chalmers, Métallurgie Physique, Dunod, Paris, 1963.

(25) A. Cornet, F. Hlawka, Propriété et Comportements des Matériaux, Ellipses édition Marketing, SA, Paris, 2010.

(26) P. G. Shewmon, Transformations in Metals, Materials Science and Engineering series, USA, 1969.

(27) W. Rastoker, J. R. Dvorak, Interpretation of Metallographie Structures, Acadimic press, London, 1965.

(28) J. Philibert, A. Vignes, Y. Béchet, P. Combrade, Metallurgie, du Minerai au Matériau, Mason, Paris, 1998.

(29) W. D. Callister, D. G. Rethwisch, Materials Science and Engineering, an Introduction, 8th ed. John Wiley & Sons, USA, 2009

(30) R. E. Smallman, A. H. W. Ngan, Modern Physical Metallurgy, Eighth Edition, USA, 2014.

(31) Amarican Society for Metals, Metals Handbook, Volume 8: Metallography, Structures and Phase Diagrams, 8th Edition, 1973

(32) J.P. Bailon, J.M. Dorlot, Des matériaux, presses internationales polytechnique de Montérial, 3eme édition, 2000

(33) E. Vivant, Dictionnaire technique Anglais-Français, Librairie militaire deL. Baudoin et C^{e}, 1885, Paris

(34) Z. Larouk, Scientific terms, université Frères Mentouri_Contantine, Algérie, 2001.

(35) F. Gonzales, D. Favez, Prof. M. Rappaz Transformations de phases - Interfaces II (2007)